Summer 8-15-2021

Vestibulospinal circuit in the larval zebrafish

Zhikai Liu
Washington University in St. Louis

WASHINGTON UNIVERSITY IN ST. LOUIS

Division of Biology and Biomedical Sciences
Neurosciences

Dissertation Examination Committee:
Martha W. Bagnall, Chair
Timothy E. Holy, Co-Chair
Bruce A. Carlson
Daniel Kerschensteiner
Lawrence H. Snyder

Vestibulospinal Circuit in the Larval Zebrafish

by
Zhikai Liu

A dissertation presented to
The Graduate School
of Washington University in
partial fulfillment of the
requirements for the degree
of Doctor of Philosophy

August 2021
St. Louis, Missouri

Table of Contents

List of Figures

Chapter 1:

Chapter 2:

Supplementary figures

Chapter 3:

Chapter 4:

Acknowledgments

My biggest thanks go to my advisor Martha Bagnall. She really changed my perspective on how to do research and how to be a good scientist. It is quite remarkable to see her doing science at such a high level and being thoughtful about everyone around her at the same time. As a scientist, Martha's efficiency to get things done impresses me the most. Her intellectual acuity is rarely seen for a junior PI, and her mastery of articulating her ideas is second to none. I am very grateful that her ways of presenting, writing and thinking had so much influence on me. I feel extremely honored to be the first Ph.D out of her lab. In many ways, Martha is the perfect mentor for me, because although I had the raw skills to work hard and learn experiments quickly, I was never a great planner or a proficient communicator. She has been very patient and passionate to help me improve over the years, and she constantly kept all aspects of my life/career in the back of her mind. I couldn't ask for a better experience in her lab. Martha is one of a kind, and I will always look up to her.

I can't be more fortunate to have another amazing mentor, Tim Holy. The breadth and depth of Tim's knowledge are hard to grasp, but he is so approachable that you could forget he is a PI. I have learned many computational skills from scratch with him. Tim has hand by hand taught me how to write Matlab and Julia scripts, derive deconvolution algorithms on the white board of his office, and debug programs for my electrophysiology analysis. Talking with Tim about science is always a treat, and his personality made a pleasant and intellectually stimulating environment for his lab.

I would also like to acknowledge my other thesis committee members, Daniel Kerschensteiner, Larry Snyder and Bruce Carlson. They gave me great advice about my research

and challenged me to think harder about my projects. Especially Daniel provided valuable feedbacks for my paper. I am also very grateful for their inputs on my scientific career.

Next I want to thank Rich Roberts, Rebecca Callahan, Saul Bello Rojas, Mohini Sengupta and Vamsi Daliparthi in the Bagnall family for their tremendous technical and emotional support. Especially Rich helped me with my early experiments to screen for fishlines that label the vestibulospinal neurons, and construct the motorized table. The lab is also well connected outside of work - I had an eye-opening experience in Rebecca's dog wedding. Saul introduced me to the best beers in Chicago, and also organized every celebration event possible for the lab. Mohini cooked the most spicy Indian food for us and Vamsi's grilling skill is off the charts. I am very thankful that they make the lab feel like home.

My fellow graduate friends made my life in St. Louis much more colorful. I want to thank Keith Johnson and Allison Soung for keeping me sane during quarantine with guitar practicing and rock climbing; Jim Hsiang for discussing many wild and interesting ideas with me during biking; my hiking mates Hao Chen, Weikang Shi and Kaining Zhang for quite a few Midwest adventures; my cohort Monica, Margaret, Rachel, Hannah, Tami, Sabin, Nicole, Shaul for making the beginning years of graduate school so much fun.

I also appreciate great discussions and feedbacks in Tim's lab meetings, especially from Xitong Liang, Cody Greer, Jerry Lee, Kelly Hill, and Yue Yang. I'd also like to thank Ju Huang and Xiaoyan Fu for teaching me patch clamp physiology and surgery skills during my rotations.

At last, I am forever grateful for the support from my family back in China. My parents always cheer me on and believe in my ability to accomplish my goals. Although I am mostly away from home, their love and care are the strongest force to keep me going forward.

Zhikai Liu

Washington University in St. Louis

August 2021

Dedicated to my grandpa.

ABSTRACT OF THE DISSERTATION

Vestibulospinal Circuit in the Larval Zebrafish

by

Zhikai Liu

Doctor of Philosophy in Biology and Biomedical Sciences

Neurosciences

Washington University in St. Louis, 2021

Assistant Professor Martha Bagnall, Chair

Professor Timothy Holy, Co-Chair

The vestibular system sense gravity and self-motion to help animals maintain body balance. Although vestibular signals inform the brain of the directions and speed of our body movements, it still remains unclear how these sensory information are processed and organized in the central nervous system. My thesis aims to illustrate neural computation underlying central vestibular tuning and the topographic organization of the vestibular circuits. First I established a novel approach to perform whole-cell recording of synaptic inputs *in vivo* during multi-axis movements in the central vestibular neurons. This technical advance allowed me to simultaneously measure presynaptic and postsynaptic tuning, along with the presynaptic convergence pattern and synaptic strengths, all at the larval zebrafish vestibulospinal nucleus. I showed that convergence of inputs with dissimilar sensory responses can create complex postsynaptic tuning, whereas convergence of inputs with similar responses mediates simpler postsynaptic tuning. This direct demonstration of how simple and complex vestibular tuning are computed centrally, resolved a major gap in the vestibular field between theoretical prediction

and experimental evidence. Next, I used serial-section electron microscopy to reconstruct a high-resolution ultrastructure of the entire vestibular peripheral circuit. I mapped the connectivity of all 91 vestibular hair cells and 105 afferents in one utricle and traced afferent projections to the vestibular brainstem. This work reveals the first known topographic map organized by both sensory tuning and developmental age in the vestibular ganglion. It also shows that the early born and late born peripheral pathways coincide with two vestibular streams encoding the phasic and tonic signals, respectively. Together my study suggests that vestibular circuits from the peripheral sensors to the central neurons are potentially organized by development and movement speed.

Chapter 1: Introduction

1.1 Vestibular system for body balance

Gravity confines our movements on earth. Maintaining proper posture is necessary for vertebrates to traverse land and water. The vestibular system detects both gravity and self-motion, to help animals stabilize the visual field and keep body balance. Head motion elicits compensatory eye movements to keep visual inputs stable on the retina, and also initiates coordinated movements of the whole body to maintain correct posture with respect to gravity (Angelaki and Cullen, 2008). Both sensorimotor responses are carried out by rapid vestibular pathway, the vestibulo-ocular reflex (VOR) and the vestibulospinal (VS) reflex. These reflexes translate mechanosensory signals from the vestibular sensors to activation of muscles with minimal temporal delay. Six different muscles are used to compensate gaze by moving the eye in the opposite direction of head motion via the VOR, which only involves eye movements in three different axes (roll, yaw and pitch) (Bronstein et al., 2015). In contrast, keeping the whole body in balance requires more complicated motor coordination with muscle groups over the entire body. Thus it is less understood how the vestibular circuits transform the sensory signals to generate proper body-stabilizing outputs.

Body posture is maintained by both limb and trunk muscles in vertebrate animals. When tilted to the side, tetrapods extend their ipsilateral hindlimb and flex their contralateral hindlimb to maintain balance. It was shown that the limb extensor and flexor are differentially activated during vestibular stimulation. During head tilt towards the ipsilateral ear (ipsiversive roll), the extensor motor neurons are activated and the flexor motor neurons are inhibited in the

spinal cord (Grillner et al., 1970, Basaldella et al., 2015); whereas during contraversive roll, the flexor motor neurons are activated and extensor motor neurons are inhibited (Grillner and Hongo, 1972, Murray et al., 2018). Axial circuits control trunk muscles, which are well recognized for their role in left-right alteration during locomotion. Namely, the left and right axial motor units are driven by distinct pre-motor inputs, with mutual inhibition onto each other to create rhythmic locomotor activity, an essential mechanism of the central pattern generator (CPG) (Marder and Bucher, 2001). However, how axial spinal circuits mediate motor control for body balance is still not clear.

The axial dorsal and ventral motor activities were recently discovered to be controlled by distinct premotor networks (Bagnall and McLean, 2014). The motor neurons innervating dorsal musculature in the larval zebrafish, receive differential presynaptic inputs compared with those innervating the ventral musculature. During bodily tilt, dorsal- and ventral-projecting motor neurons show asymmetric activities, creating a torque to correct the body orientation. Moreover, this asymmetric drive to dorsal and ventral motor circuits requires vestibular sensation. It suggests that vestibular signals harness the segregation of the intraspinal circuits to induce self-righting behavior, consistent with previous models proposed in the lampreys (Tytell et al., 2010). However, the source of the descending vestibular inputs and the targeted neurons in the spinal cord receiving these inputs, are yet to be identified.

Larval zebrafish rely mostly on their trunk muscles to maintain their posture in the water (Ehrlich and Schoppik, 2017, Ehrlich and Schoppik, 2019). They use only utricle to sense self-motion (Fig. 1.1). The vestibular information is detected by the hair cells and relayed by the vestibular afferents into the vestibulospinal nuclei in the brainstem. The vestibulospinal neurons directly excite motor neurons and pre-motor neurons in the spinal cord for motor control. The

larval zebrafish brain and spinal cord are optically transparent, and highly accessible to map neural connectivity. Thus it provides unique technical advantages to uncover the sensorimotor transformation in the vestibulospinal circuit. Moreover, larval zebrafish is a great model organism to investigate the development of the vestibular system, a vastly understudied field in mammals. The larvae develop functional vestibular circuits as early as 3 days post-fertilization (dpf) (Mo et al., 2010). Both static tilts and dynamic rotations of the larvae evoke compensatory eye movements. The wild-type animals are also able to swim reliably with the dorsal-up posture at 4 dpf (Bagnall and Schoppik, 2018). Thus my thesis aims to use the larval zebrafish to understand 1) how vestibulospinal neurons compute sensory signals from the vestibular afferents, and 2) the developmental and functional organization of the vestibular circuits.

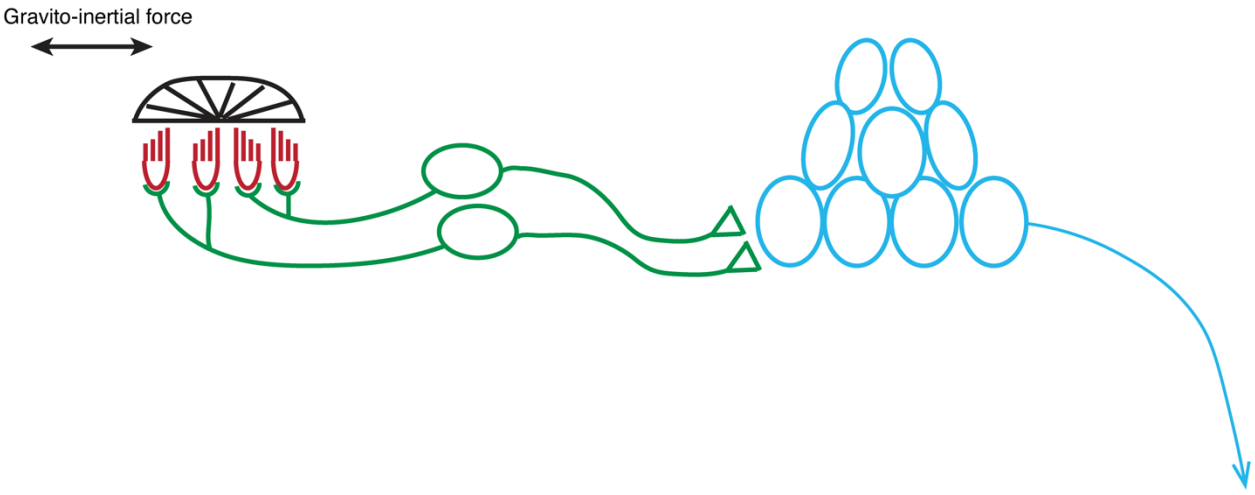

Figure 1. 1 Schematic of vestibulospinal circuit in the larval zebrafish

Gravito-inertial force on the otolith (black) is detected by hair cells (red), and the sensory signals are relayed by the vestibular afferents (green) to the vestibulospinal neurons (blue), which projects axons directly to the spinal cord to control movements.

1.2 Otolith and hair cells

Vestibular sensors consist of two parts, the semicircular canals and the otolith organs. In mammals, three semicircular canals are orthogonal in their orientation, spatially arranged to detect rotational movements in 3 different planes. Utricle and saccule, the two otolith structure, are used to detect gravity and translational movements. In both sensors, vestibular sensation is initiated by the deflection of the hair cells, by either the cupula in the canals or the calcium carbonate stone, named otoconia in the otolith organs (Eatock and Songer, 2011). In mammals, these two otolith end organs are aligned with the horizontal and parasagittal planes, to detect movements in orthogonal directions. In the larval zebrafish, the semicircular canals are not functional until about 1 month old (Beck et al., 2004, Lambert et al., 2008), and the saccule is used for hearing (Riley and Moorman, 2000). As a result, the utricle is the sole vestibular sensor, and required for both vestibulo-ocular and vestibulospinal reflexes. In the *rock solo -/-* fishline, the utricular hair cells are not able to detect self-motion or gravity due to the lack of the utricular otolith (Roberts et al., 2017). Therefore these mutant animals don't have vestibular-induced eye movement and exhibit abnormal swimming posture.

Polarization of vestibular hair bundle gives rise to direction selective tuning to motion stimuli. The preferred tuning direction of the hair cell is determined by the location of its kinocilia and stereocilia, two types of cilia built with distinct cytoskeleton structure. Each hair cell has one kinocilium and multiple stereocilia. The cilia extend from the sensory epithelium to the extracellular matrix that tether the otolith. Consequently, the hair cell cilia are mechanically deflected by the gravito-inertial force generated by gravity or acceleration on the otolith. When the hair bundle are deflected towards the kinocilia, the hair cell is depolarized most effectively.

This deflection direction is termed the preferred tuning direction, or the hair cell orientation. If the hair bundle are deflected to other directions, the hair cell is either activated or inhibited, depending on the cosine of the angle between the preferred and the actual direction (Hudspeth and Corey, 1977, Shotwell et al., 1981). This cosine tuning rule arises directly from the anatomical arrangement of the hair cell cilia and dictates the direction selectivity of hair cells.

The utricular hair cell orientation are diverse, and topographically organized. In the utricle, the macula is relatively flat and hosts hair cells that are tuned to all directions on the horizontal plane. Utricular hair cells that are located closer to each other have more similar orientation, except along the line of polarity reversal (LPR). The LPR marks the anatomical division between the hair cells that are nearby but oppositely tuned, an evolutionarily conserved feature in the otolith across many species (Deans, 2013). The majority of the utricular hair cells are tuned to ipsilateral tilt, residing on the medial side to the LPR; while the rest of the hair cells on the lateral side are tuned to contralateral tilt. However, the location of the LPR varies between species, leading to different proportions of hair cells on each side of the LPR. In mammals, the LPR is located more medially, with more hair cells tuned to contralateral tilt (Desai et al., 2005, Li et al., 2008). In fish and reptiles, the LPR is located more laterally, thus with fewer hair cells tuned to contralateral tilt (Haddon et al., 1999, Huwe et al., 2015). Such variance in the vestibular sensors could result in distinct spatial tuning and sensitivities centrally in different species.

1.3 Vestibular afferents

The vestibular afferent somata reside in the vestibular ganglion, and they relay vestibular signals from the hair cells into the brain. Each afferent connects with multiple hair cells of similar

orientation, and their synaptic connections are mediated by glutamatergic receptors. Thus, the otolith afferents' response to head tilt fit perfectly with a cosine function of the tilting angle (Fernandez and Goldberg, 1976b), and the preferred tuning direction of each afferent is aligned with the orientation of its presynaptic hair cells. The overall distribution of the otolith afferents' preferred directions also matches well with the distribution of hair cell orientation on the otolith macula (Fernandez and Goldberg, 1976a), showing that the afferents inherit their spatial tuning properties from the hair cells .

Two types of vestibular afferents are well known to encode vestibular information in different spiking patterns. The regular afferents in the otolith originate from the extrastriolar zone on the macula, and exhibit tonic firing; whereas the irregular afferents originate from the striolar zone, and exhibit phasic firing (Eatock and Songer, 2011). The coefficients of variation (CV) of inter-spike interval are relatively small in regular afferents, and the CV are by an order of magnitude higher in the irregular afferents (Goldberg et al., 1990, Goldberg and Fernandez, 1971). The regularity indicated by the CV of vestibular afferents often exhibits bimodal distribution in many species, therefore regarded as an important classifier for afferent types. It is believed that temporal dynamics of the regular and irregular afferents reflect their encoding strategies to signal head motion. Regular afferents encode vestibular stimuli linearly with firing rate, known as rate coding; while irregular afferents use precise timing of spikes to represent vestibular stimuli, known as temporal coding (Jamali et al., 2016). As a result, irregular afferents show high-pass tuning (respond stronger to high-frequency stimuli) and are more sensitive to motion transients (Goldberg, 2000). In contrast, regular afferents show flat tuning gain across different frequencies, and encode vestibular signals more accurately. Moreover, anatomically the irregular afferent have axons with larger diameters, allowing action potential to transmit with

higher conduction velocities (Goldberg and Fernandez, 1977), which is consistent with their role

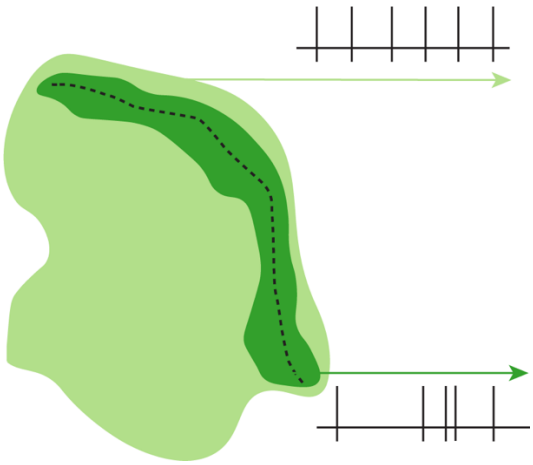

Figure 1. 2 Phasic and tonic vestibular pathways

Regular and irregular firing afferents arise from the striolar (dark green) and extrastriolar (light green) zones in the utricle. Dashed line: the line of polarity reversal

to detect fast motion signals. In summary, vestibular afferents relay self-motion signals to the brain in two distinct pathways, a phasic channel encoding preferentially high-frequency component and a tonic channel encoding preferentially low-frequency component.

1.4 Central vestibular tuning

How is head movement information encoded in the central brain? Vestibular afferents send projection into the central vestibular nuclei in the brainstem, giving rise to distinct temporal tuning properties of the central vestibular neurons (Angelaki and Dickman, 2000a, Bush et al., 1993). The tuning properties of central vestibular neurons are more complicated than those of the hair cell and afferents. The vestibular peripheral hair cells and afferents encode head tilt and translational movements in a unidirectional manner, and they also have consistent tuning phase across different direction or angles of vestibular stimulation(Fernandez and Goldberg, 1971). In the central vestibular nuclei of the monkeys, some neurons are broadly tuned to head tilt on different axes (Angelaki et al., 1993, Angelaki and Dickman, 2000a), and the tuning phase measured in each direction also differ from each other. Consistent with this data, vestibulospinal neurons in cats also exhibit a bidirectional tuning pattern (Peterson, 1970a), more complex than

those of the afferents. It was proposed that these complex tuning properties arise from the convergence of the vestibular afferents. Comprehensive computational modelling (Schor and Angelaki, 1992, Angelaki, 1991, Angelaki, 1992) from Dora Angelaki demonstrated that the central vestibular tuning is not simply the vectorial summation of its afferent inputs, even given that the synaptic input-output relationship is linear. When two afferents of different preferred tuning direction converge, the resultant postsynaptic tuning is cosine tuned only if these two afferents exhibit the same tuning phase. If the afferents' tuning phase are also different, the postsynaptic tuning is no longer unidirectional, but rather spatiotemporally complex. Especially if the afferents' are 90 degrees out of phase, the postsynaptic neuron would respond with the same tuning gain to translational stimuli on all axes. This spatiotemporal tuning model could explain the physiologically recorded sensory response of central vestibular neurons. But whether the convergence of afferents is sufficient to construct postsynaptic response *in vivo* is still unclear.

Anatomically, vestibular afferent innervations largely bypass the lateral vestibulospinal nucleus (Sato and Sasaki, 1993, Newlands et al., 2003, Carleton and Carpenter, 1984). Although electrical stimulation on afferents can elicit monosynaptic EPSPs on the vestibulospinal neurons, it remains unclear whether afferent inputs are the primary driver for their sensory tuning (Boyle et al., 1992). Other than direct afferent inputs, proprioception is known to affect the tuning of vestibulospinal neurons. Neck proprioceptors sense the torque between the head and body, which informs the brain of the relative head to body position (Goldberg and Cullen, 2011, Wilson and Schor, 1999). Commissural projection and cerebellar inputs were shown to inhibit the activities of vestibulospinal neurons. Ipsilateral excitation and commissural inhibition were suggested to work as push-pull system to synergistically generate vestibular response (Uchino et al., 1999).

Purkinje cells tonically inhibit central vestibular activities, and were implicated to provide cancellation signals for self-generated motion (Cullen, 2019). How these non-afferent inputs contribute to central vestibular tuning is still unclear.

1.5 Vestibulospinal pathway

Although central vestibular neurons in the brainstem receive direct afferent inputs and are considered secondary sensory neurons, they are anatomically segregated for their roles in regulating motor activities. The vestibulo-ocular reflex is mediated by neurons in the medial vestibular nucleus (MVN), which project to the oculomotor neurons and generate eye movements to compensate for head movements. The vestibulospinal tract regulating body posture consists of two pathways: the lateral vestibulospinal tract (LVST) and the medial vestibulospinal tract (MVST). The LVST originates from the lateral vestibular nucleus (LVN), and projects only ipsilaterally to the spinal cord (Boyle and Johanson, 2003), whereas the MVST projects to both the ipsilateral and contralateral side of the spinal cord (Kasumacic et al., 2010, Glover, 2000). Besides, the MVST and LVST also exhibit distinct longitudinal projection patterns. The descending MVST ends at the cervical level in the spinal cord, controlling primarily neck muscles, and the LVST sends collateral axons throughout the cervical and lumbar segments, controlling limb and axial trunk muscles (Kasumacic et al., 2015).

The lateral vestibulospinal (VS) nucleus giving rise to the LVST is also known as the Deiters' nucleus. The Deiters' neurons have large soma size, and innervate most spinal segments to regulate body posture (Wilson and Yoshida, 1969, Wilson et al., 1970, Wilson et al., 1978). They make direct excitatory connections with ipsilateral pre-motor and motor neurons to exert motor control. For example, bulk stimulation in the Deiters' nucleus revealed vestibulospinal

neurons excite extensor and inhibit flexor motor neurons for the ipsilateral limb muscles (Grillner and Hongo, 1972, Grillner et al., 1970). Thus the Deiters' nucleus is thought to elicit ipsilateral limb extension during bodily tilt and help animals regain body balance.

Vestibular signals are also used to regulate axial muscle activity. It was recently demonstrated that ipsilateral axial motor neurons receive distinct excitatory and inhibitory inputs from pre-motor neurons, and such input specificity requires vestibular sensation (Bagnall and McLean, 2014). LVST is a potential pathway to relay vestibular information from the sensory organs to the spinal axial circuits. Specifically, it is proposed that the axial motor circuits are modularized by their downstream musculature, and LVST descending signals regulate the activities of these modular microcircuits to generate posture-stabilizing outputs. In the larval zebrafish, the axial trunk muscles can be divided by their anatomical quadrants. Dorsal-projecting and ventral-projecting motor neurons activate their corresponding muscle groups in a body orientation dependent manner. When the fish is tilted in the roll axis, the activities in the dorsal-projecting motor neurons are stronger on the ear-down side, and weaker on the ear-up side, than the activities in ventral-projecting motor neurons. This asymmetric pattern is thought to initiate a rolling behavior to turn the animal back to the dorsal-up orientation (Bagnall and Schoppik, 2018). Again, the vestibulospinal neurons could be responsible for the asymmetric drive to the dorsal and ventral musculature for the self-right behavior.

Which spinal neurons are directly targeted by the vestibulospinal neurons for postural control? The motor neurons for hindlimb extensors were shown to receive monosynaptic excitatory inputs from the ipsilateral vestibulospinal neurons, and those for hindlimb flexors receive disynaptic inhibitory inputs (Grillner and Hongo, 1972). It indicates that descending vestibular signals coordinate activities of motor neurons and premotor neurons for proper

sensorimotor transformation, and both extensor motor neurons and ipsilaterally-projecting inhibitory interneurons are directly projected by the vestibulospinal neurons. Moreover, although the collaterals of vestibulospinal axons don't cross the midline of the spinal cord, motor neurons on the contralateral side receive disynaptic excitation and multi-synaptic inhibition from the vestibulospinal nucleus. Thus, excitatory and inhibitory spinal interneurons that project to the contralateral side are also likely direct targets of the vestibulospinal neurons.

Which axial motor neurons are the likely targets of the vestibulospinal projection? In the larval zebrafish, motor neurons are topographically organized for swimming of various speeds (McLean et al., 2007). Fast motor neurons project to medially located fast muscle fibers and slow motor neurons project to laterally located slow muscle fibers. The motor neuron somata recruited during fast swimming are born earlier and located more dorsally in the spinal cord than those recruited during slow swimming. These fast and slow spinal axial motor neurons were shown to receive inputs from distinct excitatory and inhibitory pre-motor neurons (McLean et al., 2008, Menelaou et al., 2014). In mammals, it was shown that slow extensor motor neurons receive more synaptic inputs that fast extensor motor neurons (Basaldella et al., 2015). It is yet to be examined whether slow and fast axial motor neurons receive different amounts of direct synaptic inputs from the vestibulospinal projections.

Do all vestibulospinal neurons target the same population of motor neurons and interneurons? It is almost entirely unknown how the tuning properties of the vestibulospinal neurons are associated with their role in regulating limb and axial muscle activities. Sensory tuning in vestibulospinal neurons determines the timing and amplitude of the excitation that they provide to the downstream spinal circuits. The tuning diversity of these neurons could provide some insights into the functional heterogeneity of the vestibulospinal circuit for motor control. In

cats, lateral vestibulospinal neurons were tuned to head tilt towards various angles (Schor et al., 1984b, Schor et al., 1985). Their preferred tuning directions are distributed across the roll and pitch axes. Only neurons tuned to the contralateral/nose-down head tilt were underrepresented. In VOR, central vestibular neurons tuned to a specific direction elicit eye movement toward the opposite direction, by monosynaptically exciting the oculomotor neurons that control specific eye muscle groups (Bronstein et al., 2015, Bianco et al., 2012). For vestibulospinal reflex, although vestibulospinal neurons as a population preferentially project to the extensor motor neurons, it is yet unclear whether the preferred tuning direction of an individual vestibulospinal neuron is associated with its postsynaptic targets. Central vestibular neurons have also diverse temporal tuning – most have higher tuning gain at higher stimulation frequency (high-pass) while some have flat tuning gain with respect to frequency change (Angelaki and Dickman, 2000a, Angelaki et al., 1993). High and low frequency vestibular stimuli are associated with fast and slow movement, respectively. It has not been examined whether vestibulospinal neurons with high-pass tuning are used to regulate fast locomotor activities, and those with flat gain are used to regulate slow locomotor activities.

Chapter 2: Central vestibular tuning arises from patterned convergence of otolith afferents

This chapter is adapted from the following publication:

Liu, Z., Kimura, Y., Higashijima, S.I., Hildebrand, D.G., Morgan, J.L. and Bagnall, M.W., 2020. Central vestibular tuning arises from patterned convergence of otolith afferents. *Neuron*, *108*(4), pp.748-762.

Abstract:

As sensory information moves through the brain, higher-order areas exhibit more complex tuning than lower areas. Though models predict that complexity arises via convergent inputs from neurons with diverse response properties, in most vertebrate systems convergence has only been inferred rather than tested directly. Here we measure sensory computations in zebrafish vestibular neurons across multiple axes *in vivo*. We establish that whole-cell physiological recordings reveal tuning of individual vestibular afferent inputs and their postsynaptic targets. Strong, sparse synaptic inputs can be distinguished by their amplitudes, permitting analysis of afferent convergence *in vivo*. An independent approach, serial-section electron microscopy, supports the inferred connectivity. We find that afferents with similar or differing preferred directions converge on central vestibular neurons, conferring more simple or complex tuning, respectively. Together these results provide a direct, quantifiable demonstration of feedforward input convergence *in vivo.*

2.1 Introduction

Neurons compute information from many different synaptic inputs. A central challenge in understanding neuronal circuits is determining how the tuning and connectivity of these inputs affect the resulting computations. For example, neurons in visual cortex exhibit simple or complex orientation tuning, which is thought to derive from the convergence of presynaptic inputs with distinct tuning properties (Hubel and Wiesel, 1962, Alonso and Martinez, 1998). Computational models of such input-output relationships have fundamentally shaped the way we think of information processing in the brain (Felleman and Van Essen, 1991, LeCun et al., 2015). However, these models generally require assumptions about many parameters that can only be measured with incompatible approaches: the tuning of the presynaptic population, input connectivity, and synaptic strengths, as well as the activity of the postsynaptic neuron itself. Direct measurements of these parameters simultaneously are prohibitively difficult in most systems, making it hard to define neuronal computations *in vivo*.

Vestibulospinal (VS) brainstem neurons receive direct vestibular sensory inputs from peripheral vestibular afferents (Boyle et al., 1992) and project to the spinal cord (Boyle and Johanson, 2003). Understanding the neuronal computations of VS neurons would not only inform how vestibular sensory signals are processed in the brain, but also provide a mechanistic view of sensorimotor transformation. VS neurons, like other central vestibular neurons, produce diverse responses to head movement. During head tilt or acceleration, some central vestibular neurons exhibit simple cosine-tuned responses, similar to those of the afferents: the strongest activity is evoked by movements in a preferred direction, with little or no response in the orthogonal direction. In contrast, other central vestibular neurons exhibit more complex

responses, including bidirectional responses (Peterson, 1970b) and spatiotemporally complex tuning (Angelaki et al., 1993). A vectorial model predicts that convergence of several simple cosine-tuned afferents can fully account for the response of either a simple or a complex central vestibular neuron, depending on whether those afferents are similarly tuned or differently tuned (Angelaki, 1992). However, as in other systems, this model has been technically challenging to test experimentally.

We chose to address this question in the larval zebrafish. Vestibular pathways in larval zebrafish are implicated in gaze (Bianco et al., 2012) and postural control (Ehrlich and Schoppik, 2019, Bagnall and Schoppik, 2018), similar to their functions in mammals. The VS neurons in larval zebrafish were also identified as anatomical homologs to those in mammals (Kimmel et al., 1982), indicating that they might share highly conserved functions. Moreover, the VS circuit becomes functional as early as 3 days post-fertilization (dpf) (Mo et al., 2010) in the larval zebrafish, whose small brain is exceptionally accessible for *in vivo* intracellular recordings from identified neurons. Therefore, the larval zebrafish serves as an excellent model organism to investigate how central vestibular neurons compute sensory signals in the vertebrates.

Here we establish a novel approach to record sensory evoked responses *in vivo* from VS neurons in the larval zebrafish. We find that individual afferents evoke large amplitude-invariant excitatory postsynaptic currents (EPSCs), allowing us to separate distinct afferent inputs that converge onto a given VS neuron. This provides a mechanism to simultaneously measure the sensory tuning and synaptic strength of each converging afferent, as well as the response of the postsynaptic neuron. We show that afferents with similar tuning direction preferentially converge, producing simple tuning in the VS neuron. Furthermore, the smaller number of cells with complex bidirectional responses receive input from differently tuned afferents, with

consequent simple or complex spiking. We also show that these afferent inputs suffice to predict the tuning of the VS neuron. Together, this work reveals how central neurons in the brain compute sensory information from their presynaptic inputs.

2.2 Results

Sensory evoked responses of vestibulospinal neurons *in vivo*

Traditionally, measurements of neuronal responses to vestibular stimuli have been accomplished by unit recordings (Angelaki and Dickman, 2000b, Schor et al., 1984a, Fernandez and Goldberg, 1976a). Directly measuring vestibular-evoked synaptic currents in central neurons *in vivo* has been technically challenging (Arenz et al., 2008, Chabrol et al., 2015). We designed a custom whole-cell electrophysiology rig to deliver translational motion stimuli to 4-7 dpf larval zebrafish via an air-bearing motorized sled (Fig. 2.1A). This setup allows intracellular measurement of sensory-evoked responses from vestibulospinal (VS) neurons over multiple axes *in vivo* for the first time, to the best of our knowledge. To target identified VS neurons, we generated a Tg(nefma:gal4; UAS:GFP) line, whose labelling overlaps dye backfilling from the spinal cord (Figs. 2.1D, 2.S1), consistent with evidence of *Nefm* expression in mammalian vestibular neurons (Kodama et al., 2020). We recorded spontaneous EPSCs in voltage clamp, at overall rates varying from 1 to 365 EPSC/s. Delivery of translational movement evoked corresponding modulations in EPSC frequency (Fig. 2.1B). The extent of modulation varied depending on the direction of the stimulus delivered across four different directions (Fig. 2.1C). In this example neuron, EPSC rate was modulated most strongly in the rostral-caudal (R-C) axis and weakly in the dorsal-ventral (D-V) axis, with intermediate strength responses for the diagonal directions (R/D-C/V and R/V-C/D).

Response to translational movement could derive from the vestibular or other sensory inputs. In larval zebrafish, the anterior otolith (utricle) is the sole functional vestibular sensor (Riley and Moorman, 2000). To examine whether utricular signaling is necessary for the observed tuning, we measured the sensory response of VS neurons in the *otog*$^{c.1522+2T>A}$ *-/-* (*rock solo*) animals, which lack the utricle (Mo et al., 2010, Roberts et al., 2017). Translational stimuli were ineffective at modulating EPSC rate in VS neurons of *rock solo* homozygotes, in contrast to wild-type/heterozygous siblings (representative examples, Fig. 2.1E). Across all recordings, VS neurons of *rock solo* -/- animals exhibit largely untuned EPSCs compared to siblings, as quantified by a tuning index (Fig. 2.1F). Thus, this approach reveals sensory-evoked synaptic responses encoding directional vestibular stimuli in identified VS neurons *in vivo*.

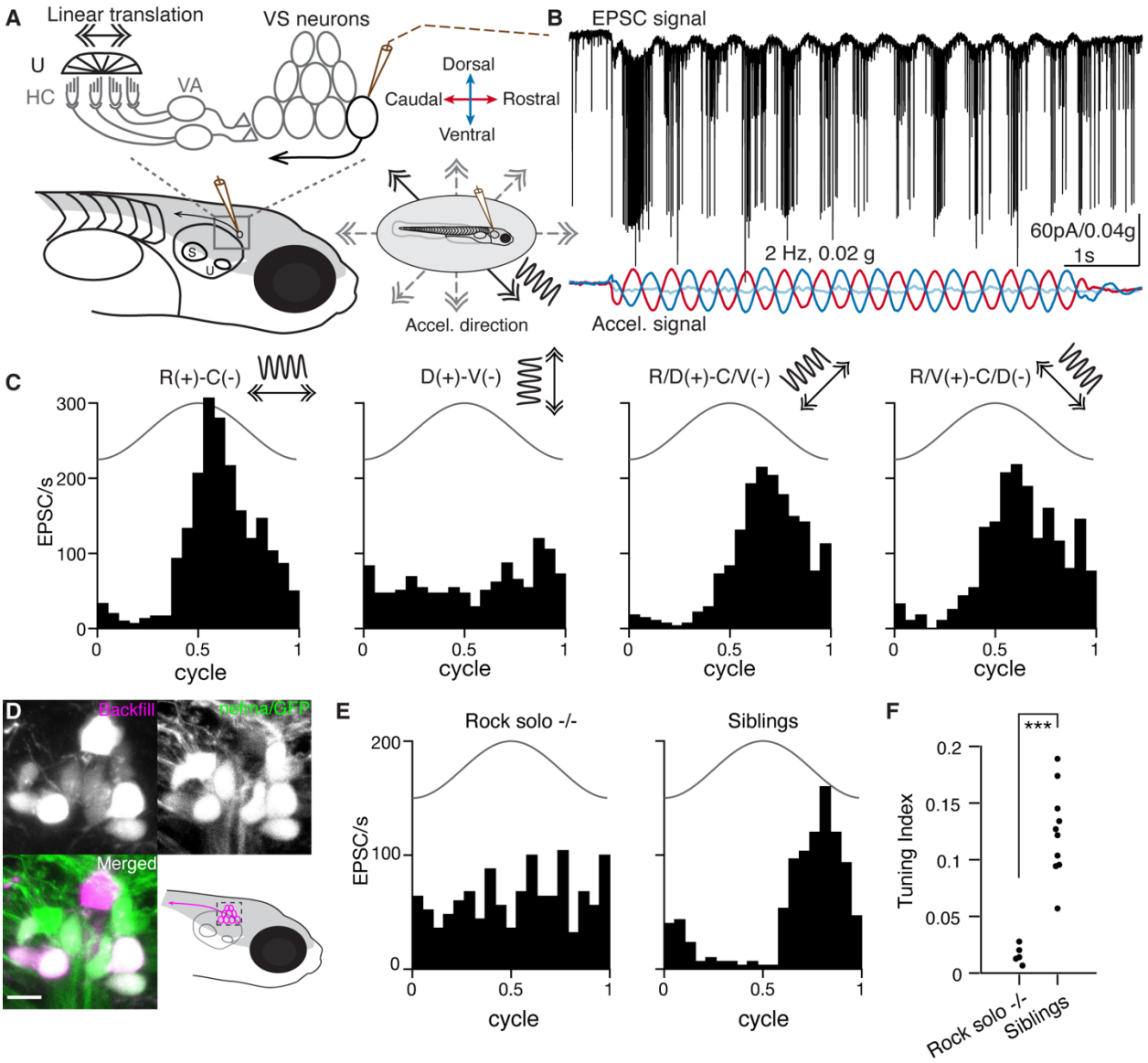

Figure 2. 1 Sensory-evoked responses in vivo in vestibulospinal (VS) neurons

A. Schematic representing *in vivo* patch clamp recording configuration and vestibular afferent circuit in larval zebrafish, U: utricle, HC: hair cells, VA: vestibular afferents, S: saccule. Inset, vestibular stimuli were delivered by a motorized table, acceleration direction indicated by the arrows and waveform by the sinusoidal curve. Solid, stimulus direction same as in B; dashed, other stimulus directions.

B. Example recording trace from a VS neuron in voltage clamp (V_{hold}: -65 mV) during 2 Hz, 0.02 g translational movement on the R/V(+)-C/D(-) axis. Membrane current and EPSC frequency are modulated by the translational movement. Black, EPSCs; colored, acceleration (same as in A) in three body axes recorded by an accelerometer (red, (R)ostral[+]-(C)audal[-]; dark blue, (D)orsal[+]-(V)entral[-]; light blue, (I)psilateral[+]-(C)ontralateral[-]).

C. Sensory-evoked EPSC responses to translation in four different directions for the same VS neuron as in B, across 12 cycles. Solid line, acceleration (2 Hz, 0.02 g).
D. Tg(nefma:gal4; UAS:GFP) (green) colabels VS neurons identified by dye backfilling (magenta) from spinal cord. Scale bar: 5 µm
E. Sensory responses of a VS neuron in the best direction in a rock solo -/- (left) and in a het/WT sibling (right).
F. Summary of tuning index in the best direction for all VS neurons recorded in rock solo -/- (9 neurons, 5 fish) and siblings (15 neurons, 10 fish). Mann-Whitney U test, p=6.7e-4

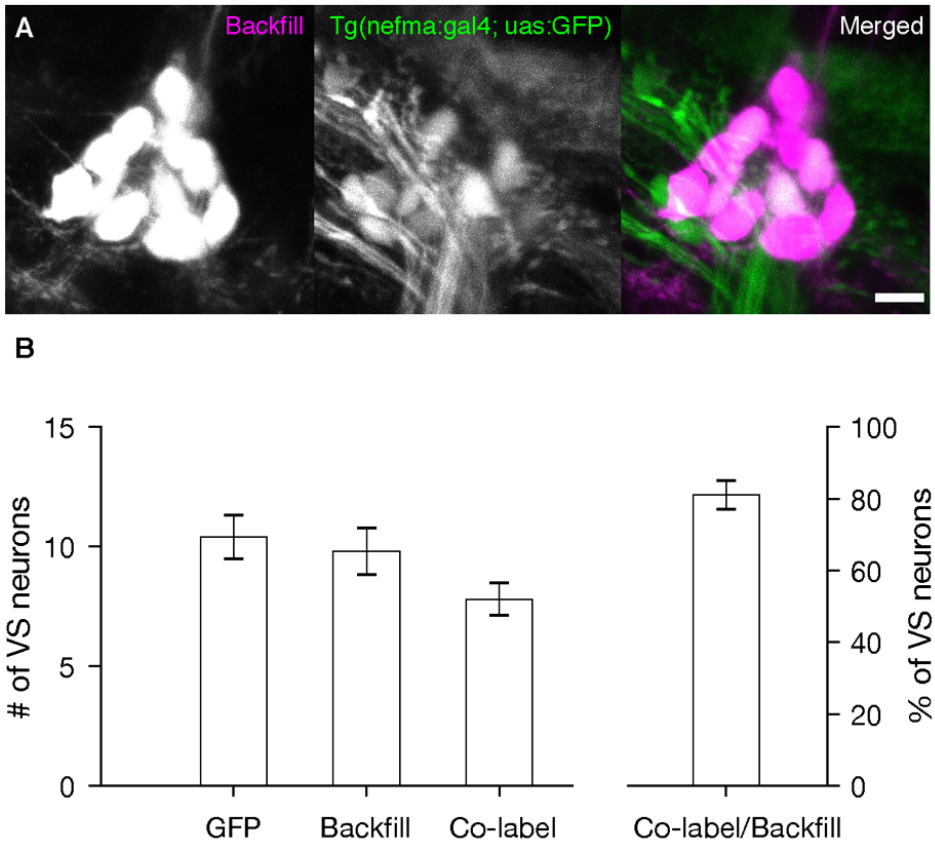

Figure 2. S 1

A. An example of labeled VS neurons by dye backfilling (magenta) from spinal cord in the Tg(nefma:gal4; uas:GFP) fishline. Scale bar: 5 µm
B. Number of labeled VS neurons (mean ± SEM) by GFP, by dye backfill from the spinal cord, and co-labeled with both on one side of the brain in the larval zebrafish (5-6 dpf). Right, percentage of VS neurons identified by backfill that are also expressing GFP.

Mixed electrical and chemical synapses mediate the transmission from otolith afferents to VS neurons

What properties define the vestibular afferent synapse onto VS neurons? In rodents, vestibular afferent synapses onto vestibulo-ocular reflex neurons exhibit amplitude-invariant synaptic transmission, mediated by specialized vesicular release machinery (Bagnall et al., 2008, McElvain et al., 2015, Turecek et al., 2017). To characterize afferent synaptic input to VS neurons, we electrically stimulated the vestibular (anterior statoacoustic) ganglion while recording from VS neurons in voltage clamp (Fig. 2.2A). Stimulation evoked a synaptic current with two components. The first component had fast kinetics with short latency (0.56 ± 0.28 ms, n=8), low jitter (0.05 ± 0.04 ms, n=8), and invariant EPSC amplitude (sd/mean: 6.7±3.9%, n=8) across trials. In contrast, the second component had slower kinetics with longer latency (2.3 ± 0.22 ms, n=5) and slightly higher jitter (0.15 ± 0.04 ms, n=5) than the early component, though still consistent with monosynaptic transmission (Wang and McLean, 2014). The second component also exhibited variable amplitudes (sd/mean: 60 ± 37%, n=4) (Fig. 2.2B). We dissected the two components of evoked EPSCs pharmacologically. Bath application of the gap junction blocker carbenoxolone (CBX, 500 μM) during afferent stimulation substantially reduced the first component of the EPSC, without abolishing the second component (Figs. 2C, E). In contrast, bath application of the AMPA receptor antagonist NBQX (10 μM) abolished the second component of synaptic current (Fig. 2.2D). Furthermore, the fast EPSCs were not reversed by changing the holding potential (Fig. S2.2), a signature behavior of electrical synaptic transmission (Akrouh and Kerschensteiner, 2013). Thus, the early and late components of afferent-evoked synaptic currents are mediated by gap junctions and AMPA receptors, respectively. Both EPSC components have low latency and jitter consistent with monosynaptic

transmission in larval zebrafish (Wang and McLean, 2014), and abrogating the early component with CBX does not affect the later component, suggesting these two components are mediated by mixed monosynaptic transmission from vestibular afferents to VS neurons. Across VS neurons, the NBQX-sensitive currents accounted for 27.1±20.2% of total charge transfer (n=7, Fig. 2.2F), demonstrating that gap junctional current is the dominant component mediating synaptic transmission.

To evaluate ultrastructural evidence for mixed synaptic transmission, we re-imaged existing serial ultrathin sections of a 5.5 dpf larval zebrafish (Hildebrand et al., 2017) at sufficiently high resolution (1-4 nm/px) to identify synaptic contacts between myelinated utricular afferents and VS neurons, identified anatomically. We found evidence for electrical transmission between utricular afferent axons and VS neurons in the form of tight junction structures, recognizable by the close apposition between pre- and post-synaptic membranes so that both membranes appear as one (Fig. 2.2G). Similarly, we identified utricular to VS chemical synapses based on the parallel adjoining membranes and vesicles clustered near a postsynaptic density (Fig. 2.2H). These data are consistent with anatomical evidence for mixed electrical / chemical transmission at this synapse in adult fish (Korn et al., 1977) and rat (Nagy et al., 2013). Together, these results demonstrate that VS neurons receive vestibular afferent inputs mediated by amplitude-invariant gap junctional (electrical) and variable amplitude glutamatergic (chemical) synapses.

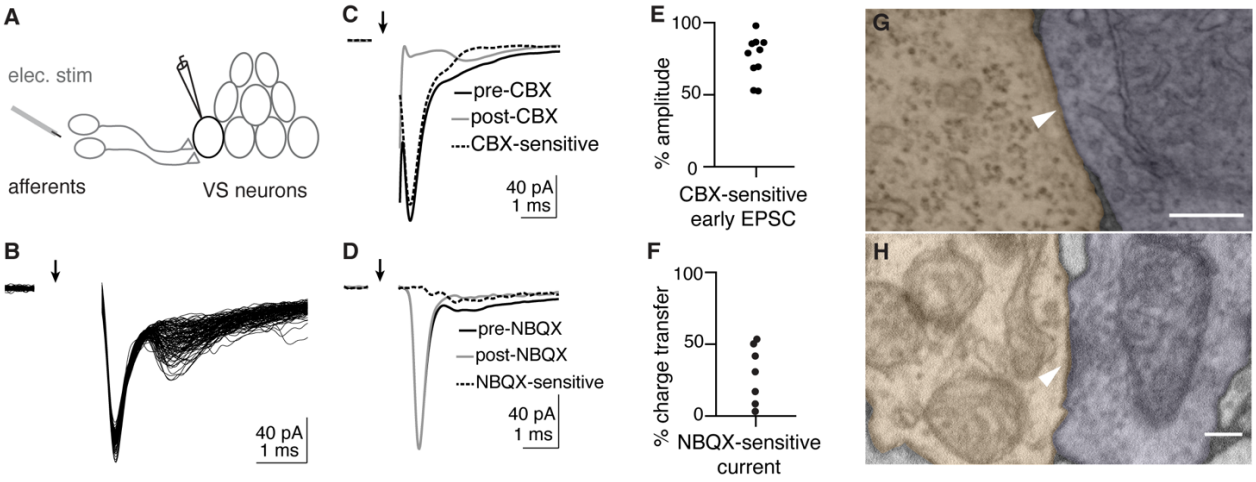

Figure 2. 2: Otolith afferent to VS neuron transmission is mediated by mixed electrical and chemical synapses

A. Schematic of whole-cell recording configuration from VS neuron while electrically stimulating otolith afferents.
B. Example EPSCs evoked by electrical stimulation of the otolith afferents; 105 EPSCs overlaid. Arrow indicates onset of stimulation. Stimulus artifact is blanked.
C. Carbenoxolone (CBX) diminishes the fast component of evoked EPSCs while slower component remains. Average traces from an example VS neuron; pre-CBX, n=100; post-CBX, n=100.
D. NBQX abolishes the second, slower component of evoked EPSCs without diminishing the early component. Pre-NBQX, n=349; post-NBQX, n=333.
E. Group data quantifying the reduction of early EPSC amplitude by CBX, n=10.
F. Group data quantifying the total charge transfer that is abolished by NBQX application, n=7.
G. Example EM image of gap junction between identified otolith afferent (pseudocolored purple) and VS neuron (peach), recognizable by the tight apposition of membranes to the exclusion of extracellular space,. Scale bar: 200 nm.
H. Example EM image of chemical synapse between otolith afferent (purple) and VS neuron (peach), characterized by the presence of synaptic vesicles, postsynaptic density, and parallel membranes at the cleft. Scale bar: 200 nm.

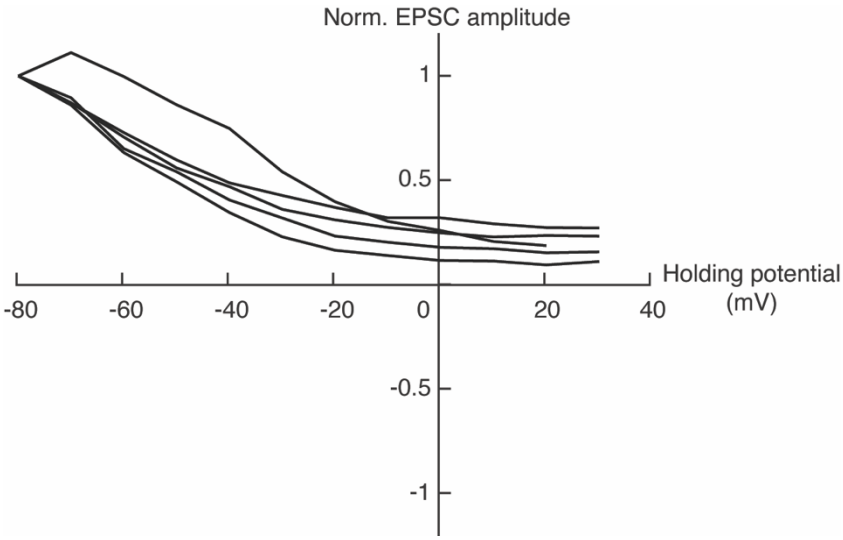

Figure 2. S 2

I-V relationship for the early EPSC component evoked by electrical stimulation on otolith afferents, normalized to EPSC amplitude at -80 mV, n=5. Note that early EPSCs do not reverse at 0 mV, consistent with electrical identity. The late EPSC (chemical) component was typically too small to measure at higher holding potential, but in some instances could be seen to reverse [data not shown], consistent with chemical identity.

Inferring afferent tuning from distinct EPSCs

Because electrically mediated EPSCs from afferents to VS neurons exhibited a fixed amplitude, we hypothesized that we could distinguish the activity of individual otolith afferents converging onto a given VS neuron by their characteristic EPSC amplitudes. Indeed, spontaneous and sensory-evoked EPSCs recorded in VS neurons often fell into distinctive size bins, as visualized in a histogram of EPSC amplitudes (Figs. 3A, B). EPSCs were sorted into three clusters with unsupervised learning (see Methods), primarily leveraging their amplitudes. Each of these EPSC clusters showed a stereotypical amplitude and waveform in this example neuron (Fig. 2.3A, inset). To test whether each cluster of EPSCs amplitudes corresponds to an individual afferent, we used an approach derived from spike sorting: temporal autocorrelation to test for refractory

periods within EPSC event times. Physiologically, one afferent cannot generate two action potentials within its refractory period (Fernandez et al., 1972); thus the EPSCs elicited by that afferent should exhibit a refractory period. The auto-correlogram of EPSCs showed the average activity of other EPSCs relative to the timepoint of the reference EPSC anchored at 0 ms (Fig. 2.3C). In this example neuron, an auto-correlogram of all EPSC event times did not show any structure around 0 ms (Fig. 2.3C, top). In contrast, an auto-correlogram within each EPSC cluster exhibited a gap in event intervals around 0 ms, suggesting a clear refractory period (Fig. 2.3C, bottom). This result was not due to limitations in event identification at brief intervals, because the fast kinetics of these EPSCs allowed us to distinguish events as close together as 0.2 ms, as seen in the all-event autocorrelogram (top), and this is much shorter than the typical refractory period (see Methods). Furthermore, cross-correlograms between EPSC clusters did not show this structure, consistent with the notion that they arise from independent inputs (Fig. 2.S3). Accordingly, we can interpret these three EPSC clusters as deriving from the activity of three distinct presynaptic afferents (Fig. 2.3D, left). Because of the high fidelity of electrical transmission, each EPSC cluster effectively reads out the spiking of an individual afferent, allowing us to measure presynaptic activity via postsynaptic recording (Fig. 2.3D, right).

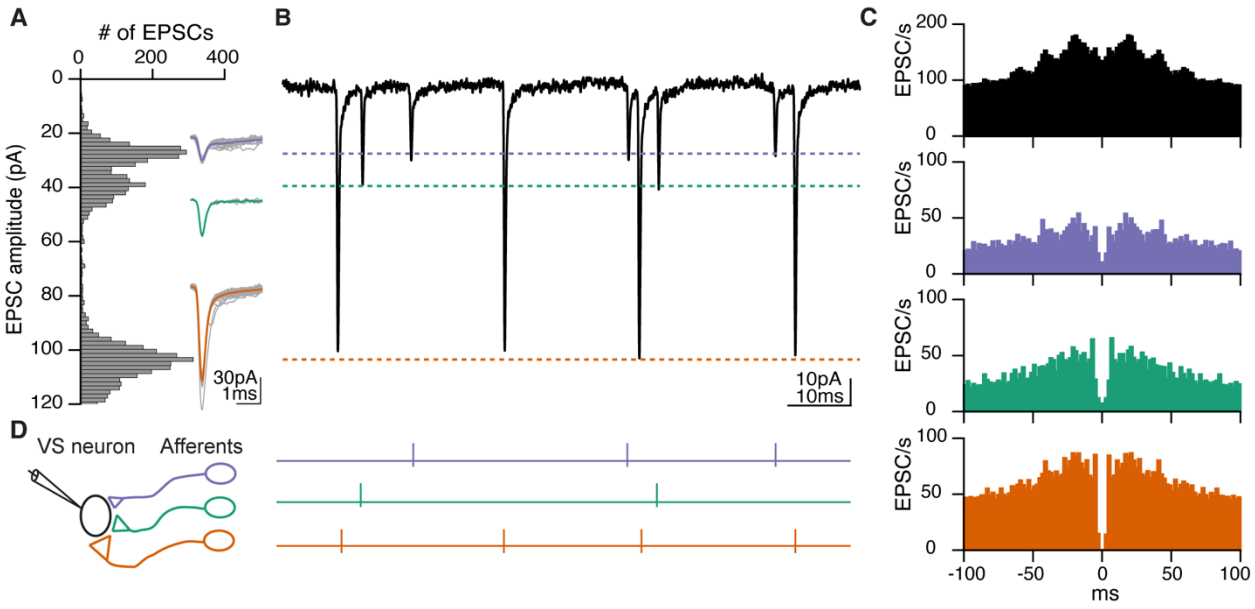

Figure 2. 3: Distinct EPSC amplitudes reflect individual afferent inputs

A. Histogram of spontaneous and sensory-evoked EPSC amplitude distribution of the same VS neuron as Fig. 2.1B. Inset, overlay of individual EPSCs (gray) and average (colored) for each amplitude bin.
B. Example trace of EPSCs exhibiting stereotypic shapes and amplitudes in three clusters, corresponding to each amplitude bin in A.
C. Auto-correlogram of all EPSCs recorded from the VS neuron (top, black) or divided into three clusters based on EPSC amplitudes (bottom, colored). Note EPSC activities around 0 ms only appears across all EPSCs, but not within each cluster.
D. Schematic of three different otolith afferents converging onto one VS neuron, each eliciting EPSCs with a distinct amplitude (represented by different synaptic sizes). Right, spike activities of three afferents inferred from B.

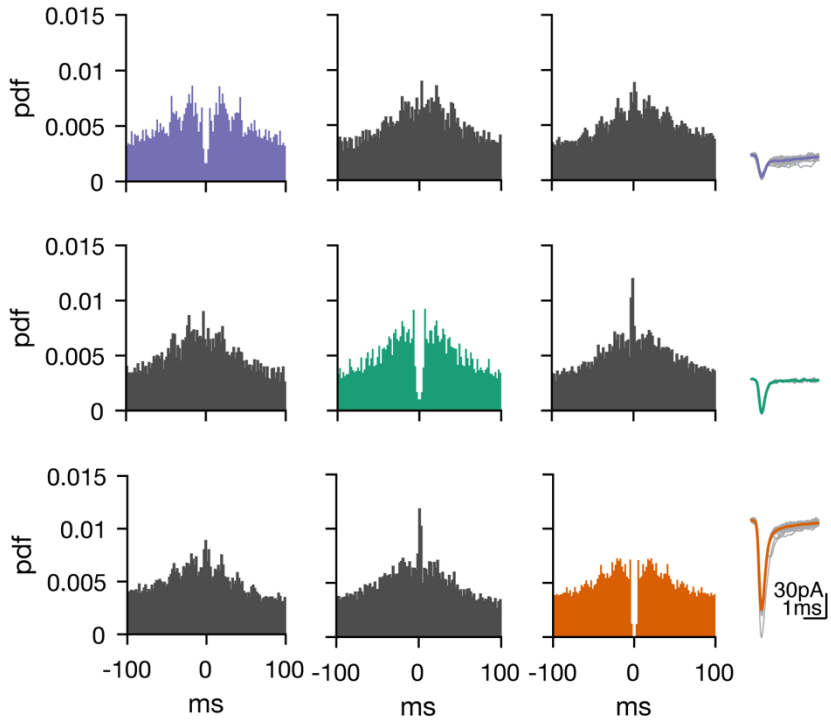

Figure 2. S 3

Auto- and cross-correlograms of three distinct EPSC clusters in one VS neuron. Note that refractory periods only appear in auto-correlograms (colored panels), not in cross-correlograms (gray).

To test this interpretation of electrophysiological data with a completely independent approach, we reconstructed the whole volume of myelinated utricular inputs onto 11 VS neurons from a high-resolution re-imaged serial-section electron microscopy (EM) dataset acquired from the right side of one 5.5 dpf larval zebrafish (Fig. 2.4A, B). We found that the connection between myelinated utricular afferents and VS neurons was relatively sparse. All VS neurons were contacted by at least two utricular afferents, but some afferents did not innervate any VS neurons (Fig. 2.4C). These reconstructions showed that a range of 2-6 afferents (mean±std: 3.4±1.4) converged onto each VS neuron (Fig. 2.4D). We compared these numbers to those derived from whole-cell physiology, where we inferred the number of convergent afferents from

the number of EPSC clusters. Across all VS neuron recordings, we found a range of 0-5 afferents (1.7±1.3) converged onto each VS neuron (Fig. 2.4E). The smaller number of afferents deduced from physiological recordings is likely because small-amplitude EPSCs were often not successfully clustered, or did exhibit refractory-period structure in autocorrelogram, suggesting they are elicited by multiple sources. Nonetheless, the result from anatomical reconstruction is largely consistent with the overall distribution of afferent contacts as measured by whole-cell physiology. Therefore, these results demonstrate that synaptic inputs from individual vestibular afferents can be separated by their stereotypic EPSC waveforms, yielding inferred afferent convergence consistent with high-resolution anatomical connectivity.

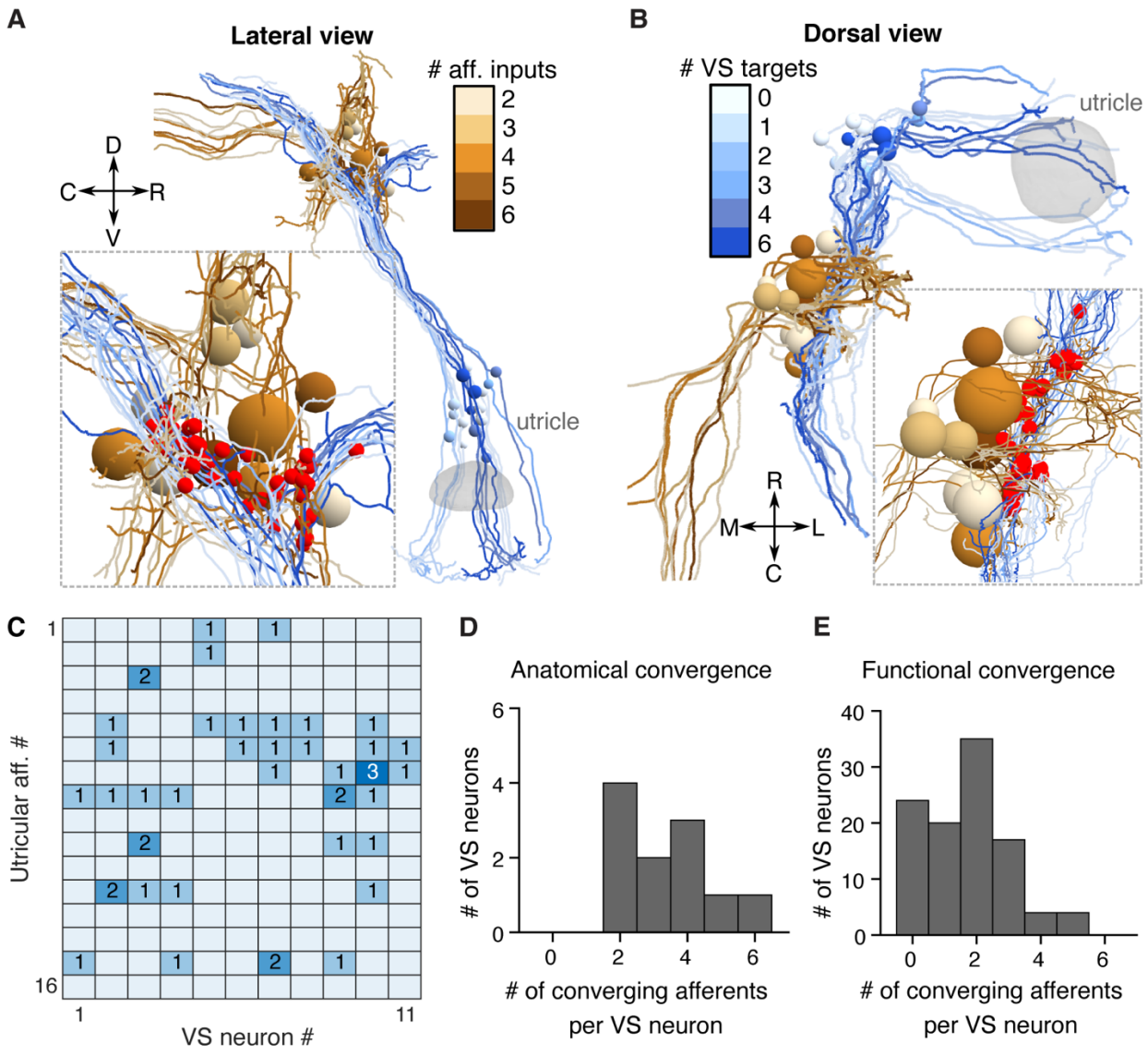

Figure 2. 4: Anatomical reconstructions reveal a similar convergence pattern as physiology

A. Serial-section EM reconstruction (lateral view) of all myelinated utricular afferents (blues) and VS neurons (browns) on the right side of one animal (5.5 dpf). Inset, identified synaptic contacts between afferents and VS neurons (red). Color scale represents number of distinct afferents synapsing with a given VS neuron (browns). VS neurons with greater number of afferent inputs are located more ventrally.
B. Dorsal view of the same reconstruction as in A. Color scale represents number of VS neurons contacted by a given afferent (blues).
C. Number of distinct synaptic contacts from each utricular afferent onto each VS neuron, based on serial-section EM reconstruction.
D. Histogram of the numbers of distinct afferents converging onto each VS neuron, as measured by serial-section EM reconstruction (11 neurons, 1 fish)

E. Histogram of the numbers of distinct afferents converging onto each VS neuron, as inferred from whole-cell physiology recording (104 neurons, 89 fish)

Spatial tuning of inferred otolith afferents

By recording from one VS neuron, we can infer the activity of its presynaptic afferents. This approach thus offers a unique opportunity to measure the sensory tuning of several convergent afferents simultaneously. To determine the spatial tuning of convergent afferent inputs, we delivered 2 Hz, $\pm$0.02 g sinusoidal translational stimuli on four directions in the horizontal plane and recorded the sensory-evoked EPSCs, as shown for an example VS neuron (Fig. 2.5A). In this example neuron, the inferred utricular afferent (EPSC cluster) with the largest synaptic amplitude responded best to caudally directed acceleration, while two others responded with varying sensitivities to rostrally directed acceleration. All cells had phase leads relative to peak acceleration (Fig. 2.5B). With these measurements, we can derive the preferred tuning direction, gain and phase of each afferent, as represented by the direction and length of a vector (Fig. 2.5B, right). To validate the consistency of the vectorial representation, we used a previously established approach (Schor et al., 1984a) to quantify the tuning vectors with separately measured responses to two circular stimuli (Fig. 2.S4 B), which showed similar preferred directions as those measured by translational stimuli (Figs. 2.S4 A-C). Across all recordings with the animal oriented side-up, tuning of afferents was strong in the rostral (30/69) and caudal (31/69) directions, but relatively weak in the dorsal (4/69) and ventral (4/69) directions, as represented by an overlay of all inferred afferent tuning vectors (Fig. 2.5C). When fish were oriented dorsal-up, the axes tested were rostral-caudal and ipsilateral-contralateral (motion along an axis from one ear to the other; ipsilateral indicates acceleration towards the side where the recorded neuron is located). In this position, most afferents were strongly tuned to acceleration

towards the contralateral direction (31/60), some exhibited preferential tuning to the acceleration to the rostral (4/60) and caudal (20/60) directions, and only 5/60 afferents were tuned to the ipsilateral direction (Fig. 2.5D). The decrease in proportion of afferents responsive to rostral translation as compared measured in the side-lying recording is likely due to the suppression of hair cells in the side-lying animal, which may have caused fewer afferents to be active. Overall, these results showed that each afferent in the larval zebrafish exhibits selective responses to different translational stimuli. Afferents overall responded best to acceleration towards the contralateral, rostral, and caudal directions, which correspond to ipsilateral, nose-up and nose-down tilts in postural change (Angelaki and Cullen, 2008), consistent with the distribution of hair cell polarity in the utricular macula (Haddon et al., 1999).

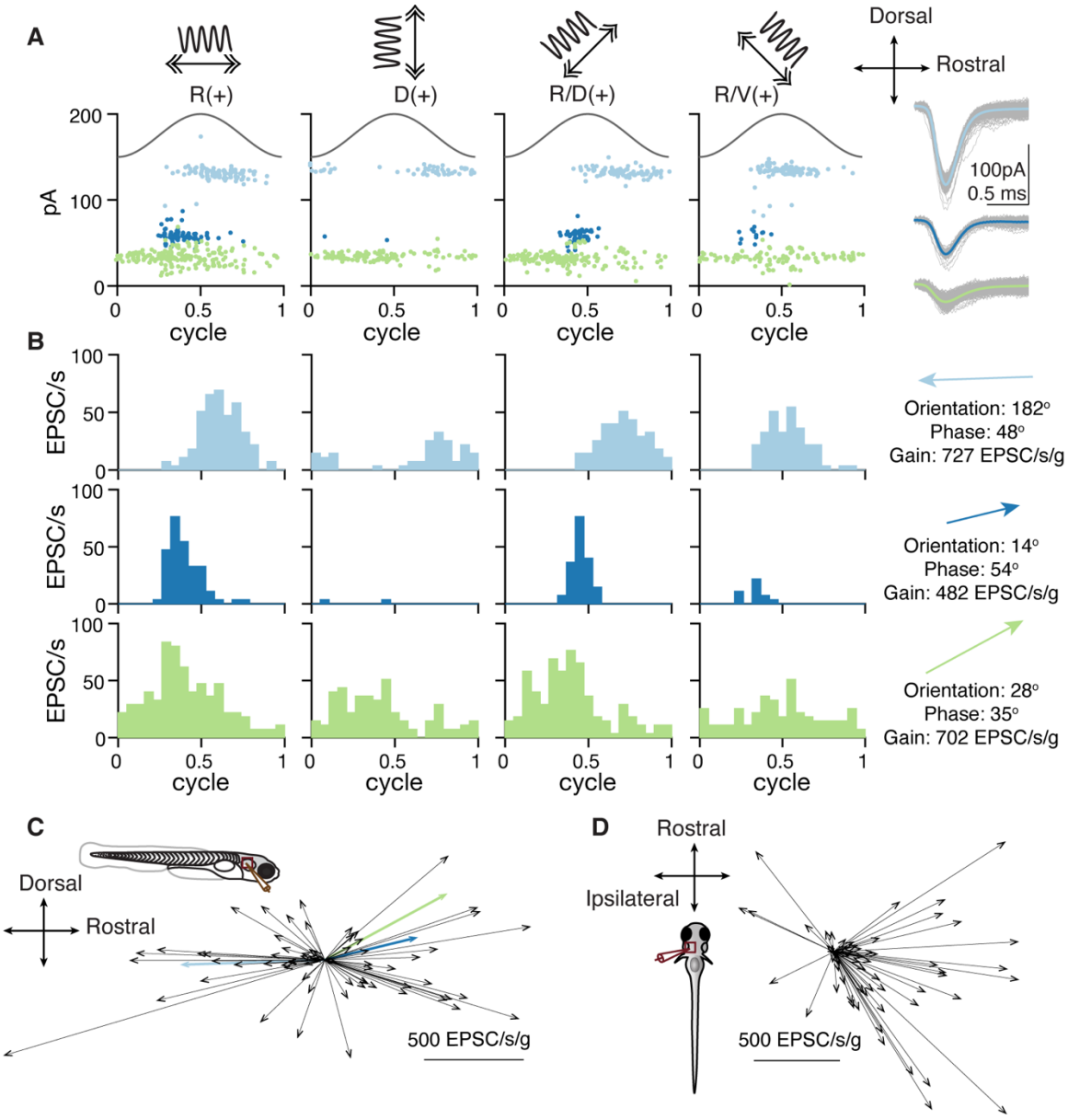

Figure 2. 5: Spatial tuning of inferred otolith afferents

A. EPSC responses of an example neuron in response to 2 Hz, 0.02 g translational stimuli (solid sinusoidal line, acceleration) along 4 different axes (top, arrows). Each dot represents one EPSC; note three EPSC clusters with distinct amplitudes. Right, overlay of individual EPSCs (gray) and average (colored) for each cluster.
B. EPSC tuning of three clusters. Right, vectors representing the maximum tuning direction, phase, and gain of each inferred afferent corresponding to an EPSC cluster.
C. Maximum tuning directions of all afferents from VS neurons recorded from fish oriented side-up. Colored arrows represent tuning of afferents in B (69 afferents, 43 neurons, 33 fish).
D. Maximum tuning directions of all inferred afferents from VS neurons recorded from fish oriented dorsal-up (60 afferents, 36 neurons, 36 fish).

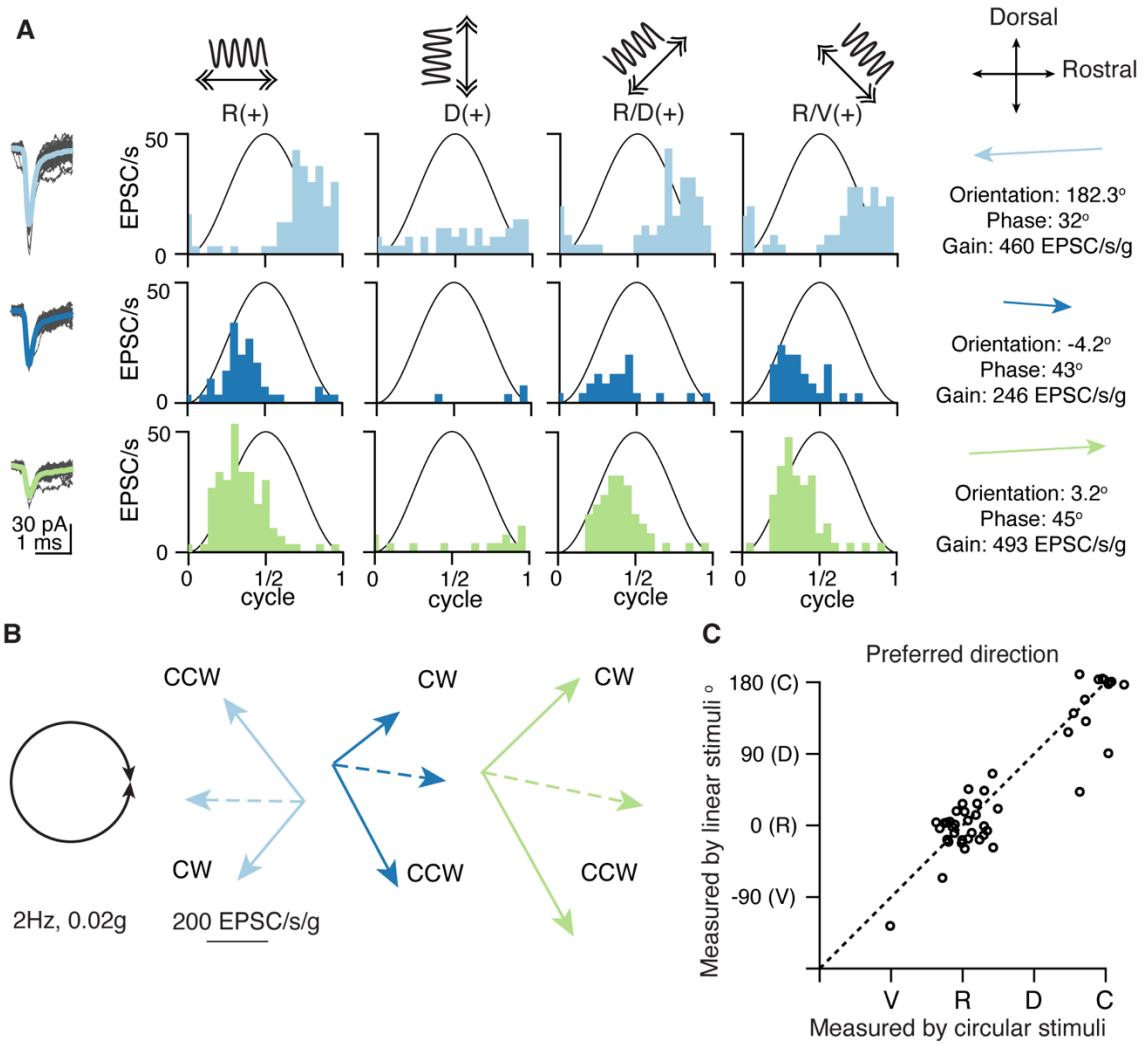

Figure 2. S 4

A. Response vectors of the three afferents converging onto one VS neuron, quantified in the same way as Fig. 2.5B

B. Response vectors of the same three afferents, measured with clockwise (CW) and counterclockwise (CCW) circular stimuli (left). Solid vectors represent the measured response with CW and CCW stimuli. The dashed vectors represent the vector sums, an estimate of the preferred tuning direction and gain as measured by circular stimuli.

C. Preferred tuning direction measured with 4-axis linear stimuli was highly correlated to preferred tuning direction measured with circular stimuli across the population of inferred otolith afferents (n=46). Dashed: unity line; R=0.92, p=5e-20.

Temporal tuning of inferred otolith afferents

The sensitivity and phase of vestibular afferents varies for motion at different frequencies (Fernandez and Goldberg, 1976b). The otolith afferents ranges from typically more jerk-tuned (tuned to the derivative of acceleration) at low frequencies to more acceleration-tuned at high frequencies. What temporal tuning profile do afferents in larval zebrafish exhibit? We applied translational stimuli with different frequencies (0.5-8 Hz, ±0.02 g) on the R-C axis. In one example neuron, all three inferred otolith afferents showed similar tuning, with progressively stronger responses to increasing frequencies of stimulation (Fig. 2.6A). Across group data, the average tuning gain in response to stimuli from 0.5 Hz to 8 Hz increased 3.3-fold (measured with stimulus amplitude 0.02 g) or 2.3-fold (measured at 0.06 g) (Fig. 2.6B). Most afferents (39/48) showed at least a 2-fold increase from 0.5 Hz to 4 Hz in tuning gain at either 0.02 g or 0.06 g. Only one afferent had relatively flat gain (< 50% increase) at both 0.02 g and 0.06 g, and its tuning was overall weak (mean gain: 1.88 and 2.24 EPSC/s respectively), suggesting it was less sensitive or not tuned on the R-C axis. Regardless of tuning direction (rostral: 44%, 21/48; caudal: 56%, 27/48), afferents exhibited a phase lead relative to peak acceleration at various tested stimulus magnitudes and frequencies (Fig. 2.6C, 2.S5A). On average, the phase lead at low frequency (0.5 Hz) was 84.0° for 0.02 g and 78.6° for 0.06 g. In other words, the peak response was almost 90° prior to peak acceleration, and therefore best described as encoding jerk at low frequencies. At high frequency (8 Hz), the phase lead was reduced to 33.6° for 0.02 g and 39.3° for 0.06 g, partway between the peaks of jerk and acceleration. The temporal dynamics of the afferents resembled those of previously reported irregular units (Goldberg et al., 1990), with low spontaneous firing rates (10.28±9.1 EPSC/s) and larger coefficients of variation (CV). The average CV across inferred afferents was 0.97±0.24, and the smallest CV was 0.5 (Fig. 2.S5B),

indicating that no regular-firing otolith afferents were detected synapsing onto VS neurons. We conclude that the otolith afferents act as a high-pass filter, encoding a mixture of acceleration and jerk, similar to irregular otolith afferents in primates (Laurens et al., 2017, Jamali et al., 2013).

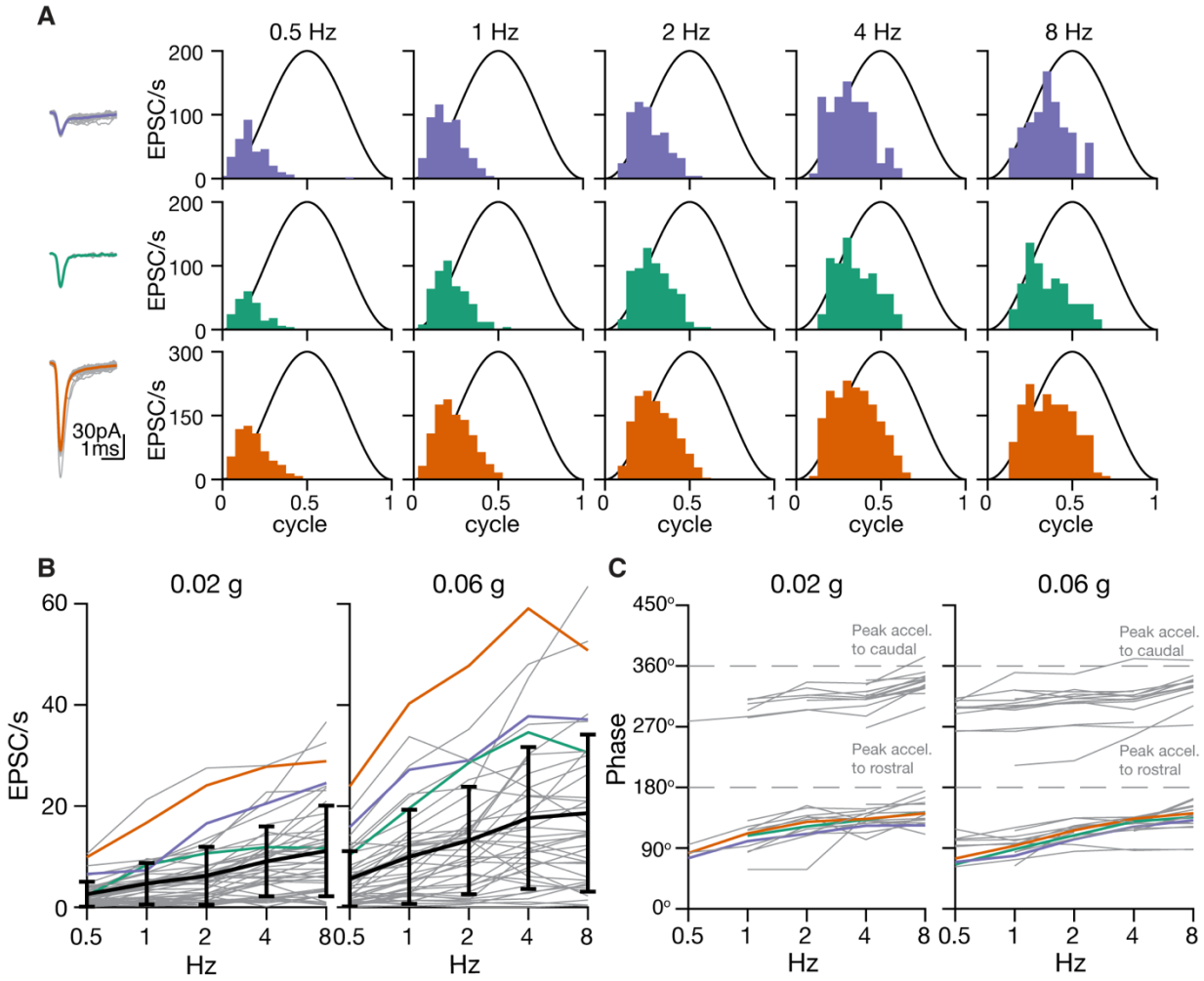

Figure 2. 6: Temporal tuning of inferred otolith afferents

A. Sensory tuning of afferent inputs to one VS neuron during translational movement at 5 different frequencies in the R(+)-C(-) axis. Left, EPSC waveforms of three different clusters recorded from one VS neuron. Right, temporal tuning profile of each EPSC cluster on the R-C axis.
B. Gains of inferred afferents across different frequencies of translational acceleration. Gray, individual afferents; colored, afferents from A; black, mean and standard deviation of gains from all afferents (0.02 g, 48 afferents; 0.06 g: 46 afferents; 25 neurons, 20 fish)

C. Phases of inferred afferents across frequencies, relative to the sinusoidal stimulus. 180° (0.5 cycle in A) represents the peak of acceleration towards rostral direction; 360° represents the peak of acceleration towards caudal direction (0 or 1 cycle in A). Data were thresholded to only include afferents whose gain was > 5 EPSC/s (0.02 g, 36 afferents; 0.06 g, 38 afferents; 25 neurons, 20 fish)

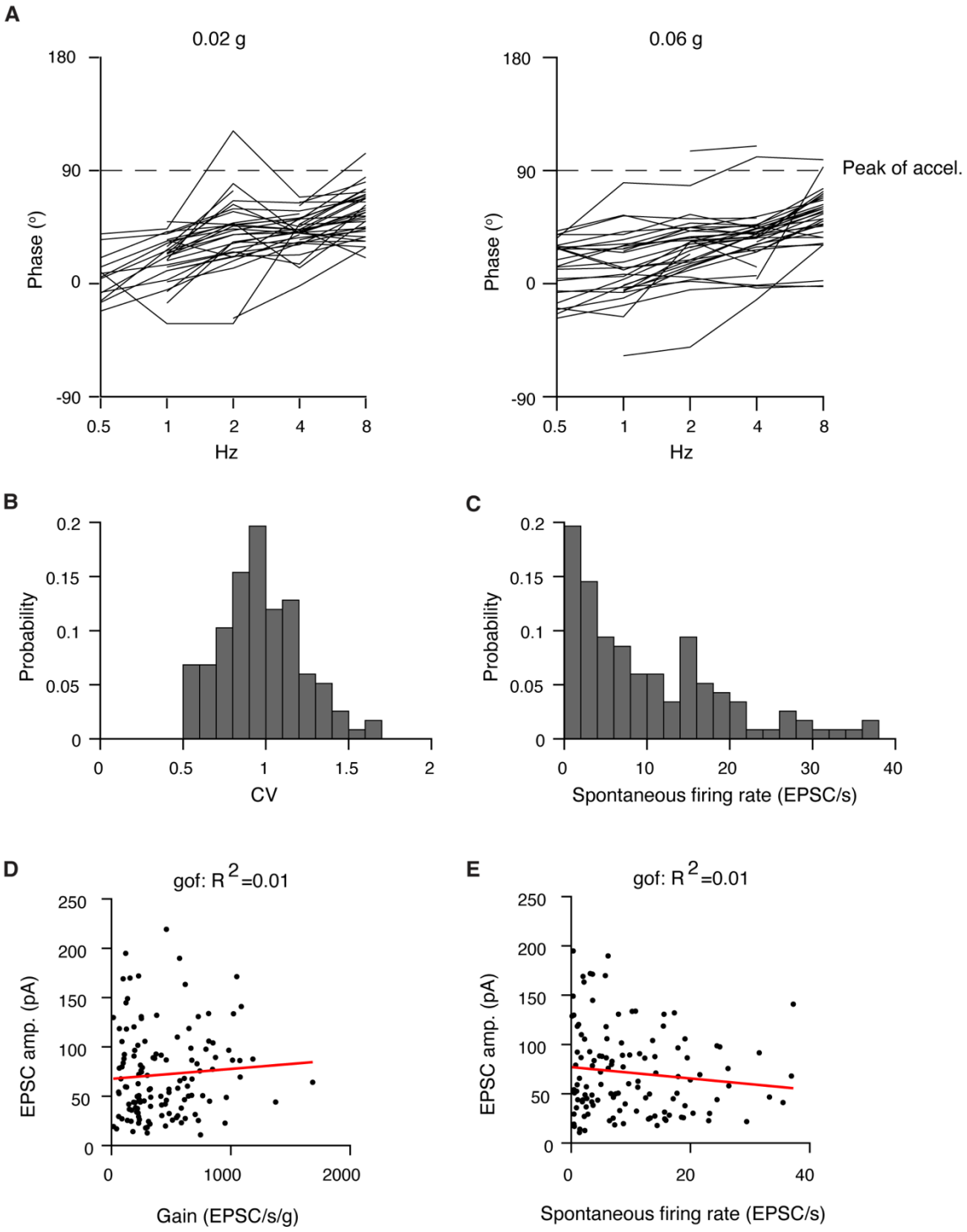

Figure 2. S 5

A. Phase lead relative to peak of acceleration (left, 0.02 g; right, 0.06 g) for all otolith afferents combined. Dashed line indicates peak of acceleration towards preferred direction (either rostral or caudal).
B. Coefficient of variations for spiking of the inferred otolith afferents in the larval zebrafish (n=117).
C. Spontaneous firing rate of inferred otolith afferents in the larval zebrafish. (n=117)
D. No correlation between tuning gain and EPSC amplitudes of inferred afferents (n=129), red: linear fit, gof: goodness of fit.
E. No correlation between spontaneous firing rate and EPSC amplitudes of inferred afferents (n=120), red: linear fit, gof: goodness of fit.

Preferential convergence

Individual VS neurons can receive inputs from afferents with similar (Fig. 2.6A) or different tuning (Fig. 2.5B). Is afferent tuning convergence random or structured? To answer this question, we compared the sensory responses of inferred afferents to 0.02 g, 2 Hz translational stimuli, using their tuning vectors quantified in the analysis of preferred spatial directions (Fig. 2.7A). The angle between the vectors indicates the similarity of convergent inputs, with a small angle (<45°) for a VS neuron with similarly tuned inputs and a large angle (>135°) for a VS neuron with differently tuned inputs. From 43 VS neurons recorded in the side-up orientation, 60% (38/63) of converging afferent pairs had small angles and 27% (17/63) had large angles. Compared to a random pairing angle distribution generated by bootstrapping, the percentage of similarly tuned convergent afferent pairs was significantly higher than chance (Fig. 2.7B, left). From 36 VS neurons recorded in the dorsal-up orientation, there were 71% (37/52) of inferred converging afferent pairs with small angles, and only 2% (1/52) with large angles due to the small number of ipsilaterally tuned afferents (Fig. 2.5D). Nonetheless, the probability of similarly tuned afferent convergence for small converging angles was significantly higher than chance (Fig. 2.7B, right). For afferent pairs with a large converging angle (45°-90°, 90°-135°,

135°-180°), their probabilities were slightly lower than the respective estimated distributions by bootstrapping. Accordingly, along a given body axis (R-C or I-C), convergent afferents are also more likely to encode similar tuning directions (Fig. 2.7C). These results suggest that afferents with similar tuning direction preferentially converge at rates exceeding what would be expected by random connectivity.

Do converging afferents also have similar tuning phase regardless of their tuning direction? Most afferents are phase-leading with 2 Hz, 0.02 g stimulation (Figs. 2.6 and 2.7D, inset), and the phase difference between afferents is small (R-C: 41° ±16°, n=177, I-C: 33° ±17°, n=60). Consequently, most afferent pairs (R-C: 68±4.6%; I-C: 68±8%) selected randomly have very small phase difference (phase diff. < 22.5°) (Fig. 2.7D). Both the probability of converging afferents having similar phase (phase diff. < 22.5°) (R-C, 73%, 75/103; I-C, 59%, 20/34) and the cumulative distribution (Fig. 2.S6) lay within the bootstrap predications on the R-C and I-C axes. Therefore, tuning phase between converging afferent pairs is similar, in accordance with their relatively homogeneous distribution.

In conclusion, we found that afferents forming synaptic connections with the same postsynaptic VS partner typically have similar spatial tuning properties. In particular, afferents with similar tuning direction preferentially converge, which may explain the long-standing observation that most VS neurons exhibit simple cosine tuning (Peterson, 1970b, Schor et al., 1984a). However, a non-negligible number of VS neurons receive convergent input from differently tuned afferents, providing a potential source for the complex spatiotemporal tuning of central vestibular neurons.

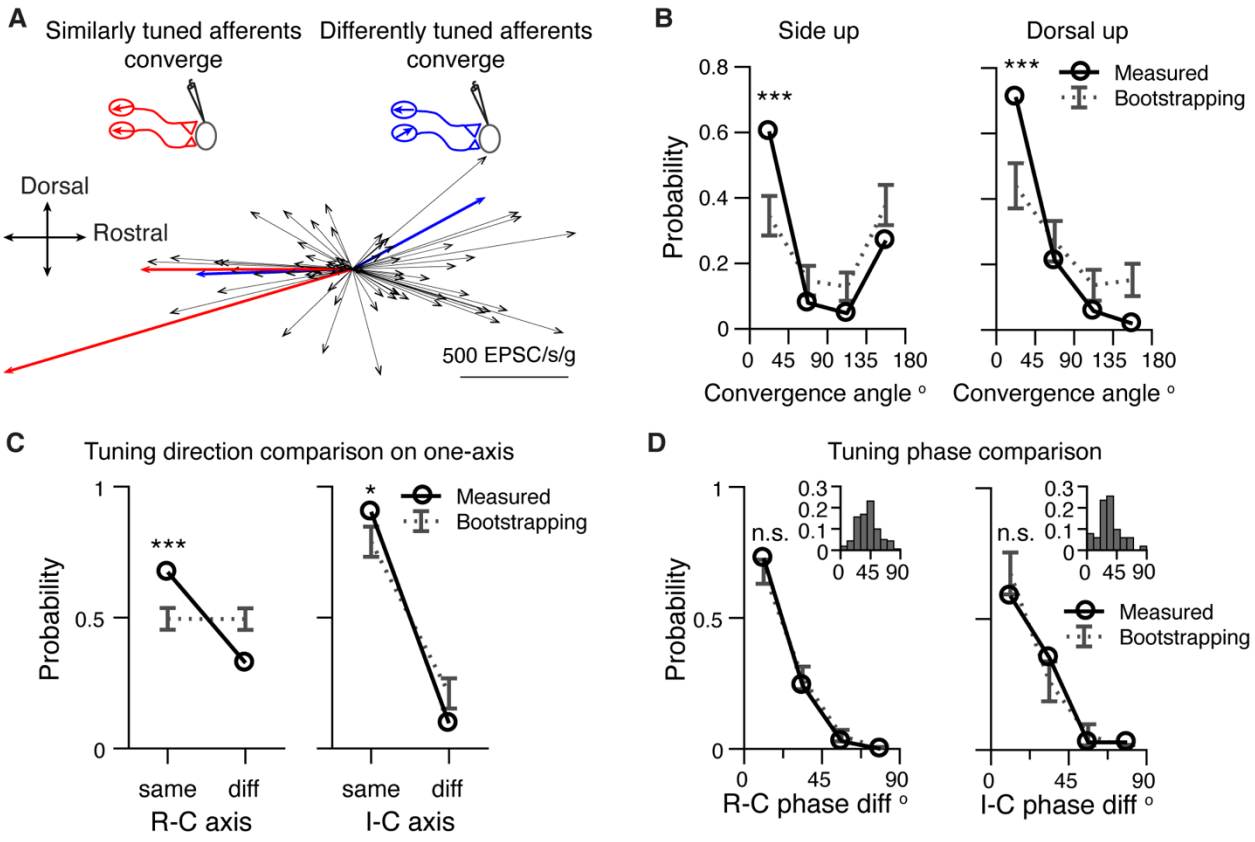

Figure 2. 7: Afferents with similar tuning direction preferentially converge

A. Example of two pairs of converging afferents from two VS neurons in side-up fish. Red, converging afferents are similarly tuned, with small converging angle between the pair; Blue: converging afferents are differently tuned, with large convergent angle between the pair.
B. Probability distribution of converging angles for measured and randomly generated afferents pairs in side-up fish and dorsal-up fish. Two tailed z-test, side up, 0-45°: p=2e-5, 135-180°: p=0.08. (63 afferent pairs); dorsal up, 0-45°: p=8e-5, 135-180°: p=0.007. (52 afferent pairs)
C. Probability distribution of converging afferents tuned to the same direction vs different direction, on the R-C and I-C axis. Two tailed z-test, R-C, same: p=1e-5, diff: p=4e-5 (150 afferent pairs); I-C, same: p=0.044, diff: p=0.044 (52 afferent pairs).
D. Probability distribution of phase difference for converging afferents, on the R-C and I-C axis. Two tailed z-test, R-C, 0-22.5° p=0.26 (103 afferent pairs); I-C, 0-22.5°, p=0.28 (34 afferent pairs). Inset: distribution of tuning phase of afferents, R-C, 177 afferents; I-C, 60 afferents; 90° represents the peak of acceleration of preferred direction (2 Hz, 0.02 g).

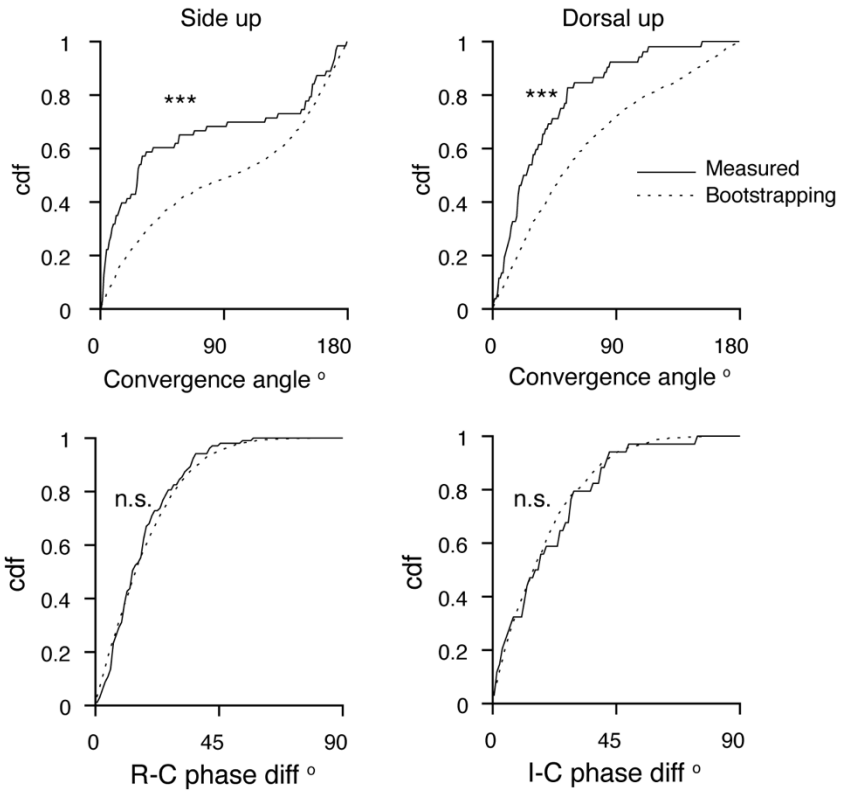

Figure 2. S 6

Cumulative distribution function of convergence angle and phase difference, in measured (solid) and randomly generated (dashed) afferent pairs. Kolmogorov-Smirnov test, p = 1.3e-5 (convergence angle, side up), 3.5e-5 (convergence angle, dorsal up), 0.46 (R-C phase difference), 0.65 (I-C phase difference)

Complex central tuning arises from divergent afferent inputs

Complex sensory tuning of central neurons is thought to arise from convergence of more simply tuned inputs with differing spatial and temporal properties in vestibular (Angelaki et al., 1993), visual (Jia et al., 2010), and somatosensory (Petersen, 2007, Roy et al., 2011) systems. For example, complex tuning such as bidirectional (Peterson, 1970b) and broadly tuned sensory responses (Angelaki, 1992) of central vestibular neurons can be computationally reconstructed from multiple modelled cosine-tuned inputs. However, directly measuring these inputs has been

technically difficult, and it is unclear whether such models can sufficiently explain the activity of central neurons. Therefore, we took advantage of the inferred afferent spiking to examine whether the tuning of VS neurons can be constructed from the convergence of otolith afferents.

During sensory stimulation, most VS neurons showed simple membrane potential responses to translational stimuli, with depolarization or spiking during only one phase of acceleration (Fig. 2.8A, top, and Supplemental Video S3). In contrast, some VS neurons exhibited multiple depolarized periods during each stimulation cycle, resulting in a complex response. In both subthreshold and spiking VS neurons depolarization or spiking exhibited two peaks per stimulus cycle (Fig. 2.8A, bottom). To examine how spiking responses are generated from afferent inputs, we measured the EPSC tuning in the same VS neurons. In the VS neuron with simple spiking responses (raster, top), sensory evoked EPSCs exhibit three distinct amplitudes (Fig. 2.8B, top), indicating that three afferents converge onto the cell. These three afferents showed similar tuning to each other, with the strongest responses for rostrally directed acceleration, consistent with the simple spike tuning. In contrast, the four inferred afferents that converge onto an example complex cell exhibited a different tuning pattern (Fig. 2.8B, bottom). Two afferents were tuned to rostrally directed acceleration and the other two to caudally directed acceleration, consistent with the bidirectional spike tuning. Some VS neurons (37/71) did not spike spontaneously or during the largest sensory stimulation we could deliver while holding the cell. Therefore, we injected a small bias current to evoke spiking in a subset of VS neurons (15/27, see Methods). Membrane potential was shifted by the bias current but its relationship to sensory stimulation was largely unaffected by this manipulation (Fig. 2.S8A), though this may not be the same response as would be seen with larger sensory stimuli. Both unidirectional and bidirectional responses were observed VS neurons, regardless of whether they were exhibiting

spontaneous or current-induced spiking. To investigate the relationship between convergent afferent tuning and VS responses, we ranked the spiking responses of VS neurons based on the similarity of EPSC inputs. The similarity index ranges from 0-1, with smaller values representing more divergent EPSC input tuning and larger value representing more similar tuning (see Methods). The spiking responses of all VS neurons is represented in a heatmap in Fig. 2.8C, with cells ordered from most similar tuning to least similar tuning. The example cells shown in Fig. 2.8B have input similarity indices of 0.45 and 0.12, respectively (Fig. 2.8C, red asterisks). VS neurons with more similar EPSC inputs (Fig. 2.8C, top) typically have more simple postsynaptic spiking responses, with action potentials occurring in just one phase of the stimulus cycle. In contrast, VS neurons with more divergent EPSC inputs (Fig. 2.8C, bottom) show more complex postsynaptic spiking responses, with action potentials at two phases of the stimulus cycle.

To quantify this relationship across the population, we compared the afferent inputs similarity with the tuning complexity of each VS neuron. The inputs similarity index is defined by the phase of afferent inputs and their EPSC amplitudes, and the tuning complexity index used the original classifier developed in visual cortical neurons to quantify the complexity of the postsynaptic neuron's membrane potential or spiking responses (Skottun et al., 1991). In this metric, neurons with simple tuning show large AC and small DC spiking responses, whereas cells with more complex (multi-phasic) activity exhibit small AC and large DC spiking responses. We found that for both subthreshold (Fig. 2.8D) and spike (Fig. 2.8E) tuning, the AC/DC ratio was positively correlated with the similarity index of afferent inputs. In other words, convergence of more similarly tuned afferents yields a more simple postsynaptic tuning, and the convergence of more differently tuned afferents generates a more complex postsynaptic tuning. Thus, the properties of converging afferents are directly linked to postsynaptic tuning,

with bidirectionally sensitive neurons derived from summation of oppositely tuned inputs. These bidirectionally sensitive neurons were only seen for the R-C axis, not the I-C axis (Fig. 2.8F), though similar bidirectional "delta" type neurons have been found in multiple axes in cats (Peterson 1970).

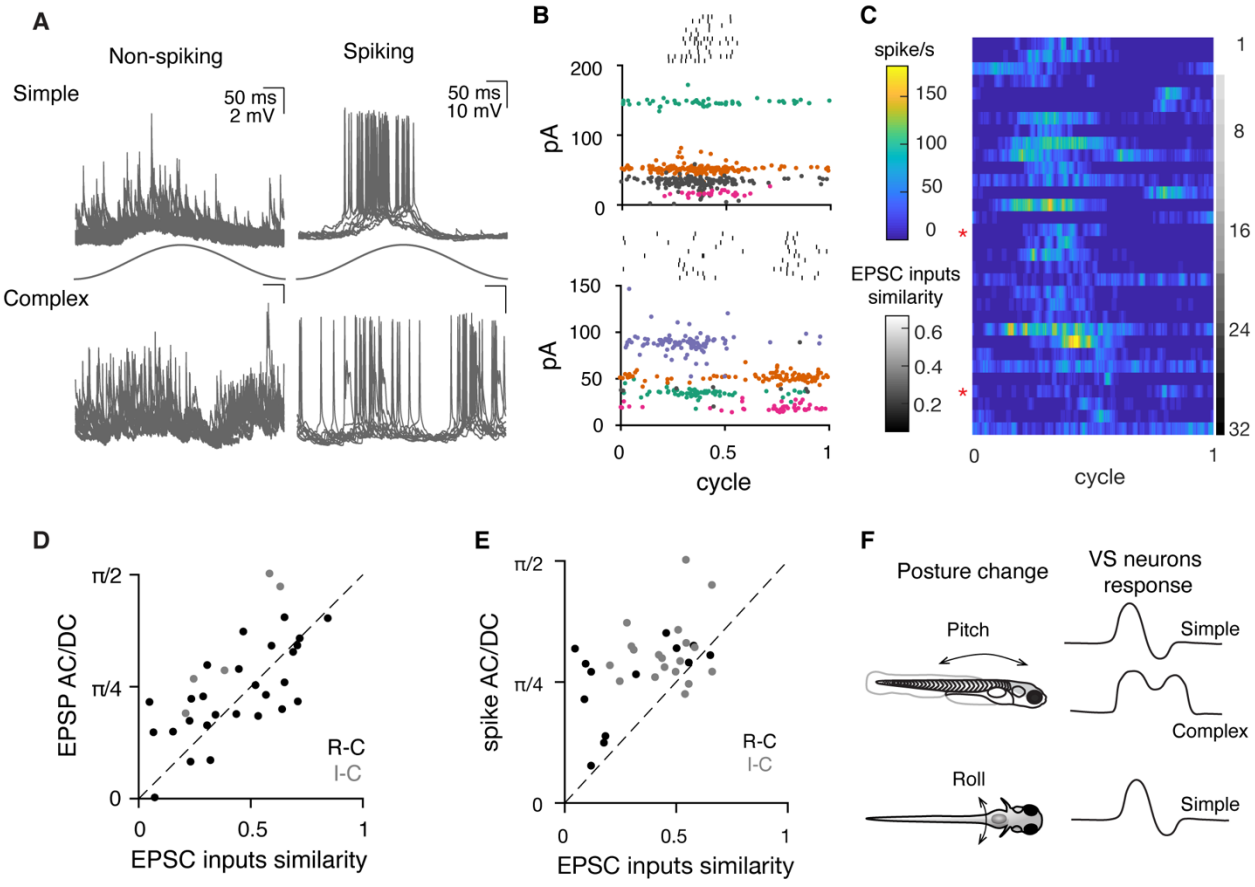

Figure 2. 8: Complex central tuning arises from divergent afferent inputs

A. Example subthreshold and spiking responses from VS neurons with simple tuning (top) or more complex, multi-phase responses (bottom) during 2 Hz, 0.02 g translational movement (11-12 cycles overlaid).
B. Example spiking cells (same as in A), showing that simple (top) and complex (bottom) spiking tuning response are constructed from afferent inputs with similar and different tuning directions, respectively. At top (black) is the sensory-evoked spike raster. Colored and gray dots represent sensory-evoked EPSCs; all the EPSCs with the same color in a panel are inferred to arise from the same afferent. Gray, EPSCs that are not necessarily from individual afferents, based on the absence of clear refractory period structure in autocorrelogram. EPSCs and rasters are from 11-12 cycles.

C. Average spiking rate of VS neurons during a cycle of sensory stimulation, ranked from more similar EPSC inputs to more different EPSC inputs, n=32. Red asterisks label the example spiking simple and complex VS neuron in A and B.
D. Correlation of EPSC inputs similarity index and EPSP AC/DC response ratio (see Methods), for all non-spiking VS neurons with multiple convergent afferents. Sensory tuning of afferent inputs and EPSPs was measured on the R-C axis (black, n=27) and I-C axis (grey, n=5). Dashed, unity line. R: 0.67, p=2.9e-5
E. Correlation of EPSC input similarity index and spike activity AC/DC ratio, for all spiking VS neurons on the R-C axis (black, n=13 recordings) and I-C axis (gray, n=19). Dashed, unity line. R: 0.48, p=5.5e-3.
F. Summary of different VS neuron responses to posture change on the pitch and roll axes.

2.3 Discussion

Sensory convergence in the central vestibular nuclei

Taking advantage of the invariant synaptic transmission of electrical synapses, we separated distinct afferent inputs that converge onto VS neurons and measured the spatial and temporal tuning of each converging afferent *in vivo*. This analysis is facilitated by the sparseness of connectivity, with < 6 afferents synapsing with each VS neuron. Our data reveal that sparse but powerful afferent synaptic contacts, located on the lateral dendrites of VS neurons, are sufficient to drive the membrane potential of the cell during sensory stimulation. These data are consistent with observations in the mammalian literature: anatomically, very few otolith afferent terminals are observed in the lateral vestibular nucleus (Newlands and Perachio, 2003), but physiologically, afferent stimulation elicits monosynaptic EPSPs in VS neurons (Boyle et al., 1992). Although these large afferent inputs drive sensory responses, VS neurons receive a wealth of non-vestibular synaptic contacts on their large dendritic arbors. This is in line with previous findings that the activity of VS neurons is regulated by locomotion (Orlovsky, 1972), proprioception (Neuhuber and Zenker, 1989), and other inputs (Sarkisian, 2000, Witts and Murray, 2019). Interestingly, lateral geniculate neurons (LGN) of the visual thalamus display a

similar pattern of connectivity, with sparse, powerful afferent inputs from retinal ganglion cells and weaker, diverse inputs from other sources (Usrey et al., 1999, Sherman, 2005). Moreover, granule cells in cerebellum also receive sparse mossy fiber inputs, and their synaptic inputs exhibit pathway-specific biophysical properties (Chabrol et al., 2015). Our findings suggest that this configuration is common to VS neurons as well.

Similarly tuned otolith afferents preferentially converge onto VS neurons (Fig. 2.7), demonstrating that feedforward excitation can generate central neurons with simple response properties. In a similar vein, thalamocortical inputs with similar angular tuning also preferentially project onto the same site in somatosensory cortex, and the preferred tuning direction of a given cortical neuron can be predicted by that of the presynaptic thalamic neuron (Bruno et al., 2003). Furthermore, we found that convergence of differently tuned afferents can yield a more complex postsynaptic response in central vestibular neurons, similar to bidirectional or complex tuning observed previously in cats (Peterson, 1970b) and primates (Angelaki and Dickman, 2000b). This result generally supports the hypothesized model (Angelaki, 1992) that the tuning of central vestibular neurons can be constructed from cosine-tuned inputs with varying spatiotemporal properties. However, we find that convergence of differently tuned afferents can also yield simple tuning in VS neurons (cells in upper left, Fig. 2.8E), suggesting other factors such as inhibition (Straka and Dieringer, 1996) and thresholding (Priebe et al., 2004) might be involved. We found no evidence for polysynaptic excitatory circuits during afferent stimulation (Fig. 2.S7 A and B), and modelling indicates that excitatory synaptic input is sufficient to predict subthreshold membrane potential and tuning (Fig. 2.S7 C-F). However, stronger stimuli might elicit inhibition and other nonlinearities. Across brain regions, sensory tuning of central neurons is constructed by a variety of mechanisms. These include afferent convergence patterns (Alonso

and Martinez, 1998, Priebe and Ferster, 2012), local excitatory or inhibitory modulation (Wilent and Contreras, 2005), and nonlinear dendritic computations (Lavzin et al., 2012). Our results demonstrate that the sensory response of a central neuron can be constructed from its afferent inputs in a direct feedforward manner.

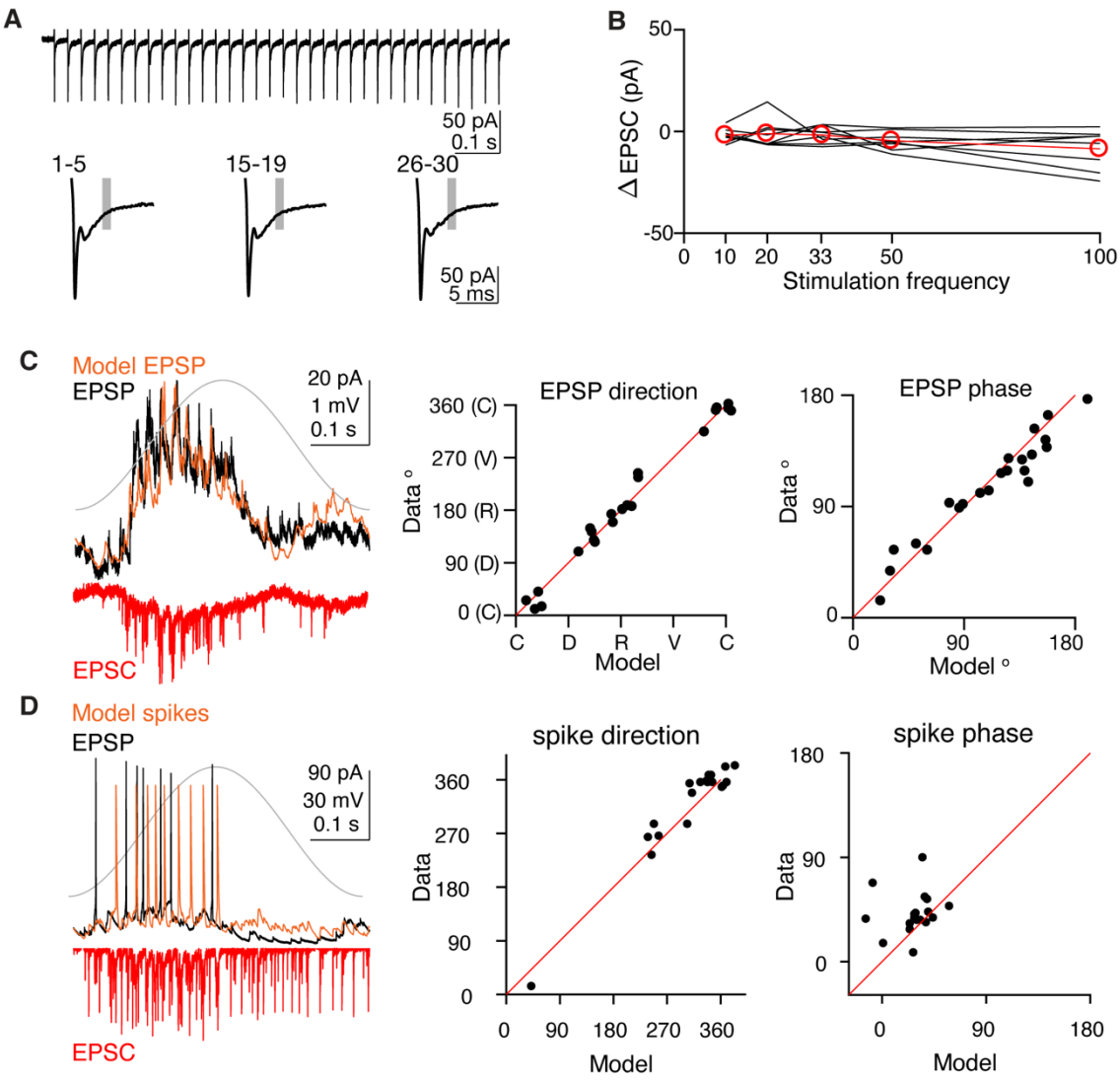

Figure 2. S 7

A. No polysynaptic EPSCs are evoked by electrically stimulating afferents. Top, EPSCs evoked by a train (33 Hz) of electrical pulses on otolith afferents. Bottom, average traces of EPSCs at the beginning (1-5), middle (15-19) and end (26-30) during the train of electric pulses. Shaded area,

4-5 ms (estimated latency of polysynaptic EPSC) after the onset of the pulse. No additional EPSCs are observed in the shaded area for all three average traces.
B. No polysynaptic EPSCs are evoked regardless of stimulation frequency of otolith afferents (n=8). ΔEPSC, difference of the average response in the shaded area (4-5 ms) to the last 5 pulses versus the first 5 pulses.
C. EPSC inputs are sufficient to explain EPSP tuning of VS neurons. Left, comparison of EPSC (red) and EPSP (black) responses recorded sequentially in the same VS neuron, to 2 Hz, 0.02 g translational movement on the R(+)-C (-) axis, as well as the model-generated EPSP (orange). Middle, tuning direction of model-generated membrane potential is consistent with that of recorded EPSPs in the same neuron. Each dot represents the maximum tuning direction of one VS neuron (n=22). Right, tuning phase of model-generated membrane potential is consistent with recorded EPSPs. Each dot represents the phase of one VS neuron in the maximum direction, (n=22). Direction: R=0.99, p=4.2e-19; Phase: R=0.97, p=1.3e-13.
D. EPSC inputs are sufficient to explain spike tuning of the VS neurons (n=19). Data as in panel C, for 19 neurons in which both EPSCs and spiking responses to translation were recorded. The inferred best direction (middle) and phase (right) of spiking were well fit between the model and the actual data. Direction: R=0.97, p=7.7e-12; Phase: R= 0.14, p=0.55.

Otolith afferent tuning properties in the larval zebrafish

The derived spatial tuning profile of afferents in the larval zebrafish is similar to the polarity of the hair cells in otolith macula, consistent with results in fish (Fay, 1984, Platt, 1977) and primates (Fernandez et al., 1972). Notably, tuning to dorsal or ventral acceleration was relatively weak for most afferents, presumably due to the horizontal orientation of the utricular membrane in the larval zebrafish inner ear. Afferents were preferentially tuned to contralateral acceleration (ipsilateral tilt) along the roll axis, consistent with the dearth of ipsilaterally tuned hair cells in larval zebrafish (Haddon et al., 1999). Thus, the absence of bidirectionally tuned neurons in the I-C axis might simply be due to the relative rarity of ipsilaterally tuned hair cells. However, it may also be related to behavioral control: fish make deliberate changes in the pitch axis to change their elevation, but not in the roll axis (Ehrlich and Schoppik, 2017) (Fig. 2.8F). In species with a more centrally located line of polarity reversal (Fernandez and Goldberg, 1976a, Tomko et al., 1981), we would predict more convergence of oppositely tuned afferents, and correspondingly more complex responses of VS neurons in the roll axis, as seen in cats (Peterson, 1970b).

A significant question in vestibular systems is whether central vestibular neurons receive selective projections from afferents with regular as opposed to irregular firing. Both regular and irregular afferents are thought to converge on VS and vestibulo-ocular reflex neurons in mammals, based on studies comparing recruitment thresholds of afferent inputs (Boyle et al., 1992). Our data provide direct evidence that vestibular inputs to VS neurons exhibit classic characteristics of irregular afferents (Eatock and Songer, 2011): high-pass tuning, low

spontaneous firing rate, and high CV of firing (Fig. 2.S5A-C). It is unknown whether regular utricular afferents exist in the larval zebrafish. Although regular utricular afferents were observed in guitarfish (Budelli and Macadar, 1979), they appear absent in toadfish (Maruska and Mensinger, 2015) and sleeper goby (Lu et al., 2004). Based on serial-section EM reconstructions, many afferents make no contacts with VS neurons (Fig. 2.4C), leading us to conclude that either regular afferents have not yet developed or that they do not contact VS neurons in the larval zebrafish.

Linear and fast synaptic transmission via gap junctions

Our data reveal that electrical synapses mediate linear synaptic transmission from otolith afferents to VS neurons. Although electrical transmission is implicated in the formation of neural circuits during development (Pereda, 2016), other sensory afferent transmission in larval zebrafish, such as at retinotectal synapses, is mediated solely by glutamate (Smear et al., 2007). This suggests that the electrical synapses we identified from vestibular afferents are perhaps not simply a feature of early larval development but play an important role in circuit computations, potentially via their amplitude-invariant transmission. Interestingly, mammalian vestibular afferent synapses also exhibit amplitude-invariant transmission in the medial vestibular nucleus (Bagnall et al., 2008) and cerebellum (Arenz et al., 2008, Chabrol et al., 2015), but via specialized glutamatergic terminals (Turecek et al., 2017, McElvain et al., 2015), indicating that frequency-independent transmission is a hallmark of vestibular signaling across vertebrates. Furthermore, mixed electrical and chemical synapses have been anatomically identified between vestibular afferents and VS neurons in both adult fish (Korn et al., 1977) and rodents (Nagy et al., 2013), suggesting the mixed synapse may be a conserved mechanism across species to implement fast, frequency-independent transmission in the lateral vestibular nucleus. The

amplitude invariance of this connection allowed us to examine whether there was any relationship between an afferent's sensory gain or firing rate and the synaptic amplitude it evokes in a VS neuron. No correlation appeared in either of these measures (Fig. 2.S5D, E), indicating that at least within this population, weaker synaptic strength is not compensated for by higher firing rates.

VS pathway underlying sensorimotor transformation

The VS pathway is important for posture control. Larval zebrafish swim at high frequencies up to 100 Hz (McLean and Fetcho, 2009) and are naturally unstable in water (Ehrlich and Schoppik, 2017). Our study examined the response of VS neurons with translational stimuli in the range of 0.04-0.12 g and 0.5-8 Hz, head movement parameters comparable to slow swimming (Voesenek et al., 2016) or small angle tilting motion in the larval zebrafish. In the roll axis all VS neurons are tuned to ipsilateral tilt (Fig. 2.S8B), consistent with data from calcium imaging (Migault et al., 2018, Favre-Bulle et al., 2018), suggesting they might excite specific motor units in the spinal cord to produce compensatory movements (Bagnall and McLean, 2014). On the pitch axis, VS neurons have more heterogeneous responses, including simple tuning to either rostral or caudal acceleration (Fig. 2.S8B), as well as complex responses (Fig. 2.8) to both directions. Thus, when the animal is destabilized by excessive nose-up or nose-down tilts, VS neurons might activate non-specific motor units, increasing the likelihood of swim bouts to regain balance (Ehrlich and Schoppik, 2017).

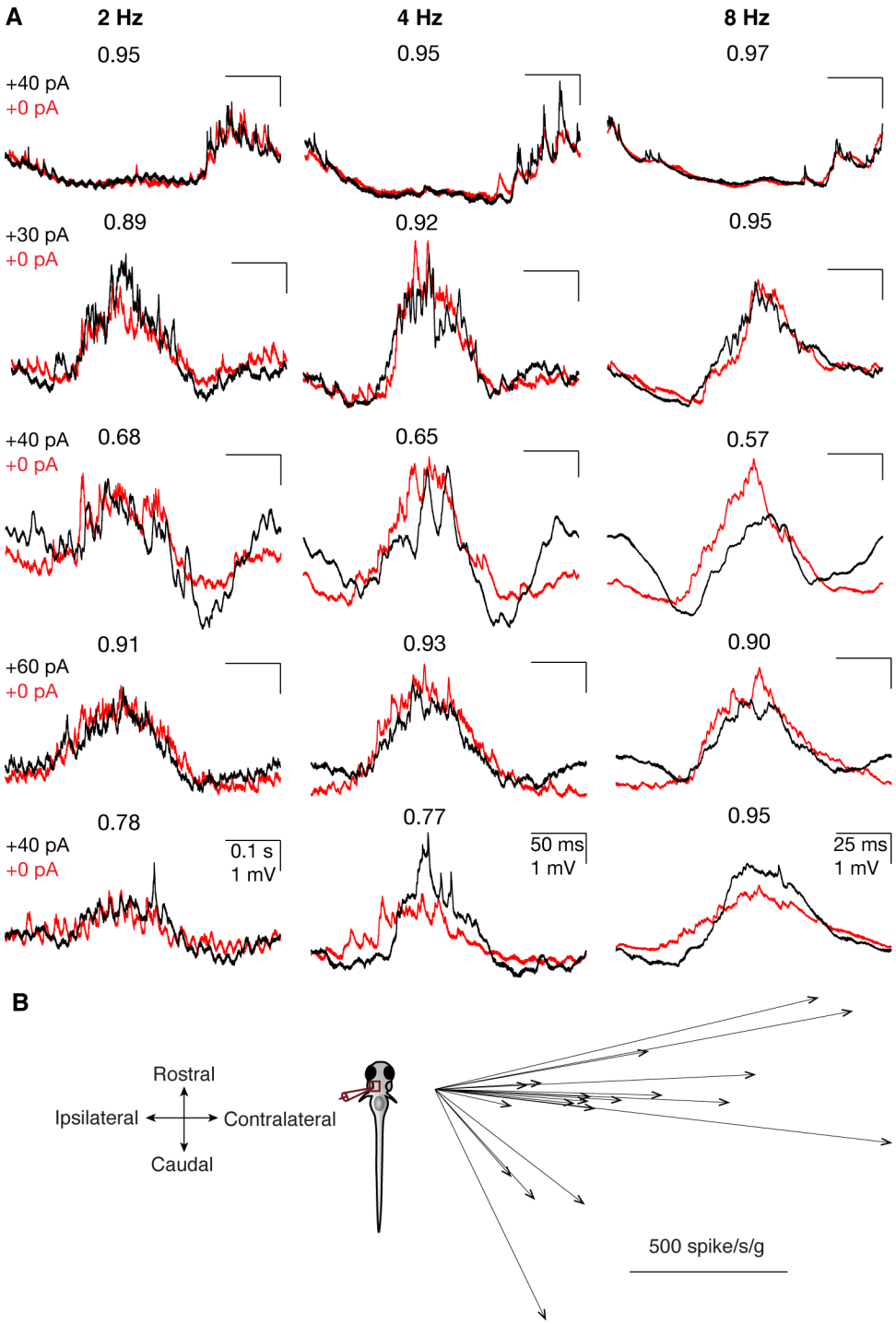

Figure 2. S 8

A. Sensory tuning of 5 different VS neurons (rows) with rheobase current injection (black) and without current injection (red). Responses are shown to three different frequencies of stimulation (columns), with baselines subtracted for easier visual comparison. After spikes were clipped from bias-injected traces, membrane potential was averaged across 10-20 cycles of 0.02 g

sinusoidal movements at the given frequencies under each condition. Numbers atop each response are the correlation coefficient of the two traces and generally indicate highly similar responses between the baseline and current injection conditions.
B. Maximum direction of spiking tuning from VS neurons (n=19) shown in Fig. 2.8. Fish were oriented dorsal up.

The high-pass tuning and phase lead of otolith afferents innervating VS neurons will make larvae most sensitive to ongoing changes in tilt or acceleration, especially at high frequency. These data are consistent with behavioral observations that larvae become more likely to swim to correct their position in the pitch axis when angular velocity (i.e., changing tilt) reaches a critical threshold (Ehrlich and Schoppik, 2017). This compensatory postural adjustment, which relies on both trunk and fins, is absent in *rock solo* larvae (Ehrlich and Schoppik, 2019), in line with our results on the absence of sensory tuning in those animals. Larval VS neurons receive similar amounts of inputs from rostrally and caudally tuned afferents, suggesting both nose-up and nose-down tilts are equally detected by the VS pathway. In contrast, the vestibulo-ocular pathway shows an anatomical bias for representation of nose-up body tilt (Schoppik et al., 2017). This bias indicates that different strategies might be involved to adjust body posture and eye position for pitch movements in larval zebrafish.

Moreover, it is important for animals to distinguish self-generated and external vestibular signals. We described the direct excitatory inputs from vestibular afferents onto the VS neurons during passive movements. How do self-generated motion signals modulate the activities of VS neurons? In the related lateral line system, locomotor signals inhibit afferent activity via brainstem efferents that preferentially suppress hair cells encoding posterior-directed deflections, which would occur during normal swim (Lunsford et al., 2019, Pichler and Lagnado, 2020). In contrast, in the mammalian vestibular system, afferent activity appears normal during self-

generated movement but central VS neurons show reduced responses, likely due to inhibition from cerebellar Purkinje cells (Cullen, 2019). In the future, it would be interesting to use *in vivo* whole-cell physiology to investigate how central vestibular neurons distinguish self-generated movements from passive movements in the larval zebrafish.

Acknowledgments

We are grateful to Dr. Timothy Holy for guidance on development of EPSC analysis and valuable feedback on the project. We thank Dr. Richard Roberts for helping set up the electrophysiology recording rig, and Drs. Rebecca Callahan, Mohini Sengupta and Mr. Saul Bello Rojas for thoughtful critiques of the paper. Drs. Daniel Kerschensteiner and David Schoppik also contributed insightful comments on the manuscript. We also acknowledge the Washington University Zebrafish Facility for fish care and Washington University Center for Cellular Imaging (WUCCI) for supporting the confocal imaging experiments. This work is supported by funding through the National Institute of Health (NIH) R00 DC012536 (M.W.B.), R01 DC016413 (M.W.B.), R21EY030623 (J.L.M.), a Sloan Research Fellowship (M.W.B.), a Leon Levy Foundation Fellowship in Neuroscience (D.G.C.H.), and the National BioResource Project in Japan (S.H.). M.W.B. is a Pew Biomedical Scholar and a McKnight Foundation Scholar. J.L.M is a recipient of a Research to Prevent Blindness Career Development Award.

Author contributions:

Y.K. and S.H. generated the *Tg(nefma:gal4, UAS:GFP)* fish line. Z.L. and M.W.B. conceived the project. Z.L. performed the electrophysiology, confocal imaging experiments and analyzed the data. M.W.B., J.L.M. and D.G.C.H. carried out the serial-section EM imaging and reconstruction. Z.L. and M.W.B. wrote the manuscript with input from all other authors.

Resource availability

Materials Availability

The fish line generated in this study have been deposited to ZFIN: Tg(nefma:gal4; uas:GFP), ZFIN ID: ZDB-ALT-200623-2

Aligned EM images are available at the following site: http://zebrafish.link/hildebrand16/data/vestibular_right

Data and Code Availability: MATLAB code for analysis is available on https://github.com/bagnall-lab/VStuning_project

2.4 Methods

All fish used for experiments were at larval stage from 4-7 dpf before the onset of sexual maturation. The age of the animals used is described in the Method details and/or indicated in the figures. All experiments and procedures were approved by the Animal Studies Committee at Washington University and adhere to NIH guidelines.

Animals were raised and maintained in the Washington University Zebrafish Facility at 28.5ºC with a 14:10 light:dark cycle. Larval zebrafish (4-7 dpf) were housed either in petri dishes or shallow tank with system water. Adult animals were maintained up to 1 year old with standard procedure.

Tg(nefma:LRL:Gal4) was established by injecting the construct containing hsp70 promoter (Kimura et al., 2014), and the insertion site was set at the upstream of the nefma gene with the CRISPR target sequence: CATCGACGGATCAATGG. The *Tg(nefma:gal4)* fish line was

generated by crossing *Tg(nefma:LRL:Gal4)* with a ubiquitous-Cre fish. The *otog*$^{c.1522+2T>A}$ -/- (rock solo) mutant is vestibular deficient due to a splice site mutation in *otogelin* (Mo et al., 2010, Roberts et al., 2017). Rock solo homozygotes on a *Tg(nefma:gal4, UAS:GFP)* background were crossed to rock solo WT/heterozygotes to produce clutches containing WT, heterozygotes and homozygotes for recording purposes. The rock solo homozygotes were identified by the absence of anterior otolith (utricle).

Method details:

Electrophysiology:

VS neurons were targeted for whole-cell patch clamp recordings based on their characteristic position and fluorescence in the *Tg(nefma:gal4, UAS:GFP)* fish. The larvae (4-7 dpf) were paralyzed by 0.1% α-bungarotoxin and embedded in a 10 mm FluoroDish (WPI) with low-melting point agarose (Camplex SeaPlaque Agarose, 2.4% in system water). Fish were immersed in extracellular solution ([in mM] NaCl 134, KCl 2.9, $MgCl_2$ 1.2, HEPES 10, glucose 10, $CaCl_2$ 2.1, osmolarity ~295 mOsm and pH ~ 7.5) and a small piece of skin above the brainstem was carefully removed by sharpened tungsten pins. The fish was transferred to an epifluorescence microscope equipped with immersion objectives (Olympus, 40x, 0.8 NA), infrared differential interference contrast optics and air-bearing sled recording table.

Patch pipettes (7-9 MΩ) were filled with internal solution ([in mM] K gluconate 125, $MgCl_2$ 2.5, HEPES 10, EGTA 10, Na_2ATP 4, Alexa Fluor 568 or 647 hydrazide 0.05-0.1, osmolarity ~295 mOsm and pH ~ 7.5). After whole-cell configuration was achieved, voltage clamp and current clamp signals were recorded at room temperature with a Multiclamp 700B, filtered at 10 kHz

(current clamp) or 2 kHz (voltage clamp), digitized at 50 kHz with Digidata 1440 (Axon Instruments), and acquired by Clampex 10 (Molecular Devices).

I-V curve measurement: CsMeO4 internal solution ([in mM] CsMeSO3 122, QX314-Cl 1, TEA-Cl 1, MgCl2 3, HEPES 10, EGTA 10, Na2-ATP 4) was used to measure the reversal potential of evoked EPSCs. In the voltage clamp mode, evoked EPSCs at different holding membrane potential (-80-40 mV) were recorded. The amplitude and sign change of EPSCs were determined to plot the I-V curve. Liquid junctional potential was calculated to adjust the measured potential.

Before the vestibular stimulus was delivered to the fish, the immersion objective was removed from the recording chamber. During the recording, series resistance was monitored every 15 s to ensure good recording quality; neurons with series resistance variation > 25% were discarded. After recording, the recorded cell was imaged with epifluorescence to confirm cell identity.

Vestibular stimulation:

The recording rig was custom-designed to allow delivering user-controlled movement to the fish during recording without losing whole-cell access. The microscope and a one-axis or two-axis air-bearing sled (Aerotech, ABL1500WB or ABL1500&1500WB) were fixed on an air table. Manipulators (Microstar) and recording platform (ThorLab) were positioned on the sled. The sled was powered with the Aerotech transformers (TM5), NPdrivers (NDRIVECP10-MXU&NDRIVECP20-MXU) and nitrogen gas (Airgas, NI UHP300). Stimuli were designed in Matlab and imported into the program by Aerotech software (Motion Designer/Composer), with additional tuning as required to compensate for the motion of the underlying air table. Movement was recorded by an accelerometer (Sparkfun, ADXL335) attached to the platform. Motion

signals were digitized at 50 kHz with Digidata 1440 (Axon Instruments), and acquired in Clampex 10 (Molecular Devices).

Fish were embedded either dorsal side up (movements on rostral-caudal and ipsilateral-contralateral axes) or left/right side up (movements on dorsal-ventral and rostral-caudal axes) and a series of frequency-varying sinusoidal translational stimulus was applied. The stimulus amplitude was set at 0.02 g or 0.06 g (min to max: 0.04 g or 0.12 g respectively), and stimulus frequency range was 0.5-8 Hz. For spatial tuning measurements, linear translation was applied on four different axes (0-180°, 45°-225°, 90°-270°, 135°-315°) on the horizontal plane. Because the two-axis sled was mounted atop a standard electrophysiology air table, there was a slight damping effect during stimulation, most noticeably at the beginning of a sinusoidal waveform. We delivered an adapted stimulus waveform to compensate for this damping effect. Across four translation stimuli, the measured stimulus from the accelerometer showed the acceleration amplitude was 0.0208 ± 0.001 g on the intended axis, and 0.0019 ± 0.0006 g on the orthogonal axis, indicating only small deviation from linearity. To record spike tuning in neurons without spontaneous firing, a rheobase current was injected to depolarize the cell (<=40 pA, 12/15; >40 pA, 3/15).

Circular stimulation: clockwise (CW) and anticlockwise (CCW) 2 Hz circular movements with direction-varying acceleration of 0.02 g, were applied at the end of the recording to measure the dynamic neural response. CW and CCW stimuli have 90° phase difference in acceleration between X and Y axes.

Otolith afferent stimulation and pharmacology

A glass pipette electrode (2-5 MΩ) filled with extracellular solution ([in mM] NaCl 134, KCl 2.9, $MgCl_2$ 1.2, HEPES 10, glucose 10, $CaCl_2$ 2.1, osmolarity ~295 mOsm and pH ~ 7.5) was connected to a stimulator (A-M systems, Model 2100), and placed in the vestibular ganglion to stimulate the vestibular afferents. A train of 0.1 ms, 1 μA - 1 mA electrical pulses at varying frequencies were delivered to elicit EPSCs in the recorded cells. At least 20 trials of evoked EPSCs were recorded to establish a stable baseline. AMPA receptors and gap junctions were blocked with 10 μM NBQX and 500 μM carbenoxolone, respectively.

Electron Microscopy:

Ultrathin serial sections of brainstem from a 5.5 dpf zebrafish were a generous loan from J. Lichtman and F. Engert. Using the published 18.8 × 18.8 × 60 nm^3 per voxel and 56.4 × 56.4 × 60 nm^3 per voxel reference map and reconstructions (Hildebrand et al., 2017), we targeted re-imaging at 4.0 × 4.0 × 60 nm^3 per voxel to the entirety of the myelinated utricular afferents (identified by their peripheral processes reaching for the utricular macula) and VS neurons (identified by their position and axonal projections into the spinal cord) on one side of the brainstem, covering ~95 μm in the rostrocaudal axis. Imaging was carried out on a Zeiss Merlin 540 FE-SEM with a solid-state backscatter detector. The ATLAS scan engine was controlled via WaferMapper (Hayworth et al., 2014). The resulting images were aligned onto the existing 56.4 × 56.4 × 60 nm^3 per voxel dataset using linear affine transformations in FIJI with the TrakEM2 plug-in (Cardona et al., 2012). In a small subset of identified synapses, we carried out further re-imaging at 1.0 × 1.0 × 60 nm^3 per voxel to visualize the hallmarks of gap junctions.

The existing reconstructions of myelinated portions of VS neurons and utricular afferents were extended to cover branches that had been missed in the original dataset. Appositions between

afferents and VS neurons were considered to be synaptic contacts if the presynapse contained vesicles, the membranes were tightly apposed and straight, and there were signs of a postsynaptic density. In cases where appositions were more difficult to determine, such as those parallel to the plane of section, vesicle clustering at a tight apposition was used as the criterion for a synapse.

EPSP Modeling

Computational modeling was carried out in NEURON 7.6 (Hines and Carnevale, 1997). Because the goal was to test whether excitatory synaptic inputs were sufficient to explain the observed subthreshold tuning, only passive conductances were implemented. For each recorded neuron, input resistance measured by small hyperpolarizing steps was scaled by a fixed factor to define gLeak_hh, which was the only parameter adjusted in the model. EPSCs recorded during sensory stimulation were fed back into the model via a GClamp (dynamic clamp) mechanism (Bagnall et al., 2011) with a reversal potential of +40 mV. The resulting modeled EPSPs were then analyzed for direction and phase dynamics and compared to the same analysis on actual recorded EPSPs from the same neuron. The same approach was applied for spiking data with the addition of SpikeOut to evoke spikes at a given threshold (Brette, 2007), which was held consistent within neurons but adjusted from one neuron to the next to match the total number of spikes elicited during stimulation.

Quantification and statistical analysis:

All analysis was implemented with custom written codes in Matlab (Mathworks).

Event detection:

EPSC events were detected by a derivative method (Bagnall and McLean, 2014). The electrical and chemical EPSCs were further separated using a deconvolution method (details described below). The kinetics of the fast EPSCs measured here were extremely rapid, with rise times around 0.4 ms and fall times similarly brief, consistent with their identity as largely electrical synaptic events (Fig. 2.2). As a consequence, we could reliably identify events with > 0.2 ms separation due to the change in rate of rise. The threshold for event identification was 6 pA.

Tuning index of all EPSCs was calculated as the vectoral sum of all events' phase, weighted by the EPSC amplitude.

$$Tuning\ index = \frac{|\sum A_j * e^{i*\theta_j}|}{\sum A_j}, i = \sqrt{-1}$$

(A_j is the amplitude of each EPSC event j, and θ_j is the phase of that event relative to the sinusoidal stimulus on each axis.)

Deconvolution analysis

Deconvolving EPSC signals not only separated EPSCs with different temporal kinetics, but also resolved overlapping events and give more accurate amplitude measurements, because a kernel is used. We assumed that the signals we observed on voltage clamp were primarily composed of electrical EPSCs and chemical EPSCs from afferents, based on our observation from the pharmacology data.

$$S = conv(w_e, s_e) + conv(w_c, s_c) + residuals$$

(w_e, w_c are the kernels of electrical and chemical components of EPSCs, both derived from their waveforms shown in Fig. 2.2, and s_e, s_c are the separated electrical and chemical signals)

A sparse deconvolution algorithm with L1 regularization, derived from FISTA (Beck and Teboulle, 2009), was applied to obtain s_e, s_c by minimizing the objective function:

$$F(s_e, s_c) \equiv \frac{1}{2}(S_{observed} - S_{reconstruct})^2 + \lambda_e * |s_e| + \lambda_c * |s_c|,$$

where:

$$S_{reconstruct} = conv(w_e, s_e) + conv(w_c, s_c)$$

λ_e and λ_c were defined by the root mean square of the signal and magnitude of kernel waveform: $\lambda_i = rms(S_{observed}) * \sqrt[2]{w_i * w_i^T}$. Maximum iteration cycle was set at 500

Clustering of electrical events

Amplitude-invariant EPSCs are mediated by gap junctions, therefore only electrical signals s_e were used to infer individual afferent inputs. A threshold of $3.5 * std(s_e)$ was used for event detection. Detected electrical events were clustered by ISO-SPLIT (Chung et al., 2017). Some clusters were merged or split manually after examination. Clusters with refractory period (threshold: probability < 0.003 within 1 ms) in auto-correlograms (100 ms) were considered from an individual afferent.

For each cluster, the tuning vector of inferred afferent k on each linear axis was quantified as:

$$z_k = \frac{\sum e^{i*\theta_j}}{N_c * A_s} * f_s, i = \sqrt{-1}$$

(θ_j is the phase of EPSC event j in cluster k. N_c is the number of cycles for sinusoidal translation, f_s [Hz] and A_s [g] are the frequency and amplitude of the stimulus. The absolute value and argument of z represent the tuning gain and the tuning phase, respectively.)

Afferent input similarity index for a VS neuron was determined as:

$$\frac{|\sum A_k * z_k|}{\sum A_k * n_k}$$

(A_k, z_k, n_k are the average EPSC amplitude, tuning vector and number of events for cluster k.)

Tuning vector quantification

Tuning in four linear axes was fitted into a 2-dimensional spatiotemporal model (Angelaki, 1992) to obtain the maximum tuning direction A_{max} and the tuning gain S_{max}, phase P_{max} in that direction. In this model, the 2-dimensional tuning of an individual afferent is described by two vectors T_{max} and T_{min} that are spatially and temporally orthogonal to each other ($A_{max} = A_{min} \pm 90°, P_{max} = P_{min} \pm 90°$). When the tuning is measured on a particular axis at A degrees, the tuning gain S for fitting is determined by

$$S_f^2 = S_{max}^2 * \cos^2(A_{max} - A) + S_{min}^2 * \sin^2(A_{max} - A)$$

The tuning phase P for fitting is determined by the argument of $z = a + b * i$ ($i = \sqrt{-1}$), where:

$$a = S_{max} * \cos(A - A_{max}) * \cos(P_{max}) + S_{min} * \sin(A - A_{max}) * \cos(P_{min})$$

$$b = S_{max} * \cos(A - A_{max}) * \sin(P_{max}) + S_{min} * \sin(A - A_{max}) * \sin(P_{min})$$

The gain and phase of T_{max} and T_{min} are fitted by:

$$\min \sum_{j=1}^{4} \left(S_j - S_f(A_j)\right)^2$$

$$\min \sum_{j=1}^{4} \left(z_j - z(A_j)\right)\right)^2, z_j = |z(A_j)| * e^{i(P_j)}$$

AC/DC response quantification

AC of membrane potential and spiking response were defined as the amplitude of sinusoidal fit (2 Hz) of the membrane potential, and the spike vectorial sum during sensory stimulation, respectively. DC of membrane potential and spiking response were defined as the average membrane potential during sensory stimulation above baseline (no stimulation), and the total spike number during sensory stimulation above baseline. For spiking responses, VS neurons with firing rate > 4 spike/cycle and spike AC or DC >1 spike/cycle were included in the analysis.

Bootstrapping:

$\binom{n_i}{2}$ afferent pairs were counted for VS neuron i with n_i distinct afferent inputs ($n_i \geq 2$). The same number of total afferent pairs $\sum_{i=1}^{m}\binom{n_i}{2}$ from all m VS neurons was randomly selected among all $\sum_{i=1}^{m} n_i$ inferred afferents to determine the convergence angle or phase difference distribution by chance, and such selection was performed 5000 times to calculate mean and standard deviation.

Statistics

Statistical methods used for testing, number of data, and p values are reported in the corresponding figure legends. Groups numbers were reported as mean $\pm$ STD, unless stated otherwise.

Chapter 3: Topographic map for a developing vestibular peripheral circuit

Abstract:

In most sensory systems, a topographic map is formed by orderly projections from the periphery to the central nervous system. Although hair cells in the vestibular end organ are oriented topographically, the organization of their postsynaptic afferents is as yet unknown. Here we report that the topographic map of vestibular afferents, at the level of the ganglion, is organized by both sensory tuning and developmental age. We used serial-section electron microscopy to reconstruct the entire vestibular peripheral circuit in one utricle of the larval zebrafish. Hair cell cilia length and location revealed their orientation and striolar identity. We found that early born myelinated vestibular afferents preferentially innervated the early born striolar hair cells, whereas the late born unmyelinated afferents preferentially innervated the late born extrastriolar hair cells. Together, our data suggests the irregular vestibular pathway originated from the striolar zone and regular vestibular pathway originated from the extrastriolar zone are topographically organized at the vestibular ganglion level in an age-dependent manner.

3.1 Introduction

The brain computes sensory information in an efficient and orderly manner. A hallmark feature of central neuronal organization of sensory signals is the topographic map. For instance, the sensory response in the visual cortex maintain the spatial pattern of stimulus in the retina, known as the retinotopy in mammals (Tootell et al., 1982). In the somatosensory cortex, the anatomical

location of each barrel is arranged similarly as the vibrissa on the whisker pad, known as the somatotopy in rodents (Petersen, 2019, Bale and Petersen, 2009). These topographic maps are constructed by highly ordered projections from the sensory periphery to the central neurons. Neural connections required for topographic maps often transmit sensory information through multiple neuronal population across the brain, while maintaining the topographic structure. Thus, uncovering the principle of neural circuit formation underlying topographic organization is important to understand how sensory signals are processed in the brain.

In the vestibular system, topographic maps were only discovered in the sensory end organs, not the central nervous system (Schor et al., 1984a, Straka et al., 2003, Glover, 2000). The polarized hair cells in the otolith sense gravity and linear acceleration via mechanical deflection. On the utricular and saccular macula, the hair cell orientations are systematically organized to detect head motion. But the preferred tuning directions of central vestibular neurons to head tilt are not topographically arranged in the brainstem, subcortical or cortical areas (Laurens et al., 2017, Cullen, 2019, Chen et al., 2010). It is still unclear whether the innervation pattern of vestibular afferent onto the hair cells and their projection pattern into the brain are particularly organized (Goldberg, 2000). Vestibular signals are used to compensate body posture and eye position for self-motion. The lack of organized anatomical structure for tuning representation limits our understanding of the sensorimotor transformation in the vestibular system.

Development plays an important role in neural circuit formation. Early born and late born neurons are often arranged in a spatial gradient pattern, dictating the connection relationship with their pre- or post-synaptic partners. In the spinal cord, early-born motor neurons and excitatory pre-motor neurons are located in the more dorsal area than their late-born counterparts (McLean

et al., 2007). The early born motor and premotor neurons preferentially connect with each other to engage in fast locomotion, whereas the late born neurons preferentially connect to engage in slow locomotion (McLean et al., 2008, Menelaou and McLean, 2012, McLean and Fetcho, 2009). In the retina of larval zebrafish, photoreceptors and ganglion cells start to differentiate in the ventro-nasal region for lateral visual field, and high acuity ventro-temporal region is the last to differentiate for frontal visual field (Schmitt and Dowling, 1999), which is consistent with the survival necessity to avoid predator at early developmental stage and catch preys at later stage (Helmbrecht et al., 2018). Therefore neural circuits also obey developmental order to be topographically organized.

In this study, we examine whether the vestibular peripheral circuit follows developmental sequence to form a topographic map. We propose that the neuronal developmental sequence governs the sensorimotor transformation of the vestibular circuits to control fast and slow movements. That is, the early born periphery and central sensory neurons preferentially wire together, giving rise to the phasic vestibular pathway encoding fast self-motion signals; whereas late born periphery and central sensory neurons preferentially wire together, giving rise to the tonic vestibular pathway encoding slow self-motion signals. Using ultra-resolution serial section electron microscopy, we reconstructed all synaptic connections between 91 hair cells and 105 afferents of one utricle in the larval zebrafish. The absolute and relative length of kinocilia and tallest stereocila of the hair cells revealed their developmental age and striolar identity. We found that 16/105 utricular afferents were fully myelinated, presumably the earliest born, while other afferents were only partially myelinated or not myelinated at all. Myelinated utricular afferents preferentially innervated early-born striolar hair cells, with more synaptic ribbons, than unmyelinated afferents. The somata of these older myelinated afferents were also positioned

more laterally in the utricular ganglion, with younger unmyelinated afferents located more medially. In adult animals, afferents derived from striolar and extrastriolar zones are known to encode phasic and tonic vestibular signals, respectively. Thus, our data suggest that the phasic pathway matures earlier to compensate for fast self-movements, and the tonic pathway develops later for slow self-movements.

3.2 Results

Serial-section EM connectome of all reconstructed vestibular afferents to hair cells in one utricle of the larval zebrafish

Gravito-inertial force acts on the utricle to deflect hair cells during vestibular stimulation (Fig. 3.1A). The vestibular signals are transmitted by the utricular ganglion afferents to the central brain. Although each afferent innervates hair cells with similar tuning directions, it is unclear if any organization governs the innervation pattern from the utricular ganglion onto the macula. To examine this, we used serial-section EM to image all synaptic connections between 105 utricular afferents and 91 utricular hair cells in one utricle of the larval zebrafish at 4nmx4nmx60nm (Fig. 3.1B, middle). On the utricular macula, hair cells were identified with the apical hair bundle extending out of the cell body towards the utricle otoconia (Fig. 3.1B, right). Hair cells were connected with afferents with a stereotypic synaptic ribbon structure (Fig. 3.1B, left bottom), formed by the *ribeye* protein at the presynaptic terminal (Lv et al., 2016). We found each hair cell formed 0-19 distinct synaptic ribbons with an individual afferent (Fig. 3.1C). Hair cells located on the rostral and caudal region of the macula were preferentially innervated by afferents whose soma are located on the rostral and caudal side of the utricular ganglion, respectively.

Thus the innervations from the utricular afferents are topographically arranged to connect with the utricular hair cells along the rostral-caudal axis.

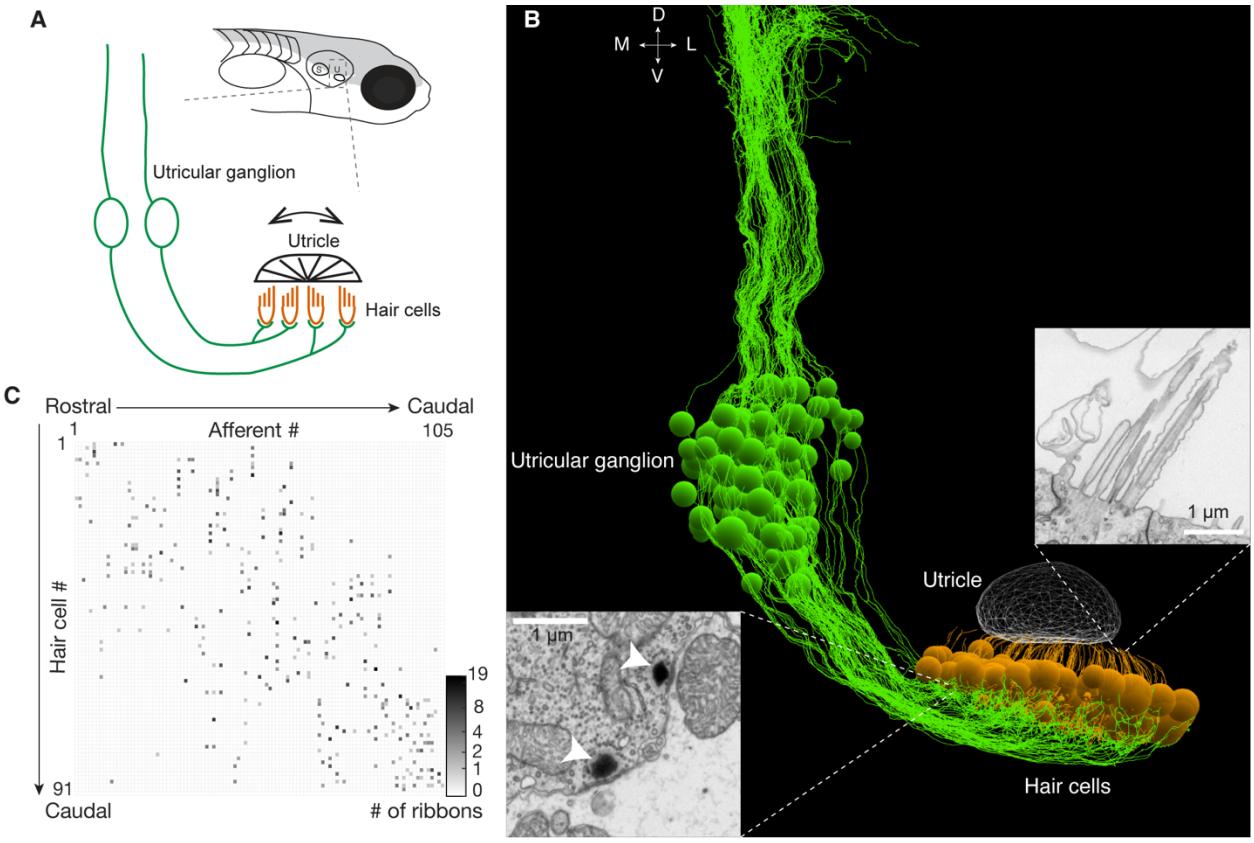

Figure 3. 1: Serial-section EM reveals the complete connectome of a utricular peripheral circuit in the larval zebrafish.

A. Schematic of utricular peripheral circuit in the larval zebrafish.
B. Serial-section EM reconstruction of 91 utricular hair cells (green) and 105 utricular afferents (orange) on the right side of a 5.5 dpf larval zebrafish. Insets: electron micrographs of hair bundle of a hair cell (right), and synaptic ribbons between a hair cell and an afferent (left).
C. Connectivity matrix between all hair cells and afferents ranked with their anatomical location on the rostral-caudal axis. Note the absence of synaptic ribbons on the bottom left and upper right sections of the matrix.

Hair cell stereocilia and kinocilia location displayed a topographic map of the utricular macula.

Hair cell orientations are systematically organized on the utricular macula (Haddon et al., 1999), but whether the tuning directions of utricular afferents form a topographic map in the vestibular ganglion, remains unknown. Mapping all innervation of afferents onto hair cells allows us to infer afferent tuning from hair cell orientation. First, we used stereocila and kinocilia location to determine the hair cell orientation in the serial-section EM dataset (Fig. 3.2A). Each hair cell has multiple stereocilia composed of actin filaments and only one kinocilium composed of microtubules, which exhibit distinct morphology in the serial-section EM images. The presence of the kinocilium and stereocilia array polarizes the hair cell bundle and gives rise to the hair cell orientation. We used the root of each cilium to indicate its anatomical location, and the cilia location of all 91 hair cells were measured across continuous sections of EM images. Thus these cilia were represented as individual points in a three-dimensional coordinate system. The orientation of each hair cell was determined as a vector from the center of the stereocilia to the kinocilium (Fig. 3.2B). The hair cell orientations were systematically organized on the horizontal plane of the macula (Fig. 3.2C), as previously observed in the larval zebrafish utricle. The line of polarity reversal (LPR) marked the division between oppositely tuned hair cells. On the medial side of LPR, hair cells (77/91) were oriented mostly towards the lateral side. On the lateral side, a single array of hair cells (14/91) were oriented towards the medial side. To quantify the hair cell topography, we compared the physical distance and orientation similarity between hair cells located medially to the LPR. We found two hair cells located closer to each other exhibited more similar orientation, and those located more distant to each other exhibited more dissimilar

orientation (Fig. 3.2D). In all, the hair cell stereocilia and kinocilia in the serial-section EM images revealed the topographic map of hair cell orientations in the larval zebrafish utricle.

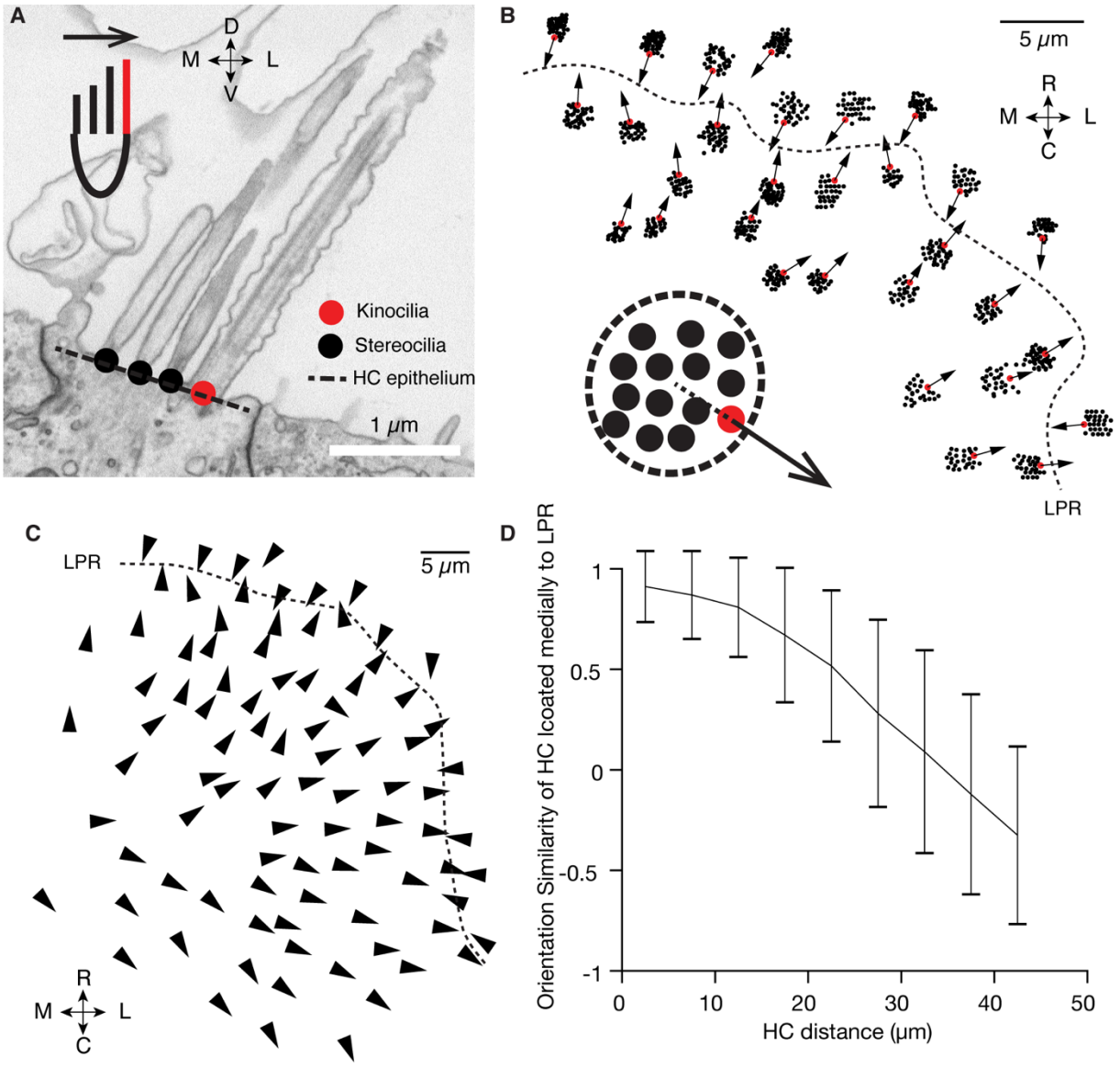

Figure 3. 2: Hair cell orientation is determined by its cilia location

A. Anatomical location of stereocilia and kinocilia reveals hair cell polarity
B. Examples of hair cell orientations along the line of polarity reversal (LPR). Hair cell orientation is measured as a vector from the center of stereocilia to the kinocilium.
C. Hair cell orientations are topographically organized on the utricular macula.
D. Hair cell orientation similarity are negatively correlated with hair cell distance, which are measured with their kinocilia location.

Complete connectome between afferents and hair cells revealed a topographic map of afferent tuning directions in the utricular ganglion

Does the rostral-caudal arrangement of the afferent innervation transform the systematically organized hair cell map to a topographic map organized by afferent tuning in the utricular ganglion? To answer this, we first inferred the tuning direction of each afferent based on the innervated hair cell orientations and synaptic ribbon counts (Fig. 3.3A, left). The tuning vector represents the preferred direction of the afferent responding to head tilt. We found that each afferent innervated 1-8 hair cells (Fig. 3.3A, middle), and those innervated hair cells had similar orientation with each other (Fig. 3.3A, right). Utricular afferent soma were hard to access for tracing or recordings in the adult vertebrate vestibular ganglion. It is yet unknown whether the tuning directions of the utricular ganglion cells are topographically organized. We found that on the caudal region of the utricular ganglion, the afferents were tuned to mostly ipsilateral tilt or caudal tilt; whereas on the rostral region of the utricular ganglion, the afferents were tuned to rostral tilt (Fig. 3.3B). The majority of afferents (93/104) innervated onto the medial side of the utricular macula with respect to the LPR. The afferents that innervate hair cells on the lateral side of the LPR (11/104) were located on the medial-rostral region of the ganglion. To quantify the afferent tuning topography, we compared the soma distance and tuning similarity between afferents that innervate hair cells on the medial side of the LPR. We found two afferents with closer soma showed more similar preferred tuning direction. and those with more distant soma showed more dissimilar preferred tuning direction (Fig. 3.3C). Together, our results show the first known tuning map of utricular afferents, and their preferred tuning directions are topographically organized in the utricular ganglion.

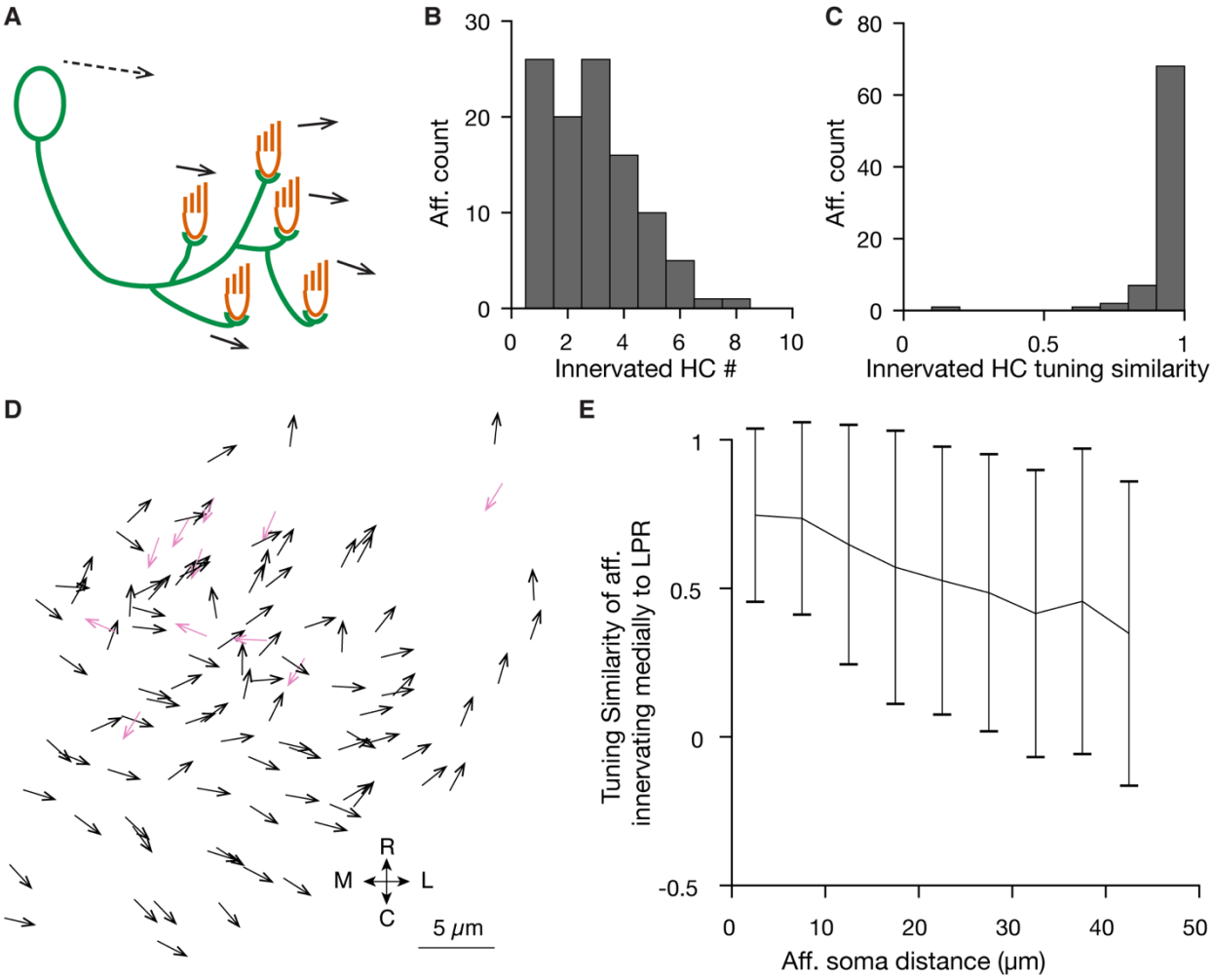

Figure 3. 3: Utricular afferent soma are topographically organized by their sensory tuning.

A. Afferent tuning is inferred from presynaptic hair cell orientations and synaptic ribbon numbers.
B. Histogram of the numbers of distinct hair cells innervated by each afferent.
C. Histogram of the tuning similarity of the two most differently tuned hair cells innervated by each afferent (included only if two or more distinct hair cells are innervated). Note no tuning similarity is less than 0 (90^{o} apart), thus no afferent innervation straddles the LPR.
D. Topographic map of the afferent soma organized by their inferred tuning directions. Black, afferents innervating the medial side of LPR; pink, afferents innervating the lateral side of the LPR.
E. Afferent tuning similarity are negatively correlated with their soma distance.

Stereocilia and kinocilia length revealed the striolar identity and developmental age of the utricular hair cells.

The phasic and tonic vestibular pathways preferentially encode fast and slow self-motion signals, respectively. But how these sensory signals of different speed are translated to regulate fast and slow locomotion remains unclear. The phasic vestibular pathway originates from the striolar zone on the macula, where the hair cells are early born during development. The tonic vestibular pathway originates from the extrastrialar zone, where the hair cells are late born. To identify early born striolar and late born striolar hair cells in the larval zebrafish, we first measured the length of the kinocilium and the tallest stereocilium of each hair cell (Fig. 3.4A). It was previously shown in both rodents and turtles that, in the striolar zone the kinocilia and the tallest stereocilia of the hair cells have similar length (K/S ratio close to 1), while in the extrastriolar zone the kinocilia are longer than the tallest stereocilia for the hair cells (K/S ratio > 2) (Li et al., 2008, Xue and Peterson, 2006). We found that in the larval zebrafish the length of kinocilia and stereocilia range from 1 μm to 10 μm (Fig. 3.4B). Some hair cells had both short kinocilia and stereocilia (<5 μm), presumed still developing or new-born. For more mature hair cells, one group had both kinocilia and stereocilia longer than 5 μm with K/S ratio close to 1, consistent with that of the striolar hair cells. Another group had kinocilia longer than 5 μm but stereocilia shorter than 5 μm, with the K/S ratios larger than 1.7, consistent with that of the extrastriolar hair cells. Furthermore, the identified striolar group were located in a band near the LPR on the macula (Fig. 3.4C), and the identified extrastriolar group were found exclusively outside of the band, which are in accordance with the topography of the striolar and extrastriolar zone in other species. The developing and new-born hair cells were located in the periphery of the macula, while the more mature striolar and extrastriolar hair cells were located in the center. This is

consistent with previous studies showing that the hair cells develop first in the central striolar zone and gradually grow out to the periphery (Jiang et al., 2017). Together, we established that the absolute length of the hair cell cilia indicates their developmental age, and the relative length between kinocilia and tallest stereocilia indicates their striolar identity.

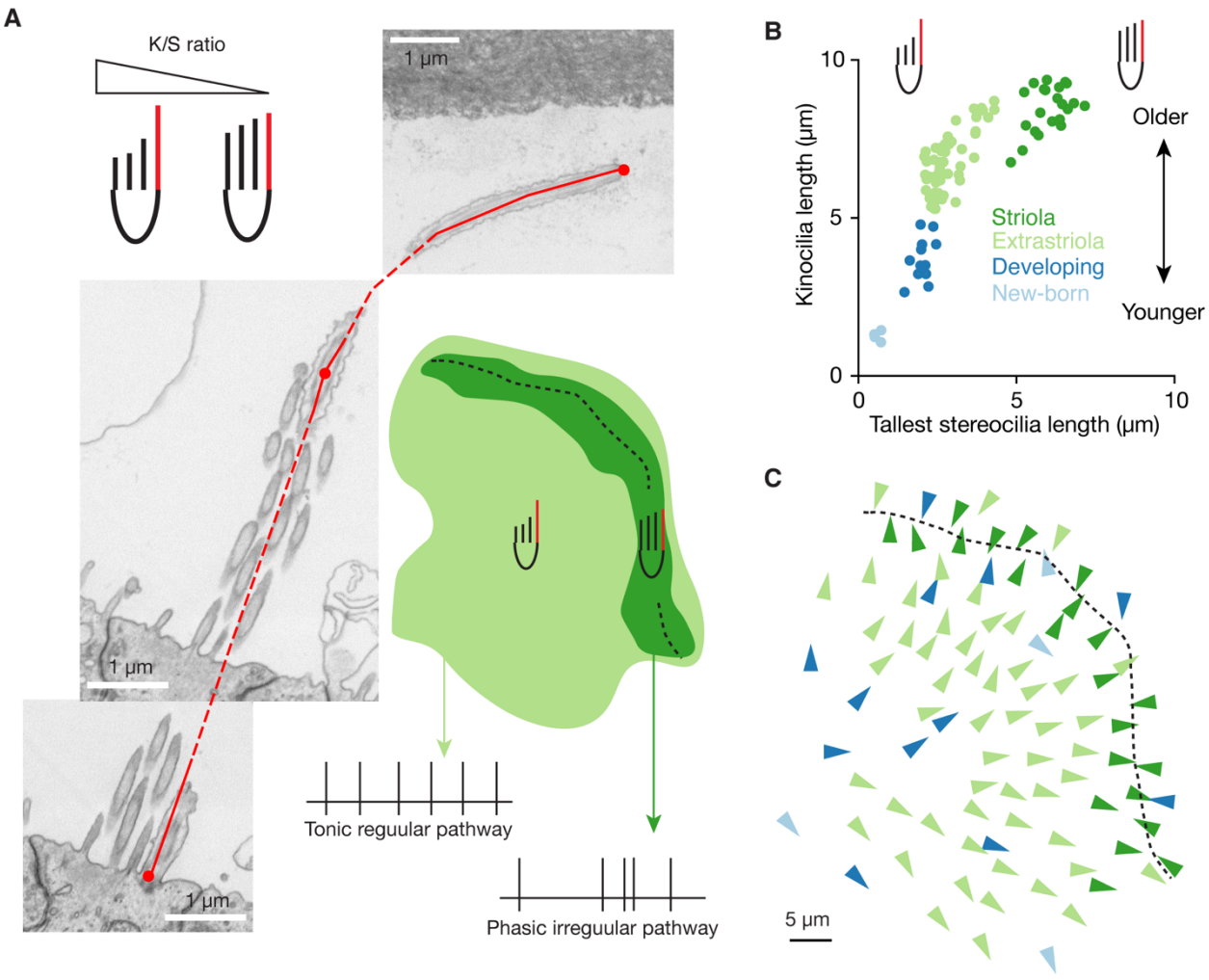

Figure 3. 4: Hair cell kinocilia and stereocilia length indicate their developmental age, and striolar identity.

A. Hair cell cilia length is measured by tracing from its root to apex across multiple EM sections. The length ratio (K/S ratio) of the kinocilia (red) and tallest stereocilia (black) was implicated to differentiate the striolar (dark green) and extrastriolar (light green) hair cells, which give rise to the irregular and regular vestibular pathway, respectively.
B. Four groups of hair cells categorized by their kinocilia and tallest stereocilia length.
C. Topographic map of four hair cell groups on the utricular macula.

The myelinated afferents are located more medially in the ganglion and have more total synaptic ribbons than the unmyelinated afferents.

Are older hair cells preferentially innervated by older afferents? We infer the developmental sequence of the afferents by examining their myelination status. Early born neurons are myelinated first during development. We found in our dataset, only 16/105 afferents were fully myelinated, presumed the earliest born, and others were either partially myelinated or not myelinated at all (Fig. 3.5A). In the utricular ganglion, the myelinated afferent somata were located more laterally compared to the unmyelinated afferent somata (Fig. 3.5B). This anatomical disparity between mature and immature afferents is consistent with previous studies examining utricular ganglion development sequence by protein photo-conversion (Vemaraju et al., 2012). The myelinated and unmyelinated afferents innervate distinct areas of the macula (Fig. 3.5C), suggesting they receive different hair cell inputs. Moreover, the myelinated afferents formed more total synaptic ribbons with hair cells than the unmyelinated afferents (Fig. 3.5D), which is in line with that myelinated afferents are more mature than the unmyelinated afferents. In summary, we found myelination and total synaptic ribbon number indicate the maturity of the afferents, and afferent soma are topographically organized by developmental age in the utricular ganglion.

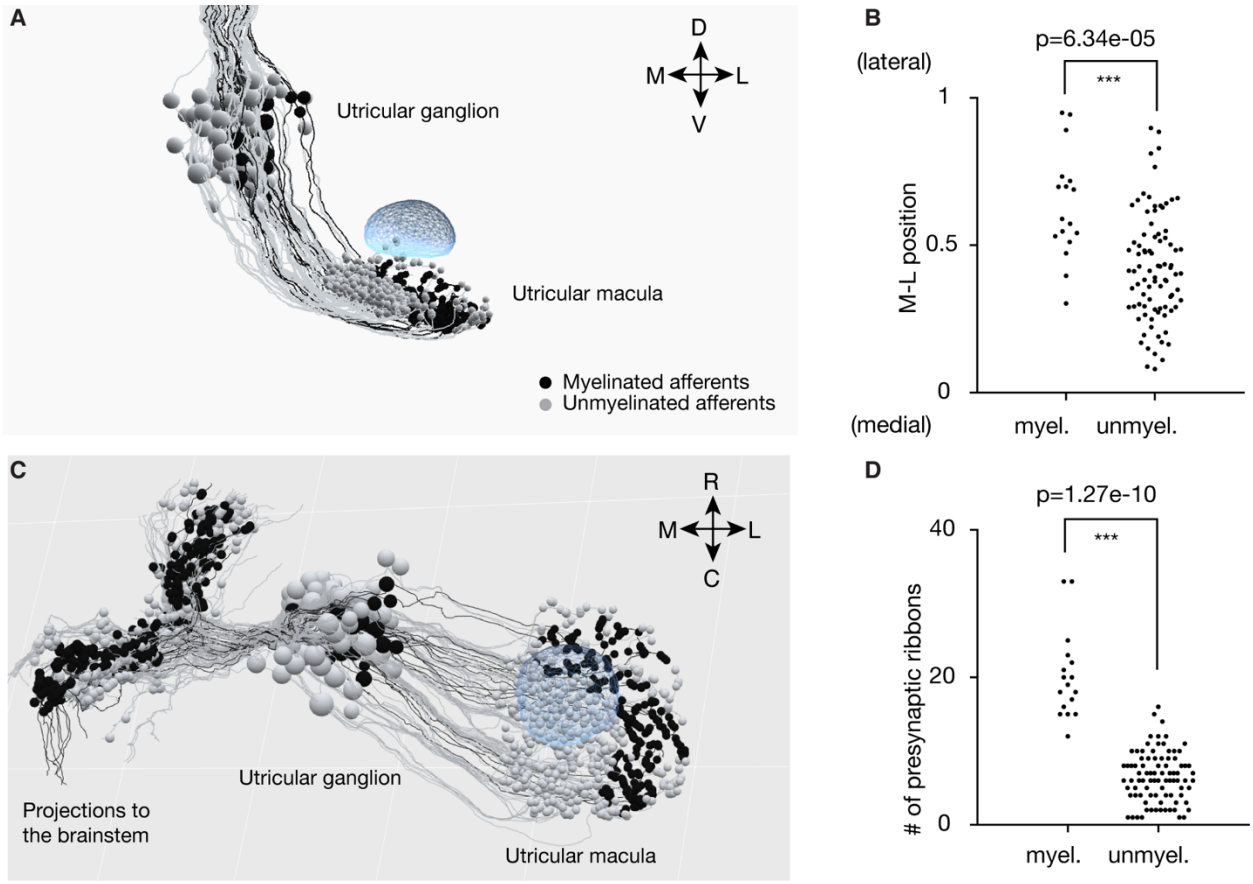

Figure 3. 5: Myelination reveals developmental organization in the utricular ganglion

A. Serial EM reconstruction (front view) of myelinated and unmyelinated utricular afferents.
B. Myelinated afferents soma are located more laterally than the unmyelinated ones in the ganglion.
C. Dorsal view of the same reconstruction as in (A). Note the myelinated and unmyelinated afferents exhibit distinct afferent innervation patterns onto the macula.
D. Myelinated afferents have more presynaptic ribbons than the unmyelinated ones.

Myelinated and unmyelinated afferents preferentially innervated striolar and extrastriolar hair cells, respectively

Striolar hair cells and myelinated afferents are earlier born and anatomically segregated from the extrastriolar hair cells and unmyelinated afferents. Do afferent innervations preferentially connect older afferents with older hair cells, and younger afferents with younger hair cells? We

found that afferents innervating the striolar hair cells were located on the lateral side of the ganglion (Fig. 3.6A), which overlaps with the myelinated afferent territory. Afferents innervating new-born and developing hair cells were located on the medial side of the ganglion, which were mostly unmyelinated afferents. Moreover, myelinated afferents preferentially received presynaptic inputs from striolar hair cells (50% of all inputs) and the remainder from extrastriolar hair cells (Fig. 3.6B). In contrast, unmyelinated afferents received the bulk of their inputs from extrastriolar hair cells (80%) with smaller proportions from striolar and developing/newborn population. Our results showed that indeed myelinated afferents preferentially innervated striolar hair cells, and unmyelinated afferents preferentially innervated extrastriolar hair cells.

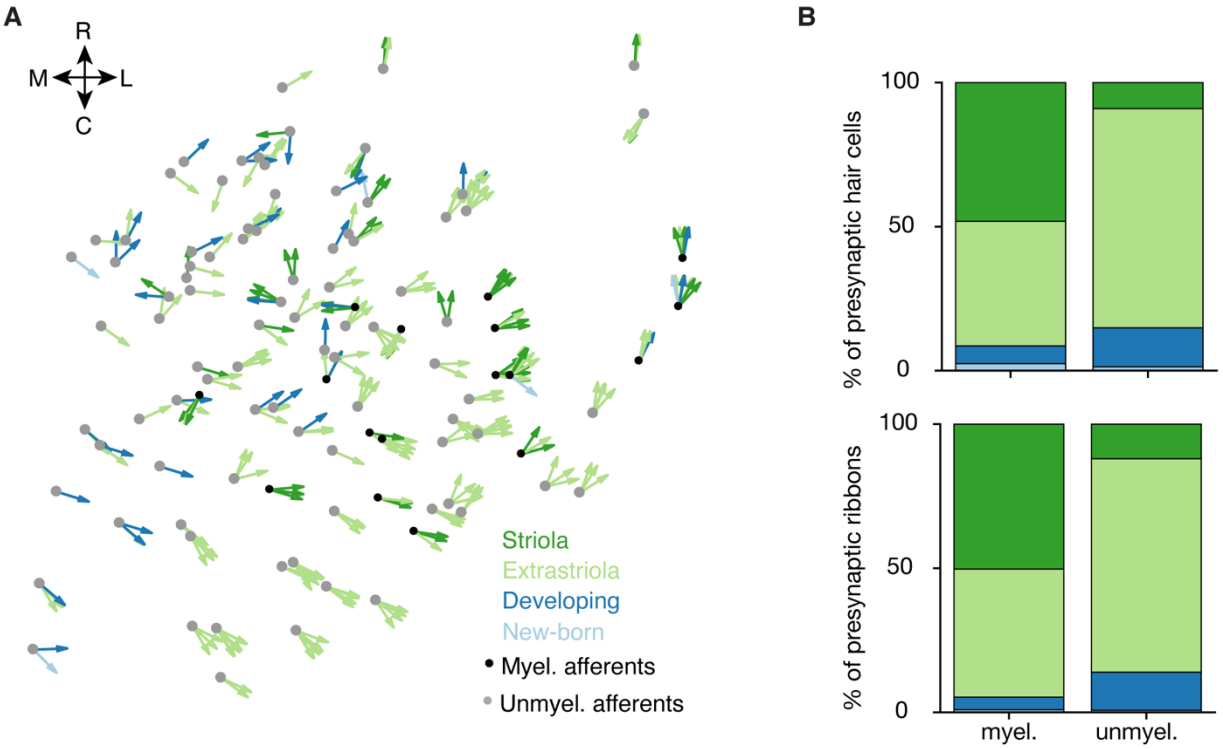

Figure 3. 6: Myelinated afferents preferentially contact striolar hair cells

A. Topographic map of innervated hair cell groups organized by myelinated (black) and unmyelinated (gray) afferent soma location in the ganglion. Arrows on each dot represent innervated hair cell orientation (directions) and group identity (colors).

B. Percentage for each group of presynaptic hair cells innervated by myelinated and unmyelinated afferents, quantified with hair cell number (top) and synaptic ribbon number (bottom).

3.3 Discussion

Our study demonstrates that the developmental sequence of neurons governs the connectivity of the vestibular peripheral circuits in the larval zebrafish. It shows that the utricular afferents are topographically organized in the utricular ganglion by both sensory tuning direction and developmental age. The afferents in the rostral and caudal regions of the ganglion are tuned to rostral and caudal head tilt respectively. Earlier born myelinated afferents are located on the lateral side of the ganglion and later born unmyelinated ones are located more medially. Moreover, the myelinated afferents preferentially connect with the striolar hair cells on the utricular macula, whereas the unmyelinated afferents preferentially connect with the extrastriolar hair cells. Striolar and extrastriolar pathways drive phasic and tonic sensory responses in the vertebrates. Our results imply a phasic-to-tonic developmental sequence that may correlate with development of motor control from coarse to fine.

Striolar and extrastriolar hair cells in the larval zebrafish

We identified striolar and extrastriolar hair cells in the larval zebrafish utricle by the relative length between their kinocilia and tallest stereocilia (K/S ratio). It shows the striolar zone and extrastriolar zone of the utricular macula for the first time in the larval zebrafish. We found that the striolar zone covers a central stripe of the macula along the line of polarity reversal (LPR), and the extrastriolar zone occupies a larger area in the outskirt of the macula surrounding the

striolar zone. This striolar topography is similar to that in the utricle of other species. Hair cells in the striolar and extrastriolar zone, also have distinct somatic and synaptic morphology in various vertebrate animals (Desai et al., 2005, Li et al., 2008, Xue and Peterson, 2006). Some features such as calyceal synapses are present in mammals (Eatock and Songer, 2011), not the fish, making it difficult to reliably identify striolar zone across species. Our data indicates the K/S ratio of hair cell cilia could be a common classifier for hair cell striolar identity,

The distinct K/S ratio of striolar and extrastriolar hair cells are also observed in mammals and turtles: striolar kinocilia are similar in height with the tallest stereocilia, and extrastriolar kinocilia is significantly longer than the tallest stereocilia. Longer stereocilia were suggested to make striolar hair bundle stiffer than the extrastriolar hair cell bundle (Spoon et al., 2011), which could result in potential difference of interaction with fluid-forced and point-forced stimulus (Nam et al., 2005). Our finding suggests that the difference between hair bundle length in striolar and extrastriolar zone is a common feature in the utricle across species that might contribute to the sensitivity or dynamics of vestibular signaling.

Our results show that striolar hair cells have longer kinocilia than extrastriolar hair cells, which is the opposite of what was observed in other animals. A possible explanation could be that the hair cells are still growing the larval zebrafish utricle, and striolar hair cells were shown to be born earlier than the extrastriolar hair cells. Thus the striolar hair cells are more mature and have longer cilia in general.

Regular and irregular afferents

The afferents in the phasic and tonic pathways are often referred as the irregular and regular afferents in the vestibular system, originating from the striolar and extrastriolar zone of the

utricular macula (Eatock and Songer, 2011). Our results show that the myelinated afferents preferentially connect with striolar hair cells, and unmyelinated afferents with extrastriolar hair cells. Thus we extrapolate that these afferents will develop to be irregular-like and regular-like afferents respectively in the adult fish.

Anatomically, irregular afferents innervate the striolar zone, and form calyceal synapses with the hair cells in mammals; whereas the regular afferents innervate the extrastriolar zone, and make button synapses with the hair cells. However, this synaptic morphological difference can't be used to distinguish early developing afferents because of the lack of calyceal synapses in fish. Irregular and regular afferents exhibit distinct firing patterns, and are classified by their coefficient of covariation of inter-spike intervals. In larval zebrafish, only irregular utricular afferents were observed with electrophysiology recordings (Liu et al., 2020). Regular utricular afferent are absent in adult toadfish (Maruska and Mensinger, 2015) and sleeper goby (Lu et al., 2004), but present in guitar fish (Budelli and Macadar, 1979). Thus it still needs to be addressed whether vestibular afferents will eventually display the regular firing pattern in the adult zebrafish.

Topographic map for vestibular tuning

Our results show the utricular afferent soma are organized by tuning directions, which reveals the first known topographic map in the utricular ganglion. Sensory stimuli are often relayed to central nervous system by orderly projections to form topographic maps. Although utricular hair cell orientation indicate the direction of head tilt, these tuning directions don't form topographic maps in the central vestibular nuclei. In the utricular ganglion, although the afferents tuned to rostral and caudal head tilt are spatially organized in the ganglion, the afferents tuned to

ipsilateral and contralateral head tilt, are intermingled. In the vestibulospinal nucleus of cats (Peterson, 1970a), there is no topographic map for neurons tuned to any direction of tilt, which suggests vestibular afferent projections to the brainstem most likely don't follow sensory tuning principle. Moreover, some central vestibular neurons receive convergence of differently tuned afferents, which leads to more complex tuning than the afferents. These neurons could be respond to head tilts towards multiple directions with similar tuning gain (Angelaki, 1993). Thus the central vestibular neurons might adopt different strategies to encode head tilt directions. It would be interesting to investigate how these signals are eventually used to inform the motor circuits for proper outputs to maintain body balance.

Developmental organization of the vestibular periphery

Our results also shows the utricular afferent soma are organized by developmental age. Is this developmental organization maintained in the central vestibular nuclei? Striolar hair cells innervated by the myelinated afferents, are known to give rise to the phasic pathway that encode preferentially fast self-motion, while the extrastriolar hair cells innervated by the unmyelinated afferents, give rise to the tonic pathway that encode preferentially slow self-motion. Thus the more mature pathway is potentially used for fast vestibular signals, and the less mature pathway for slow vestibular signals. Development also governs the functional organization of other neural circuit. In the cerebellum, the early-born granule cells send their parallel fibers into the deep molecular layer and granule cells born at later times send their parallel fibers to progressively more superficial positions, although the sensorimotor information carried by these neurons are similarly diverse (Markwalter et al., 2019). In the spinal cord, motor neurons and premotor neurons engaged during fast swim are born earlier than those engaged during slow swim (McLean and Fetcho, 2009, McLean et al., 2007). The soma of fast motor neurons and excitatory

premotor neurons are located more dorsally than the slow ones. A second type of developmental map is subcellular organization. The fast inhibitory premotor neurons project preferentially onto the axon initial segment of the motor neuron axons, to effectively silence the motor output; whereas the slow inhibitory premotor neurons project to the perisomatic and dendritic area of the motor neurons, providing weaker inhibition during locomotion (Kishore et al., 2020). Therefore, the neuronal developmental sequence of plays an important role in organizing neural circuits to relay sensory information and execute motor control (Fig. 3.7). It would be interesting to investigate whether motor and pre-motor neurons associated with escape, posture and eye movements follow developmental organization, and how they are targeted by early and late born sensory pathways.

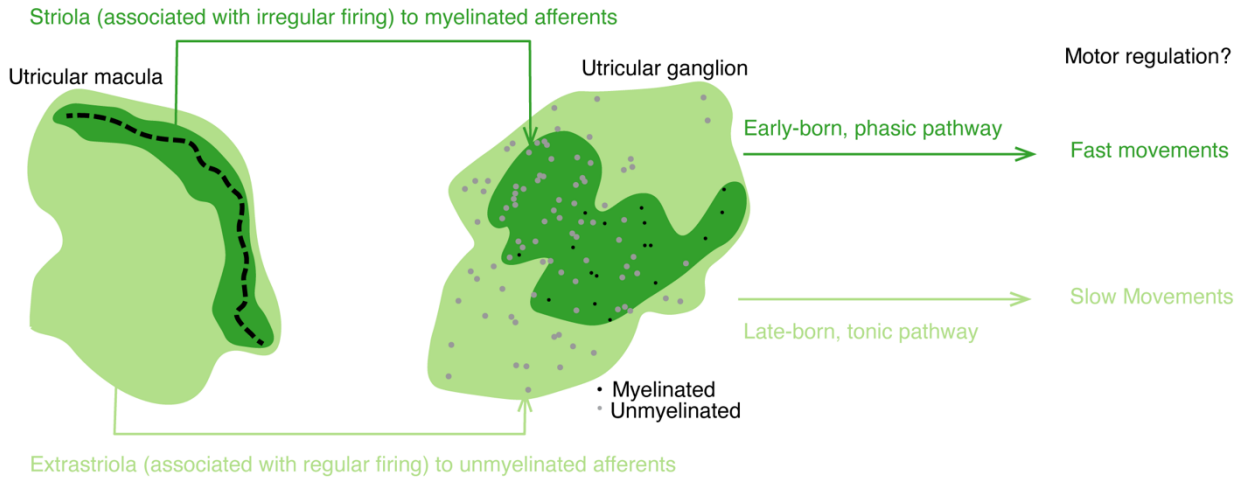

Figure 3. 7: Proposed vestibular organization for sensorimotor transformation

Phasic and tonic pathways follow developmental sequence. Early born afferents encoding fast self-motion and late born afferents encoding slow self-motion arising from the striolar and extrastriolar zones, respectively.

Acknowledgments

We are grateful to Dr. Joshua L. Morgan for guidance on serial-section EM imaging and analysis. We also acknowledge the Washington University Center for Cellular Imaging (WUCCI) for supporting the experiments. This work is supported by funding through the National Institute of Health (NIH) R00 DC012536 (M.W.B.), R01 DC016413 (M.W.B.), a Sloan Research Fellowship (M.W.B.). M.W.B. is a Pew Biomedical Scholar and a McKnight Foundation Scholar.

3.4 Methods

An ultrathin (60 nm thick) serial section library of a 5.5 dpf larval zebrafish was obtained by Hildebrand and colleagues as reported (Hildebrand et al., 2017). Wafers containing the relevant portions of the vestibular system were reimaged at an axial resolution of 4.0 x 4.0 nm/px at the Washington University Center for Cellular Imaging on a Zeiss Merlin 540 FE-SEM with a solid-state backscatter detector (cite WUCCI in acknowledgments and maybe grants). Vestibular regions were targeted using the published dataset in which the myelinated afferents have been partially reconstructed. WaferMapper software (Hayworth et al., 2014) was used to control an ATLAS scan engine for automated focus and acquisition (Morgan et al., 2016). The volume covered ~100 µm in the rostro-caudal axis, 150 µm in the mediolateral axis, and 100 µm in the dorsoventral axis, in an irregular shape designed to capture the afferent peripheral and central processes. The resulting images were aligned onto the original 18.8 nm/px dataset using custom written modifications to the TrakEM2 plugin (Cardona et al., 2012) in FIJI.

All active utricular afferents were identified by stepping through the entire anterior macula twice and marking every ribbon synapse. Every postsynaptic process was followed as far as possible, either joining up with a previously traced myelinated afferent or all the way to the soma in the vestibular ganglion. Approximately 3% of processes adjacent to ribbons could not be followed due to the quality or ambiguity of the images.

Kinocilia and the tallest stereocilia were traced from the apical surface of each hair cell to their distal tips. The kinocilium was recognizable based on its distinctive structure (Fig. 3.2A). Ciliary length was calculated as the sum of the Euclidean point-to-point distances. Positions of all cilia were plotted at the epithelial plane and a three-dimensional tuning vector for each hair cell was derived from the center of mass of all stereocilia to the kinocilium. Hair cell vectorial lengths were typically short in the dorsal-ventral axis relative to their extent in the other two axes, consistent with the mostly horizontal orientation of the utricular macula, and therefore for the purposes of analysis we focused exclusively on their projection in the horizontal plane.

Chapter 4: Conclusion and future directions

How are the vestibular signals computed in the larval zebrafish brain? I used whole-cell physiology and serial-section electron microscopy to investigate the neuronal computation of the central vestibular neurons and neural connectivity of the vestibular peripheral circuit. My results showed that vestibular afferents converge with distinct patterns to construct the sensory response in the central vestibular neurons. The convergence of similarly tuned afferent produces simple central vestibular tuning and the convergence of differently tuned afferent produces complex central vestibular tuning. It provides physiological evidence that sensory responses in central vestibular neurons are generated by direct feedforward excitation from the afferents. These data are in general consistent with the computational models theorized by Dora Angelaki, which largely explains the complex spatiotemporal properties of central vestibular tuning in mammals. Anatomical reconstruction of the vestibular peripheral circuit by serial-section EM showed that the innervations from vestibular afferents to the utricular hair cells follow a developmental order, and these afferents were topographically organized by age in the ganglion. This reveals the first known topographic map in the utricular ganglion. It suggests the phasic vestibular pathway encoding fast self-motion arises from early born vestibular afferents and hair cells, and the tonic pathway encoding slow self-motion arises from the late born vestibular afferents and hair cells. Thus, my study indicates that the vestibular peripheral circuits are organized in an age-dependent manner to transmit sensory signals into the brain.

Vestibulospinal projections to the spinal cord

The vestibulospinal neurons exhibit either simple or complex tuning to translational movements and head tilt, and project directly into the spinal cord for motor control. Head tilt direction needs to be properly translated to produce appropriate self-righting behavior, but very little is known about how the tuning complexity of the vestibulospinal neuron affects its downstream motor targets.

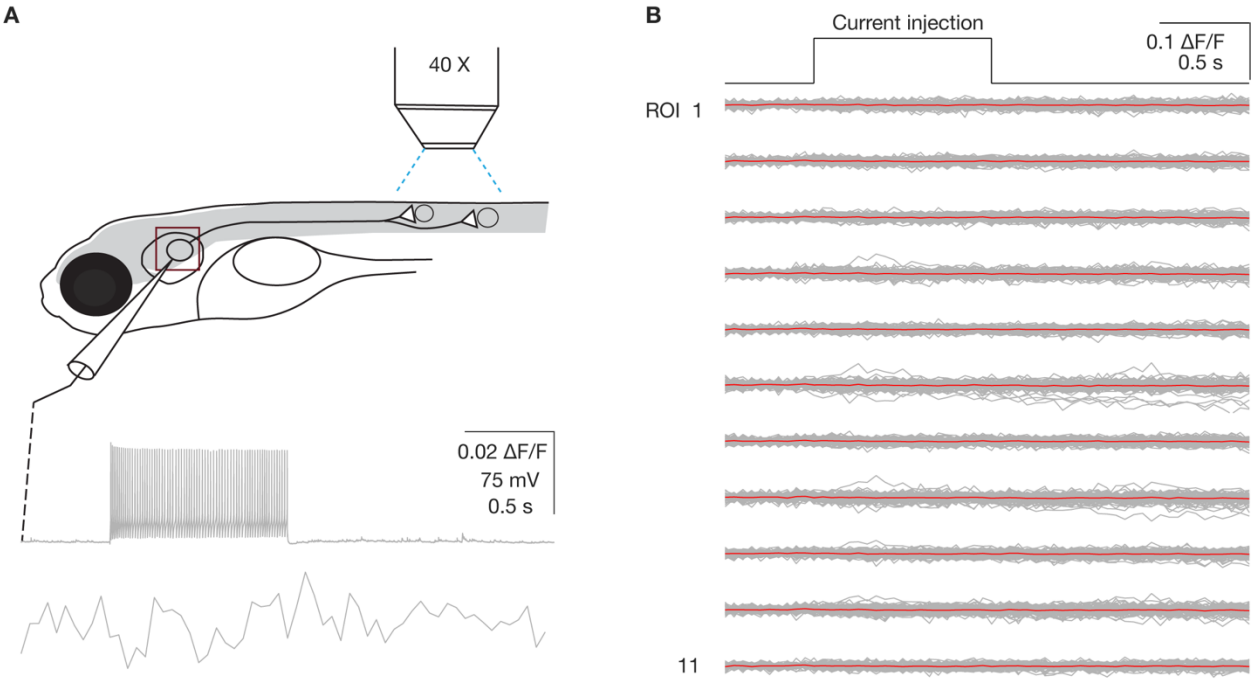

Figure 4. 1: Stimulating one vestibulospinal neuron doesn't invoke calcium response in spinal motor neurons

A. Imaging calcium response from spinal motor neurons a mnx:GCaMP5g fish, while inducing spiking activity in one vestibulospinal neuron with 1s current injection. Bottom: example traces of induced spiking activity in the vestibulospinal neuron and calcium response in a spinal motor neuron
B. Mean calcium response (red) of 11 regions of interest (ROIs) with 100 trials of 1 s current injection. ROI 1-10 are motor neurons, and ROI 11 covers the background as the control. Mean firing rate of the vestibulospinal neuron: 71.7 spike/s.

To answer this, I first examined whether vestibulospinal neurons directly project to axial motor neurons to exert motor control. Preliminary paired patch clamp recording data from Dr. Martha

Bagnall showed that activation of vestibulospinal neurons elicited monosynaptic EPSPs in some motor neurons but not the others (data not shown). Which axial motor neurons are preferentially targeted by the vestibulospinal neurons? I imaged the calcium response from the motor neurons in a mnx:GCaMP5g fishline, while intracellularly recording from one vestibulospinal neuron (Fig 4.1A). Current injection induced spiking activities in the vestibulospinal neurons, however there was not significant change in the calcium response of any motor neurons, compared to the background noise (Fig 4.1B). The most possible explanation is that the activating only one vestibulospinal neuron was not sufficient to elicit action potentials in the motor neurons, thus the calcium response is undetectable. It would be interesting to use voltage indicator to examine the potential subthreshold activities in the motor neurons. A huge advantage of imaging in larval zebrafish spinal is the accessibility to monitor the activity of a large pool of motor and pre-motor neurons simultaneously. A few directions could be explored in this regard. First, it was shown for mammalian limb extensors, motor neurons innervating the slow muscle groups are preferentially targeted by vestibulospinal projections compared to those innervating the fast muscle groups. Are vestibulospinal neurons projecting to the axial motor neurons in a similar pattern? In the larval zebrafish, fast motor neurons are earlier born and located more dorsally than the slow ones. Thus it should be tested if ventrally located motor neurons are the primary targets of the vestibulospinal pathway. Second, vestibulospinal axons span the entire rostral-caudal axis of the spinal cord. Do vestibulospinal neurons have different connectivity with motor or pre-motor neurons in the rostral and caudal spinal segments? It was recently shown that longitudinal motor control via specific intraspinal connectivity is important for locomotion. Excitatory and inhibitory spinal pre-motor axons also span multiple spinal segments and target distinct motor neurons in each segment for rostral-caudal coordination (Callahan et al., 2019,

Sengupta et al., 2020). Though the organization of spinal motor circuits along the longitudinal axis still needs to be clarified, the rostral-caudal specificity of vestibular-induced motor control is mostly uncharted, which could be an interesting topic to investigate in the future.

Central vestibular organization

Serial-section EM reconstruction revealed a developmental order of vestibular peripheral circuits. Earlier born striolar hair cells were primarily innervated by earlier born vestibular afferents, which were suggested to develop as the phasic/irregular vestibular pathway; whereas the later born extrastriolar hair cells were primarily innervated by later born vestibular afferents, which were suggested to develop as the tonic/regular vestibular pathway. Are vestibular afferent projections to the central brain arranged in a similar developmental order, which would lead to an organized central vestibular circuitry by the movement speed? To investigate this, I first examined the projections of the 105 vestibular afferents to 14 vestibulospinal neurons reconstructed from the EM dataset in Chapter 3. I found that all 14 vestibulospinal neurons were myelinated and they were contacted by both myelinated and unmyelinated afferents. In the future, I will identify if any unmyelinated vestibulospinal neurons were contacted by the afferents, and compare the presynaptic afferent age of the younger and older vestibulospinal neurons. I hypothesize that the myelinated vestibulospinal neurons receive more myelinated afferent inputs than the unmyelinated ones, which would indicate early born vestibulospinal neurons are activated by fast self-motion signals to exert motor control on fast movements. Moreover, another age-dependent recruitment mechanism was recently shown in the spinal inhibitory circuit to regulate fast and slow movements. Early born commissural inhibitory neuron innervate primarily the spike initiation zone of the motor neuron axon, whereas the late born neurons display perisomatic and dendritic innervations onto the motor neurons. This enables a

stronger capability for early born inhibitory neurons to silence the motor output. Do vestibular afferents of different ages provide varying degrees of excitation to vestibulospinal neurons via innervation onto different postsynaptic compartments? I measured the distance of each synaptic contact of all vestibular afferents to the vestibulospinal soma (Fig. 4.2).

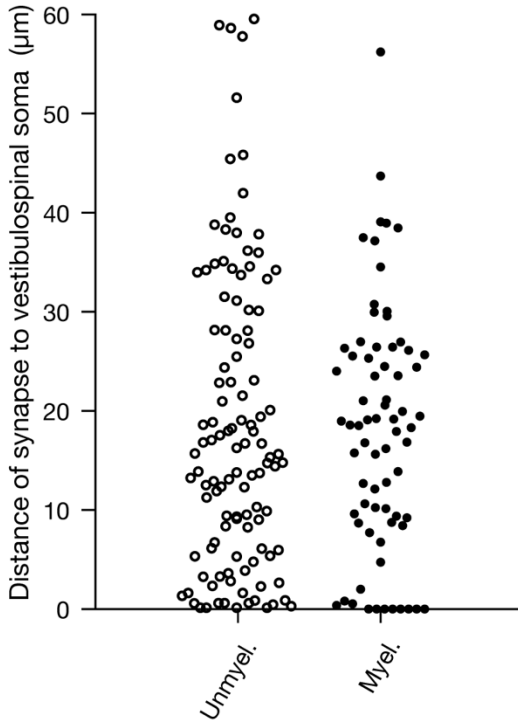

Figure 4. 2: Synapses of myelinated and unmyelinated afferents exhibit similar distance to postsynaptic soma

Myelinated (dots) and unmyelinated (circles) afferents synapse onto vestibulospinal neurons both perisomatically (=0 µm) and dendritically (> 0 µm). Their synaptic distance to vestibulospinal soma don't show significant difference. Mann-Whitney U test; p = 0.8.

I found that both myelinated and unmyelinated afferents had perisomatic and dendritic innervation onto vestibulospinal neurons. Their synaptic contact to soma distance ranged from 0 to 65 µm (18.2+13.9 µm), and there were no significant difference of such distance between the myelinated and unmyelinated afferents (p=0.8). Thus, early born and late born afferents don't show distinct anatomical innervation patterns onto the postsynaptic compartments of the vestibulospinal neurons. In mammals, the vestibulospinal nucleus doesn't seem to have topographic map organized by sensory tuning. Are the vestibulospinal neurons in the larval zebrafish similarly disorganized? In the future, it would be interesting to study how vestibular

afferents innervated onto other central vestibular neurons, and whether the innervation is governed by developmental age or sensory tuning.

Efference copy

My data showed that the direct excitatory inputs from the afferents suffice to explain the postsynaptic response in the vestibulospinal neurons during passive movements. It was shown that central vestibular neuronal activities are silenced during active movement, compared to their activities during passive motion. How do animals distinguish self-generated vs external vestibular stimuli? One prevalent hypothesis is that an internal efference copy of motor command was used to suppress central vestibular activities during active movements. More strikingly, when animals experience self-generated and external motion simultaneously, the central vestibular neurons could selectively cancel the self-generated component, and only encode the external motion (Brooks and Cullen, 2013). Cerebellar inputs are a potential source of inhibition during active movements. Purkinje cells in the cerebellum send GABAergic projections directly to the vestibulospinal nucleus (Ito et al., 1968, Kani et al., 2010, Hamling et al., 2015), and cerebellar circuits are known to generate predictive signals from sensory inputs and motor commands. In accordance, the deep cerebellar neurons exhibited strong tuning sensitivity to unexpected head movements, and weak tuning sensitivity to expected movements (Brooks et al., 2015). The internal predictive model of the cerebellum can be altered by learning to adapt a new relationship between motor commands and resultant movements. In some preliminary experiments, IPSCs were also observed in recordings from the vestibulospinal neurons with Cs-based internal solutions (data not shown). But the source of these IPSC inputs remains unknown. In the future, one could examine whether the activation of Purkinje neurons could elicit monosynaptic IPSCs in the vestibulospinal neurons, and then test how cerebellar-

derived IPSCs are associated with locomotion activity, which could be monitored by ventral root recordings in the larval zebrafish.

References:

AKROUH, A. & KERSCHENSTEINER, D. 2013. Intersecting Circuits Generate Precisely Patterned Retinal Waves. *Neuron,* 79**,** 322-334.

ALONSO, J. M. & MARTINEZ, L. M. 1998. Functional connectivity between simple cells and complex cells in cat striate cortex. *Nature Neuroscience,* 1**,** 395-403.

ANGELAKI, D. E. 1991. DYNAMIC POLARIZATION VECTOR OF SPATIALLY TUNED NEURONS. *Ieee Transactions on Biomedical Engineering,* 38**,** 1053-1060.

ANGELAKI, D. E. 1992. SPATIOTEMPORAL CONVERGENCE (STC) IN OTOLITH NEURONS. *Biological Cybernetics,* 67**,** 83-96.

ANGELAKI, D. E. 1993. GENERATION OF 2-DIMENSIONAL SPATIAL AND TEMPORAL PROPERTIES THROUGH SPATIOTEMPORAL CONVERGENCE BETWEEN ONE-DIMENSIONAL NEURONS. *Ieee Transactions on Biomedical Engineering,* 40**,** 686-692.

ANGELAKI, D. E., BUSH, G. A. & PERACHIO, A. A. 1993. 2-DIMENSIONAL SPATIOTEMPORAL CODING OF LINEAR ACCELERATION IN VESTIBULAR NUCLEI NEURONS. *Journal of Neuroscience,* 13**,** 1403-1417.

ANGELAKI, D. E. & CULLEN, K. E. 2008. Vestibular system: The many facets of a multimodal sense. *Annual Review of Neuroscience,* 31**,** 125-150.

ANGELAKI, D. E. & DICKMAN, J. D. 2000a. Spatiotemporal processing of linear acceleration: primary afferent and central vestibular neuron responses. *J Neurophysiol,* 84**,** 2113-32.

ANGELAKI, D. E. & DICKMAN, J. D. 2000b. Spatiotemporal processing of linear acceleration: Primary afferent and central vestibular neuron responses. *Journal of Neurophysiology,* 84**,** 2113-2132.

ARENZ, A., SILVER, R. A., SCHAEFER, A. T. & MARGRIE, T. W. 2008. The contribution of single synapses to sensory representation in vivo. *Science,* 321**,** 977-80.

BAGNALL, M. W., HULL, C., BUSHONG, E. A., ELLISMAN, M. H. & SCANZIANI, M. 2011. Multiple Clusters of Release Sites Formed by Individual Thalamic Afferents onto Cortical Interneurons Ensure Reliable Transmission. *Neuron,* 71**,** 180-194.

BAGNALL, M. W., MCELVAIN, L. E., FAULSTICH, M. & DU LAC, S. 2008. Frequency-independent synaptic transmission supports a linear vestibular behavior. *Neuron,* 60**,** 343-52.

BAGNALL, M. W. & MCLEAN, D. L. 2014. Modular organization of axial microcircuits in zebrafish. *Science (New York, N.Y.),* 343**,** 197-200.

BAGNALL, M. W. & SCHOPPIK, D. 2018. Development of vestibular behaviors in zebrafish. *Current Opinion in Neurobiology,* 53**,** 83-89.

BALE, M. R. & PETERSEN, R. S. 2009. Transformation in the Neural Code for Whisker Deflection Direction Along the Lemniscal Pathway. *Journal of Neurophysiology,* 102**,** 2771-2780.

BASALDELLA, E., TAKEOKA, A., SIGRIST, M. & ARBER, S. 2015. Multisensory Signaling Shapes Vestibulo-Motor Circuit Specificity. *Cell,* 163**,** 301-312.

BECK, A. & TEBOULLE, M. 2009. A Fast Iterative Shrinkage-Thresholding Algorithm for Linear Inverse Problems. *Siam Journal on Imaging Sciences,* 2**,** 183-202.

BECK, J. C., GILLAND, E., TANK, D. W. & BAKER, R. 2004. Quantifying the ontogeny of optokinetic and vestibuloocular behaviors in zebrafish, medaka, and goldfish. *Journal of Neurophysiology,* 92**,** 3546-3561.

BIANCO, I. H., MA, L. H., SCHOPPIK, D., ROBSON, D. N., ORGER, M. B., BECK, J. C., LI, J. M., SCHIER, A. F., ENGERT, F. & BAKER, R. 2012. The tangential nucleus controls a gravito-inertial vestibulo-ocular reflex. *Current Biology,* 22**,** 1285-1295.

BOYLE, R., GOLDBERG, J. M. & HIGHSTEIN, S. M. 1992. Inputs from regularly and irregularly discharging vestibular nerve afferents to secondary neurons in squirrel monkey vestibular nuclei. III. Correlation with vestibulospinal and vestibuloocular output pathways. *J Neurophysiol,* 68**,** 471-84.

BOYLE, R. & JOHANSON, C. 2003. Morphological properties of vestibulospinal neurons in primates. *Annals of the New York Academy of Sciences,* 1004**,** 183-195.

BRETTE, R. 2007. Exact simulation of integrate-and-fire models with exponential currents. *Neural Computation,* 19**,** 2604-2609.

BRONSTEIN, A. M., PATEL, M. & ARSHAD, Q. 2015. A brief review of the clinical anatomy of the vestibular-ocular connections-how much do we know? *Eye,* 29**,** 163-170.

BROOKS, J. X., CARRIOT, J. & CULLEN, K. E. 2015. Learning to expect the unexpected: rapid updating in primate cerebellum during voluntary self-motion. *Nature Neuroscience,* 18**,** 1310-+.

BROOKS, J. X. & CULLEN, K. E. 2013. The Primate Cerebellum Selectively Encodes Unexpected Self-Motion. *Current Biology,* 23**,** 947-955.

BRUNO, R. M., KHATRI, V., LAND, P. W. & SIMONS, D. J. 2003. Thalamocortical angular tuning domains within individual barrels of rat somatosensory cortex. *Journal of Neuroscience,* 23**,** 9565-9574.

BUDELLI, R. & MACADAR, O. 1979. STATO-ACOUSTIC PROPERTIES OF UTRICULAR AFFERENTS. *Journal of Neurophysiology,* 42**,** 1479-1493.

BUSH, G. A., PERACHIO, A. A. & ANGELAKI, D. E. 1993. ENCODING OF HEAD ACCELERATION IN VESTIBULAR NEURONS .1. SPATIOTEMPORAL RESPONSE PROPERTIES TO LINEAR ACCELERATION. *Journal of Neurophysiology,* 69**,** 2039-2055.

CALLAHAN, R. A., ROBERTS, R., SENGUPTA, M., KIMURA, Y., HIGASHIJIMA, S. & BAGNALL, M. W. 2019. Spinal V2b neurons reveal a role for ipsilateral inhibition in speed control. *Elife,* 8.

CARDONA, A., SAALFELD, S., SCHINDELIN, J., ARGANDA-CARRERAS, I., PREIBISCH, S., LONGAIR, M., TOMANCAK, P., HARTENSTEIN, V. & DOUGLAS, R. J. 2012. TrakEM2 Software for Neural Circuit Reconstruction. *Plos One,* 7.

CARLETON, S. C. & CARPENTER, M. B. 1984. DISTRIBUTION OF PRIMARY VESTIBULAR FIBERS IN THE BRAIN-STEM AND CEREBELLUM OF THE MONKEY. *Brain Research,* 294**,** 281-298.

CHABROL, F. P., ARENZ, A., WIECHERT, M. T., MARGRIE, T. W. & DIGREGORIO, D. A. 2015. Synaptic diversity enables temporal coding of coincident multisensory inputs in single neurons. *Nat Neurosci,* 18**,** 718-27.

CHEN, A. H., DEANGELIS, G. C. & ANGELAKI, D. E. 2010. Macaque Parieto-Insular Vestibular Cortex: Responses to Self-Motion and Optic Flow. *Journal of Neuroscience,* 30**,** 3022-3042.

CHUNG, J. E., MAGLAND, J. F., BARNETT, A. H., TOLOSA, V. M., TOOKER, A. C., LEE, K. Y., SHAH, K. G., FELIX, S. H., FRANK, L. M. & GREENGARD, L. F. 2017. A Fully Automated Approach to Spike Sorting. *Neuron,* 95**,** 1381-1394 e6.
CULLEN, K. E. 2019. Vestibular processing during natural self-motion: implications for perception and action. *Nature Reviews Neuroscience,* 20**,** 346-363.
DEANS, M. R. 2013. A balance of form and function: Planar polarity and development of the vestibular maculae. *Seminars in Cell & Developmental Biology,* 24**,** 490-498.
DESAI, S. S., ZEH, C. & LYSAKOWSKI, A. 2005. Comparative morphology of rodent vestibular periphery. I. Saccular and utricular maculae. *Journal of Neurophysiology,* 93**,** 251-266.
EATOCK, R. A. & SONGER, J. E. 2011. Vestibular hair cells and afferents: two channels for head motion signals. *Annu Rev Neurosci,* 34**,** 501-34.
EHRLICH, D. E. & SCHOPPIK, D. 2017. Control of Movement Initiation Underlies the Development of Balance. *Current Biology,* 27**,** 334-344.
EHRLICH, D. E. & SCHOPPIK, D. 2019. A primal role for the vestibular sense in the development of coordinated locomotion. *Elife,* 8.
FAVRE-BULLE, I. A., VANWALLEGHEM, G., TAYLOR, M. A., RUBINSZTEIN-DUNLOP, H. & SCOTT, E. K. 2018. Cellular-Resolution Imaging of Vestibular Processing across the Larval Zebrafish Brain. *Curr Biol,* 28**,** 3711-3722 e3.
FAY, R. R. 1984. THE GOLDFISH EAR CODES THE AXIS OF ACOUSTIC PARTICLE MOTION IN 3 DIMENSIONS. *Science,* 225**,** 951-954.
FELLEMAN, D. J. & VAN ESSEN, D. C. 1991. Distributed Hierarchical Processing in the Primate Cerebral Cortex. *Cerebral Cortex,* 1**,** 1-47.
FERNANDEZ, C. & GOLDBERG, J. M. 1971. PHYSIOLOGY OF PERIPHERAL NEURONS INNERVATING SEMICIRCULAR CANALS OF SQUIRREL MONKEY .2. RESPONSE TO SINUSOIDAL STIMULATION AND DYNAMICS OF PERIPHERAL VESTIBULAR SYSTEM. *Journal of Neurophysiology,* 34**,** 661-+.
FERNANDEZ, C. & GOLDBERG, J. M. 1976a. PHYSIOLOGY OF PERIPHERAL NEURONS INNERVATING OTOLITH ORGANS OF SQUIRREL-MONKEY .1. RESPONSE TO STATIC TILTS AND TO LONG-DURATION CENTRIFUGAL FORCE. *Journal of Neurophysiology,* 39**,** 970-984.
FERNANDEZ, C. & GOLDBERG, J. M. 1976b. PHYSIOLOGY OF PERIPHERAL NEURONS INNERVATING OTOLITH ORGANS OF SQUIRREL-MONKEY .3. RESPONSE DYNAMICS. *Journal of Neurophysiology,* 39**,** 996-1008.
FERNANDEZ, C., GOLDBERG, J. M. & ABEND, W. K. 1972. RESPONSE TO STATIC TILTS OF PERIPHERAL NEURONS INNERVATING OTOLITH ORGANS OF SQUIRREL-MONKEY. *Journal of Neurophysiology,* 35**,** 978-+.
GLOVER, J. C. 2000. Neuroepithelial 'compartments' and the specification of vestibular projections. *Cerebellar Modules: Molecules, Morphology, and Function,* 124**,** 3-21.
GOLDBERG, J. M. 2000. Afferent diversity and the organization of central vestibular pathways. *Experimental Brain Research,* 130**,** 277-297.
GOLDBERG, J. M. & CULLEN, K. E. 2011. Vestibular control of the head: possible functions of the vestibulocollic reflex. *Experimental Brain Research,* 210**,** 331-345.
GOLDBERG, J. M., DESMADRYL, G., BAIRD, R. A. & FERNANDEZ, C. 1990. THE VESTIBULAR NERVE OF THE CHINCHILLA .4. DISCHARGE PROPERTIES OF UTRICULAR AFFERENTS. *Journal of Neurophysiology,* 63**,** 781-790.

GOLDBERG, J. M. & FERNANDEZ, C. 1971. PHYSIOLOGY OF PERIPHERAL NEURONS INNERVATING SEMICIRCULAR CANALS OF SQUIRREL MONKEY .3. VARIATIONS AMONG UNITS IN THEIR DISCHARGE PROPERTIES. *Journal of Neurophysiology,* 34**,** 676-+.

GOLDBERG, J. M. & FERNANDEZ, C. 1977. CONDUCTION TIMES AND BACKGROUND DISCHARGE OF VESTIBULAR AFFERENTS. *Brain Research,* 122**,** 545-550.

GRILLNER, S. & HONGO, T. 1972. Vestibulospinal Effects on Motoneurones and Interneurones in the Lumbosacral Cord. *Progress in Brain Research,* 37**,** 243-262.

GRILLNER, S., HONGO, T. & LUND, S. 1970. VESTIBULOSPINAL TRACT . EFFECTS ON ALPHA-MOTONEURONES IN LUMBOSACRAL SPINAL CORD IN CAT. *Experimental Brain Research,* 10**,** 94-+.

HADDON, C., MOWBRAY, C., WHITFIELD, T., JONES, D., GSCHMEISSNER, S. & LEWIS, J. 1999. Hair cells without supporting cells: further studies in the ear of the zebrafish mind bomb mutant. *J Neurocytol,* 28**,** 837-50.

HAMLING, K. R., TOBIAS, Z. J. C. & WEISSMAN, T. A. 2015. Mapping the development of cerebellar Purkinje cells in zebrafish. *Developmental Neurobiology,* 75**,** 1174-1188.

HAYWORTH, K. J., MORGAN, J. L., SCHALEK, R., BERGER, D. R., HILDEBRAND, D. G. C. & LICHTMAN, J. W. 2014. Imaging ATUM ultrathin section libraries with WaferMapper: a multi-scale approach to EM reconstruction of neural circuits. *Frontiers in Neural Circuits,* 8.

HELMBRECHT, T. O., DAL MASCHIO, M., DONOVAN, J. C., KOUTSOULI, S. & BAIER, H. 2018. Topography of a Visuomotor Transformation. *Neuron,* 100**,** 1429-+.

HILDEBRAND, D. G. C., CICCONET, M., TORRES, R. M., CHOI, W., QUAN, T. M., MOON, J., WETZEL, A. W., SCOTT CHAMPION, A., GRAHAM, B. J., RANDLETT, O., PLUMMER, G. S., PORTUGUES, R., BIANCO, I. H., SAALFELD, S., BADEN, A. D., LILLANEY, K., BURNS, R., VOGELSTEIN, J. T., SCHIER, A. F., LEE, W. A., JEONG, W. K., LICHTMAN, J. W. & ENGERT, F. 2017. Whole-brain serial-section electron microscopy in larval zebrafish. *Nature,* 545**,** 345-349.

HINES, M. L. & CARNEVALE, N. T. 1997. The NEURON simulation environment. *Neural Computation,* 9**,** 1179-1209.

HUBEL, D. H. & WIESEL, T. N. 1962. RECEPTIVE FIELDS, BINOCULAR INTERACTION AND FUNCTIONAL ARCHITECTURE IN CATS VISUAL CORTEX. *Journal of Physiology-London,* 160**,** 106-&.

HUDSPETH, A. J. & COREY, D. P. 1977. SENSITIVITY, POLARITY, AND CONDUCTANCE CHANGE IN RESPONSE OF VERTEBRATE HAIR CELLS TO CONTROLLED MECHANICAL STIMULI. *Proceedings of the National Academy of Sciences of the United States of America,* 74**,** 2407-2411.

HUWE, J. A., LOGAN, G. J., WILLIAMS, B., ROWE, M. H. & PETERSON, E. H. 2015. Utricular afferents: morphology of peripheral terminals. *Journal of Neurophysiology,* 113**,** 2420-2433.

ITO, M., KAWAI, N. & UDO, M. 1968. ORIGIN OF CEREBELLAR-INDUCED INHIBITION OF DEITERS NEURONES .3. LOCALIZATION OF INHIBITORY ZONE. *Experimental Brain Research,* 4**,** 310-&.

JAMALI, M., CARRIOT, J., CHACRON, M. J. & CULLEN, K. E. 2013. Strong Correlations between Sensitivity and Variability Give Rise to Constant Discrimination Thresholds across the Otolith Afferent Population. *Journal of Neuroscience,* 33**,** 11302-11313.

JAMALI, M., CHACRON, M. J. & CULLEN, K. E. 2016. Self-motion evokes precise spike timing in the primate vestibular system. *Nature Communications,* 7.
JIA, H., ROCHEFORT, N. L., CHEN, X. & KONNERTH, A. 2010. Dendritic organization of sensory input to cortical neurons in vivo. *Nature,* 464**,** 1307-1312.
JIANG, T., KINDT, K. & WU, D. K. 2017. Transcription factor Emx2 controls stereociliary bundle orientation of sensory hair cells. *Elife,* 6.
KANI, S., BAE, Y. K., SHIMIZU, T., TANABE, K., SATOU, C., PARSONS, M. J., SCOTT, E., HIGASHIJIMA, S. & HIBI, M. 2010. Proneural gene-linked neurogenesis in zebrafish cerebellum. *Developmental Biology,* 343**,** 1-17.
KASUMACIC, N., GLOVER, J. C. & PERREAULT, M. C. 2010. Segmental patterns of vestibular-mediated synaptic inputs to axial and limb motoneurons in the neonatal mouse assessed by optical recording. *Journal of Physiology-London,* 588**,** 4905-4925.
KASUMACIC, N., LAMBERT, F. M., COULON, P., BRAS, H., VINAY, L., PERREAULT, M.-C. & GLOVER, J. C. 2015. Segmental Organization of Vestibulospinal Inputs to Spinal Interneurons Mediating Crossed Activation of Thoracolumbar Motoneurons in the Neonatal Mouse. *Journal of Neuroscience,* 35**,** 8158-8169.
KIMMEL, C. B., POWELL, S. L. & METCALFE, W. K. 1982. Brain neurons which project to the spinal cord in young larvae of the zebrafish. *The Journal of comparative neurology,* 205**,** 112-27.
KIMURA, Y., HISANO, Y., KAWAHARA, A. & HIGASHIJIMA, S. 2014. Efficient generation of knock-in transgenic zebrafish carrying reporter/driver genes by CRISPR/Cas9-mediated genome engineering. *Scientific Reports,* 4.
KISHORE, S., CADOFF, E. B., AGHA, M. A. & MCLEAN, D. L. 2020. Orderly compartmental mapping of premotor inhibition in the developing zebrafish spinal cord. *Science,* 370**,** 431-436.
KODAMA, T., GITTIS, A., SHIN, M., KELLEHER, K., KOLKMAN, K., MCELVAIN, L., LAM, M. & DU LAC, S. 2020. Graded co-expression of ion channel, neurofilament, and synaptic genes in fast-spiking vestibular nucleus neurons. *J Neurosci*.
KORN, H., SOTELO, C. & BENNETT, M. V. L. 1977. The lateral vestibular nucleus of the toadfish Opsanus tau: Ultrastructural and electrophysiological observations with special reference to electrotonic transmission. *Neuroscience*.
LAMBERT, F. M., BECK, J. C., BAKER, R. & STRAKA, H. 2008. Semicircular canal size determines the developmental onset of angular vestibuloocular reflexes in larval Xenopus. *Journal of Neuroscience,* 28**,** 8086-8095.
LAURENS, J., LIU, S., YU, X. J., CHAN, R., DICKMAN, D., DEANGELIS, G. C. & ANGELAKI, D. E. 2017. Transformation of spatiotemporal dynamics in the macaque vestibular system from otolith afferents to cortex. *Elife,* 6.
LAVZIN, M., RAPOPORT, S., POLSKY, A., GARION, L. & SCHILLER, J. 2012. Nonlinear dendritic processing determines angular tuning of barrel cortex neurons in vivo. *Nature,* 490**,** 397-401.
LECUN, Y., BENGIO, Y. & HINTON, G. 2015. Deep learning. *Nature,* 521**,** 436-444.
LI, A., XUE, J. & PETERSON, E. H. 2008. Architecture of the mouse utricle: macular organization and hair bundle heights. *Journal of Neurophysiology,* 99**,** 718-733.
LIU, Z. K., KIMURA, Y., HIGASHIJIMA, S., HILDEBRAND, D. G. C., MORGAN, J. L. & BAGNALL, M. W. 2020. Central Vestibular Tuning Arises from Patterned Convergence of Otolith Afferents. *Neuron,* 108**,** 748-+.

LU, Z., XU, Z. & BUCHSER, W. J. 2004. Coding of acoustic particle motion by utricular fibers in the sleeper goby, Dormitator latifrons. *Journal of Comparative Physiology a-Neuroethology Sensory Neural and Behavioral Physiology,* 190**,** 923-938.

LUNSFORD, E. T., SKANDALIS, D. A. & LIAO, J. C. 2019. Efferent modulation of spontaneous lateral line activity during and after zebrafish motor commands. *Journal of Neurophysiology,* 122**,** 2438-2448.

LV, C. X., STEWART, W. J., AKANYETI, O., FREDERICK, C., ZHU, J., SANTOS-SACCHI, J., SHEETS, L., LIAO, J. C. & ZENISEK, D. 2016. Synaptic Ribbons Require Ribeye for Electron Density, Proper Synaptic Localization, and Recruitment of Calcium Channels. *Cell Reports,* 15**,** 2784-2795.

MARDER, E. & BUCHER, D. 2001. Central pattern generators and the control of rhythmic movements. *Current Biology,* 11**,** R986-R996.

MARKWALTER, K. H., YANG, Y., HOLY, T. E. & BONNI, A. 2019. Sensorimotor Coding of Vermal Granule Neurons in the Developing Mammalian Cerebellum. *Journal of Neuroscience,* 39**,** 6626-6643.

MARUSKA, K. P. & MENSINGER, A. F. 2015. Directional sound sensitivity in utricular afferents in the toadfish Opsanus tau. *Journal of Experimental Biology,* 218**,** 1759-1766.

MCELVAIN, L. E., FAULSTICH, M., JEANNE, J. M., MOORE, J. D. & DU LAC, S. 2015. Implementation of linear sensory signaling via multiple coordinated mechanisms at central vestibular nerve synapses. *Neuron,* 85**,** 1132-44.

MCLEAN, D. L., FAN, J., HIGASHIJIMA, S., HALE, M. E. & FETCHO, J. R. 2007. A topographic map of recruitment in spinal cord. *Nature,* 446**,** 71-5.

MCLEAN, D. L. & FETCHO, J. R. 2009. Spinal Interneurons Differentiate Sequentially from Those Driving the Fastest Swimming Movements in Larval Zebrafish to Those Driving the Slowest Ones. *Journal of Neuroscience,* 29**,** 13566-13577.

MCLEAN, D. L., MASINO, M. A., KOH, I. Y. Y., LINDQUIST, W. B. & FETCHO, J. R. 2008. Continuous shifts in the active set of spinal interneurons during changes in locomotor speed. *Nature neuroscience,* 11**,** 1419-29.

MENELAOU, E. & MCLEAN, D. L. 2012. A gradient in endogenous rhythmicity and oscillatory drive matches recruitment order in an axial motor pool. *J Neurosci,* 32**,** 10925-39.

MENELAOU, E., VANDUNK, C. & MCLEAN, D. L. 2014. Differences in the morphology of spinal V2a neurons reflect their recruitment order during swimming in larval zebrafish. *J Comp Neurol,* 522**,** 1232-48.

MIGAULT, G., VAN DER PLAS, T. L., TRENTESAUX, H., PANIER, T., CANDELIER, R., PROVILLE, R., ENGLITZ, B., DEBREGEAS, G. & BORMUTH, V. 2018. Whole-Brain Calcium Imaging during Physiological Vestibular Stimulation in Larval Zebrafish. *Curr Biol,* 28**,** 3723-3735 e6.

MO, W., CHEN, F. Y., NECHIPORUK, A. & NICOLSON, T. 2010. Quantification of vestibular-induced eye movements in zebrafish larvae. *Bmc Neuroscience,* 11.

MORGAN, J. L., BERGER, D. R., WETZEL, A. W. & LICHTMAN, J. W. 2016. The Fuzzy Logic of Network Connectivity in Mouse Visual Thalamus. *Cell,* 165**,** 192-206.

MURRAY, A. J., CROCE, K., BELTON, T., AKAY, T. & JESSELL, T. M. 2018. Balance Control Mediated by Vestibular Circuits Directing Limb Extension or Antagonist Muscle Co-activation. *Cell Reports,* 22**,** 1325-1338.

NAGY, J. I., BAUTISTA, W., BLAKLEY, B. & RASH, J. E. 2013. Morphologically mixed chemical-electrical synapses formed by primary afferents in rodent vestibular nuclei as revealed by immunofluorescence detection of connexin36 and vesicular glutamate transporter-1. *Neuroscience,* 252**,** 468-88.
NAM, J. H., COTTON, J. R. & GRANT, J. W. 2005. Effect of fluid forcing on vestibular hair bundles. *Journal of Vestibular Research-Equilibrium & Orientation,* 15**,** 263-278.
NEUHUBER, W. L. & ZENKER, W. 1989. CENTRAL DISTRIBUTION OF CERVICAL PRIMARY AFFERENTS IN THE RAT, WITH EMPHASIS ON PROPRIOCEPTIVE PROJECTIONS TO VESTIBULAR, PERIHYPOGLOSSAL, AND UPPER THORACIC SPINAL NUCLEI. *Journal of Comparative Neurology,* 280**,** 231-253.
NEWLANDS, S. D. & PERACHIO, A. A. 2003. Central projections of the vestibular nerve: a review and single fiber study in the Mongolian gerbil. *Brain Research Bulletin,* 60**,** 475-495.
NEWLANDS, S. D., VRABEC, J. T., PURCELL, I. M., STEWART, C. M., ZIMMERMAN, B. E. & PERACHIO, A. A. 2003. Central projections of the saccular and utricular nerves in macaques. *Journal of Comparative Neurology,* 466**,** 31-47.
ORLOVSKY, G. N. 1972. ACTIVITY OF VESTIBULOSPINAL NEURONS DURING LOCOMOTION. *Brain Research,* 46**,** 85-&.
PEREDA, A. E. 2016. Developmental functions of electrical synapses. *Journal of Physiology-London,* 594**,** 2561-2562.
PETERSEN, C. C. H. 2007. The functional organization of the barrel cortex. *Neuron,* 56**,** 339-355.
PETERSEN, C. C. H. 2019. Sensorimotor processing in the rodent barrel cortex. *Nature Reviews Neuroscience,* 20**,** 533-546.
PETERSON, B. W. 1970a. DISTRIBUTION OF NEURAL RESPONSES TO TILTING WITHIN VESTIBULAR NUCLEI OF CAT. *Journal of Neurophysiology,* 33**,** 750-+.
PETERSON, B. W. 1970b. Distribution of neural responses to tilting within vestibular nuclei of the cat. *J Neurophysiol,* 33**,** 750-67.
PICHLER, P. & LAGNADO, L. 2020. Motor Behavior Selectively Inhibits Hair Cells Activated by Forward Motion in the Lateral Line of Zebrafish. *Current Biology,* 30**,** 150-+.
PLATT, C. 1977. HAIR CELL DISTRIBUTION AND ORIENTATION IN GOLDFISH OTOLITH ORGANS. *Journal of Comparative Neurology,* 172**,** 283-297.
PRIEBE, N. J. & FERSTER, D. 2012. Mechanisms of Neuronal Computation in Mammalian Visual Cortex. *Neuron,* 75**,** 194-208.
PRIEBE, N. J., MECHLER, F., CARANDINI, M. & FERSTER, D. 2004. The contribution of spike threshold to the dichotomy of cortical simple and complex cells. *Nature Neuroscience,* 7**,** 1113-1122.
RILEY, B. B. & MOORMAN, S. J. 2000. Development of utricular otoliths, but not saccular otoliths, is necessary for vestibular function and survival in zebrafish. *J Neurobiol,* 43**,** 329-37.
ROBERTS, R., ELSNER, J. & BAGNALL, M. W. 2017. Delayed Otolith Development Does Not Impair Vestibular Circuit Formation in Zebrafish. *J Assoc Res Otolaryngol,* 18**,** 415-425.
ROY, N. C., BESSAIH, T. & CONTRERAS, D. 2011. Comprehensive mapping of whisker-evoked responses reveals broad, sharply tuned thalamocortical input to layer 4 of barrel cortex. *Journal of Neurophysiology,* 105**,** 2421-2437.

SARKISIAN, V. H. 2000. Input-output relations of Deiters' lateral vestibulospinal neurons with different structures of the brain. *Archives Italiennes De Biologie,* 138**,** 295-353.
SATO, F. & SASAKI, H. 1993. MORPHOLOGICAL CORRELATIONS BETWEEN SPONTANEOUSLY DISCHARGING PRIMARY VESTIBULAR AFFERENTS AND VESTIBULAR NUCLEUS NEURONS IN THE CAT. *Journal of Comparative Neurology,* 333**,** 554-566.
SCHMITT, E. A. & DOWLING, J. E. 1999. Early retinal development in the zebrafish, Danio rerio: Light and electron microscopic analyses. *Journal of Comparative Neurology,* 404**,** 515-536.
SCHOPPIK, D., BIANCO, I. H., PROBER, D. A., DOUGLASS, A. D., ROBSON, D. N., LI, J. M. B., GREENWOOD, J. S. F., SOUCY, E., ENGERT, F. & SCHIER, A. F. 2017. Gaze-Stabilizing Central Vestibular Neurons Project Asymmetrically to Extraocular Motoneuron Pools. *J Neurosci,* 37**,** 11353-11365.
SCHOR, R. H. & ANGELAKI, D. E. 1992. THE ALGEBRA OF NEURAL RESPONSE VECTORS. *Annals of the New York Academy of Sciences,* 656**,** 190-204.
SCHOR, R. H., MILLER, A. D., TIMERICK, S. J. & TOMKO, D. L. 1985. Responses to head tilt in cat central vestibular neurons. II. Frequency dependence of neural response vectors. *J Neurophysiol,* 53**,** 1444-52.
SCHOR, R. H., MILLER, A. D. & TOMKO, D. L. 1984a. Responses to head tilt in cat central vestibular neurons. I. Direction of maximum sensitivity. *J Neurophysiol,* 51**,** 136-46.
SCHOR, R. H., MILLER, A. D. & TOMKO, D. L. 1984b. Responses to head tilt in cat central vestibular neurons. I. Direction of maximum sensitivity. *Journal of neurophysiology,* 51**,** 136-146.
SENGUPTA, M., DALIPARTHI, V., ROUSSEL, Y., BUI, T. V. & BAGNALL, M. W. 2020. Spinal V1 neurons inhibit motor targets locally and sensory targets distally to coordinate locomotion.
SHERMAN, S. M. 2005. Thalamic relays and cortical functioning. *In:* CASAGRANDE, V. A., GUILLERY, R. W. & SHERMAN, S. M. (eds.) *Cortical Function: a View from the Thalamus.*
SHOTWELL, S. L., JACOBS, R. & HUDSPETH, A. J. 1981. DIRECTIONAL SENSITIVITY OF INDIVIDUAL VERTEBRATE HAIR-CELLS TO CONTROLLED DEFLECTION OF THEIR HAIR BUNDLES. *Annals of the New York Academy of Sciences,* 374**,** 1-10.
SKOTTUN, B. C., DE VALOIS, R. L., GROSOF, D. H., MOVSHON, J. A., ALBRECHT, D. G. & BONDS, A. B. 1991. Classifying simple and complex cells on the basis of response modulation. *Vision Res,* 31**,** 1079-86.
SMEAR, M. C., TAO, H. Z. W., STAUB, W., ORGER, M. B., GOSSE, N. J., LIU, Y., TAKAHASHI, K., POO, M. M. & BAIER, H. 2007. Vesicular glutamate transport at a central synapse limits the acuity of visual perception in zebrafish. *Neuron,* 53**,** 65-77.
SPOON, C., MORAVEC, W. J., ROWE, M. H., GRANT, J. W. & PETERSON, E. H. 2011. Steady-state stiffness of utricular hair cells depends on macular location and hair bundle structure. *Journal of Neurophysiology,* 106**,** 2950-2963.
STRAKA, H. & DIERINGER, N. 1996. Uncrossed disynaptic inhibition of second-order vestibular neurons and its interaction with monosynaptic excitation from vestibular nerve afferent fibers in the frog. *Journal of Neurophysiology,* 76**,** 3087-3101.

STRAKA, H., HOLLER, S., GOTO, F., KOLB, F. P. & GILLAND, E. 2003. Differential spatial organization of otolith signals in frog vestibular nuclei. *Journal of Neurophysiology,* 90**,** 3501-3512.
TOMKO, D. L., PETERKA, R. J. & SCHOR, R. H. 1981. RESPONSES TO HEAD TILT IN CAT 8TH NERVE AFFERENTS. *Experimental Brain Research,* 41**,** 216-221.
TOOTELL, R. B. H., SILVERMAN, M. S., SWITKES, E. & DEVALOIS, R. L. 1982. DEOXYGLUCOSE ANALYSIS OF RETINOTOPIC ORGANIZATION IN PRIMATE STRIATE CORTEX. *Science,* 218**,** 902-904.
TURECEK, J., JACKMAN, S. L. & REGEHR, W. G. 2017. Synaptotagmin 7 confers frequency invariance onto specialized depressing synapses. *Nature,* 551**,** 503-506.
TYTELL, E. D., HSU, C.-Y., WILLIAMS, T. L., COHEN, A. H. & FAUCI, L. J. 2010. Interactions between internal forces, body stiffness, and fluid environment in a neuromechanical model of lamprey swimming. *Proceedings of the National Academy of Sciences of the United States of America,* 107**,** 19832-19837.
UCHINO, Y., SATO, H., KUSHIRO, K., ZAKIR, M., IMAGAWA, M., OGAWA, Y., KATSUTA, M. & ISU, N. 1999. Cross-striolar and commissural inhibition in the otolith system. *Ann N Y Acad Sci,* 871**,** 162-72.
USREY, W. M., REPPAS, J. B. & REID, R. C. 1999. Specificity and strength of retinogeniculate connections. *Journal of Neurophysiology,* 82**,** 3527-3540.
VEMARAJU, S., KANTARCI, H., PADANAD, M. S. & RILEY, B. B. 2012. A Spatial and Temporal Gradient of Fgf Differentially Regulates Distinct Stages of Neural Development in the Zebrafish Inner Ear. *Plos Genetics,* 8.
VOESENEK, C. J., PIETERS, R. P. M. & VAN LEEUWEN, J. L. 2016. Automated Reconstruction of Three-Dimensional Fish Motion, Forces, and Torques. *Plos One,* 11.
WANG, W. C. & MCLEAN, D. L. 2014. Selective Responses to Tonic Descending Commands by Temporal Summation in a Spinal Motor Pool. *Neuron,* 83**,** 708-721.
WILENT, W. B. & CONTRERAS, D. 2005. Dynamics of excitation and inhibition underlying stimulus selectivity in rat somatosensory cortex. *Nature Neuroscience,* 8**,** 1364-1370.
WILSON, V. J., GACEK, R. R., UCHINO, Y. & SUSSWEIN, A. J. 1978. Properties of central vestibular neurons fired by stimulation of the saccular nerve. *Brain Research,* 143**,** 251-261.
WILSON, V. J. & SCHOR, R. H. 1999. The neural substrate of the vestibulocollic reflex - What needs to be learned. *Experimental Brain Research,* 129**,** 483-493.
WILSON, V. J. & YOSHIDA, M. 1969. Comparison of effects of stimulation of Deiters' nucleus and medial longitudinal fasciculus on neck, forelimb, and hindlimb motoneurons. *Journal of neurophysiology,* 32**,** 743-758.
WILSON, V. J., YOSHIDA, M. & SCHOR, R. H. 1970. Supraspinal monosynaptic excitation and inhibition of thoracic back motoneurons. *Experimental Brain Research,* 11**,** 282-295.
WITTS, E. C. & MURRAY, A. J. 2019. Vestibulospinal contributions to mammalian locomotion. *Current Opinion in Physiology,* 8.
XUE, J. B. & PETERSON, E. H. 2006. Hair bundle heights in the utricle: Differences between macular locations and hair cell types. *Journal of Neurophysiology,* 95**,** 171-186.